CONCEPTUAL DESIGN AND PERFORMANCE ANALYSIS OF FREQUENCY-TUNED CAPACITIVE DISCHARGE REACTORS

BY

VEN-YEN TSAI

Bachelor of Engineering
Chung Yuan Christian University
Taiwan, Republic of China
1978

Master of Science
Mississippi State University
Starkville, Mississippi
1986

Submitted to the Faculty of the
Graduate College of the
Oklahoma State University
in Partial Fulfillment of
the Requirements for
the Degree of
DOCTOR OF PHILOSOPHY
May, 1991

CONCEPTUAL DESIGN AND PERFORMANCE ANALYSIS OF

FREQUENCY-TUNED CAPACITIVE

DISCHARGE REACTORS

Thesis Approved:

Arland H. Johannes

Thesis Adviser

Dean of the Graduate College

ACKNOWLEDGMENTS

I deeply appreciate Dr. Arland H. Johannes, my thesis adviser, for assigning me such an 'original thinker' problem from which I have learned 'the élite of research is insight, not numbers'. I also would like to thank him for his invaluable guidance as reflected in this work.

I express sincere gratitude to my other committee members, Dr. Ruth C. Erbar, Dr. Khaled A. M. Gasem and Dr. John N. Veenstra for their helpful suggestions in the course of this work. If the thesis is a slice of the author's life, it is also an image of his relations with others from whom he has benefited directly or indirectly. Special thanks are reserved for Mr. Charles Baker, laboratory manager, for his assistance during my experimental work.

I am indebted to my parent, brothers and sisters for their concern, love and support. To my children Jerry and Teresa, something more than I can give is due. Through those times when the task seems unending, my wife, Ernestine, is always there to make the road a little smoother. I owe a special debt to her patience and encouragement.

TABLE OF CONTENTS

Chapter Page

LIST OF TABLES

LIST OF FIGURES

Figure Page

LIST OF SYMBOLS

A_s	heat transfer area, cm^2
C	dynamic capacitance of reactor, pf
C_a	capacitance of air gap, pf
C_d	glass capacitance of discharge reactor, pf
C_i	capacitance of the inner tube, pf
C_o	capacitance of the outer tube, pf
C_p	heat capacity of gas, J/g °C
C_t	capacitance of two glass tubes in series, pf
D_1	inner diameter of the inner tube, cm
D_2	outer diameter of the inner tube, cm
D_3	inner diameter of the outer tube, cm
D_4	outer diameter of the outer tube, cm
Dev	deviation
$C_{t\,i}$	capacitance of reactor i, pf
$C_{t\,j}$	capacitance of reactor j, pf
E_i	inception stress, kV/cm
f	frequency, Hz
f_b	breakdown frequency, Hz
$f_{b\,i}$	measured breakdown frequency of reactor i, Hz
$f_{b\,exp}$	measured breakdown frequency, Hz
$f_{b\,cal}$	calculated breakdown frequency, Hz
f_o	starting frequency for specific frequency range of the oscillator, Hz

f_r	frequency at rated voltage, Hz
f_u	uniform breakdown frequency, Hz
h	overall heat transfer coefficient, W/m °C
i	instantaneous discharge current, A
I_s	effective current of reactor, mA
I_{scal}	estimated effective current of reactor, mA
I_{sexp}	measured effective current of reactor, mA
I_p	effective Primary Current, mA
j	instantaneous charging current, A
k	ion mobility, cm^2/Vs
K_d	dielectric constant of barrier
K_g	dielectric constant of gas
L	length of the discharge zone, m
M	mass flow rate, g/s
Mc	MC_p, W/°C
P	pressure, mm Hg
PE	probable error
Q	flow rate of gas, cm^3/min
r	inner conductor radius, cm
R	discharge resistance, ohm
SD	standard deviation
t_o	discharge time, s
T	temperature, °C
T_c	effluent gas temperature of reactor C, °C
T_d	effluent gas temperature of reactor D, °C
T_e	effluent gas temperature, °C
T_o	inlet gas temperature, °C

T_w	wall temperature, °C
U	sinusoidal voltage, V
V_m	instantaneous maximum voltage, V
U_d	instantaneous voltage across glass gap, pf
U_a	instantaneous voltage across air gap, pf
V_a	gas breakdown voltage, V
V_b	breakdown voltage, V
V_b'	modified breakdown voltage, V
V_{bexp}	experimental breakdown voltage, V
V_{bi}	measured breakdown voltage of reactor i, V
V_p	primary voltage, V
V_o	voltage at starting frequency, V
V_r	rate voltage of the transformer, V
V_s	effective secondary voltage, V
W_a	apparent discharge power, W
W_p	primary power, W
W_s	discharge power, W
W_t	total system power input, W
X_a	TCE conversion
X_{apre}	estimated conversion
Z	compressibility factor
w	$2\pi f$, rad/s
δ	relative density (=1 at 76 cm Hg and 25 °C)
μ	constant
α	variable
Φ	variable
β_1	constant

β_2	constant
ϵ	heating factor

CHAPTER I

INTRODUCTION

The use of electrical discharges for chemical synthesis has been investigated intensively in the past. The development and commercial utilization of these methods, however, remain rather limited. The major reasons for such limited development are a low energy yield due to the decomposition of product in the discharge and the complexity of the effect of the actual discharge and operational variables on yields. From a discharge destruction standpoint, however, electrical discharges are very powerful in the decomposition or transformation of chemical compounds. Recently, interest in alternating current discharges as an air purification system has been renewed with emphasis on toxic compounds. Interest stems from environmental concerns (36). Atmospheric pressure silent discharges have received particular attention.

A conventional silent discharge reactor powered by an untuned transformer needs a higher voltage to break down gas molecules and has a lower power factor. This also increases the power loss from the transformer.

Recent work (18, 25, 29) has shown that a more uniform silent glow discharge is formed in a capacitive-inductive

discharge reactor when the transformer is tuned from a power source with an oscillator, since power input varies considerably with frequency. It also appears that this discharge system is very efficient. This system can operate at a lower frequency and at atmospheric pressure. The energy required to generate the discharge can be supplied at a low cost without appreciably increasing the gas temperature. This avoids the use of electrode cooling. Microwave and radiofrequency discharge techniques are by comparison very expensive even though both discharges have been proved to be very efficient for the decomposition of toxic compounds.

In this research, coaxial capacitive discharge reactors are considered since the electrical circuit of a capacitive-inductive discharge reactor is quite complex and difficult to treat theoretically. In addition, present ozone generators utilize capacitive silent discharges. The results of this study can be used to design and optimize operation of ozonizers. Although a large number of investigators have studied discharge chemistry, little work has dealt with the discharge system from an engineering viewpoint. Furthermore, before the technique can be applied on a commercial scale, some basic understanding must be obtained to optimize design, discharge and operational variables on the conversion of reactant and the energy input. The aim of the present investigation is therefore to uncover broad trends that can provide a more conceptual

approach to the design, scale-up and operation of frequency-tuned capacitive discharge reactors.

Trichloroethylene (TCE) was chosen as the toxic agent to evaluate the use of a frequency-tuned discharge reactor system for the treatment of toxic chemical vapors. TCE is one of Volatile Organic Compounds (VOC's) observed in contaminated groundwaters.

The specific objectives of this research are:

1. conduct open-circuit and non-destructive tests to get a better understanding of the system characteristics;
2. conduct breakdown tests using discharge reactors to explore design variables of discharge reactors;
3. develop a power model to provide information on power input and current in the discharge;
4. conduct destructive tests on gaseous TCE to examine the destruction efficiency for various discharge reactors;
5. determine optimum operational criterion for high destruction efficiency and low total system power input;
6. correlate kinetic data to obtain a semi-empirical equation to aid in the design of discharge reactors.

CHAPTER II

LITERATURE REVIEW

Gas Breakdown and Breakdown Voltage

Broadly speaking, electrical breakdown of gases can be described as the transition from an insulation to a conducting state. A gas has a very low conductivity resulting from relatively few electrons and positive and negative ions. This number can be increased many thousand times by heating gas or by irradiation with a radioactive source. However, to reach a conducting state, an electric field must be applied to energize electrons.

When the electron gains more energy than the ionization energy of the gas molecules, then it is capable of ionizing. The new electron together with the primary one repeats the process, and a avalanche of electrons finally occurs. Such generations of rapidly succeeding avalanches can produce a space of slow positive ions in the gap, which favor the ionization conditions for the electrons, and so produce the rapid current growth leading to breakdown. This discharge can be maintained when the applied voltage is larger than a minimum value which is often referred to as the threshold voltage of the self-maintained discharge.

A manifestation of discharge or breakdown is emission of

light, sometimes accompanied by audible noise and by current fluctuations (8). McInally (23) measured light emission and ozone formation in an ozonizer. He found that when the applied voltage was large enough to excite the discharge, the wave form of the current ceased to be sinusoidal. The light output from the ozonizer was found to coincide with the high frequency periods of the ozonizer current. Fuji and Takemura (13) observed that the discharge appeared to have innumerable fine hairs stretching in an ozonizer. None were detected in the declining phase. This behavior was ascribed to the action of the wall charges and the confined breakdown channels. High frequency currents superposed on the fundamental one at the maximum of the current wave form.

The determination of breakdown voltage is the first step in the design of discharge reactors. The major factors in evaluating the breakdown voltage are reviewed.

Works and Dakin (9) investigated the effect of various types of current sources on breakdown. Their results showed that the variation of the alternating current breakdown voltages with increasing pressure correlated closely with positive direct current sparking results. It appeared that the positive half-cycle of an alternating current voltage was more effective in initiating breakdown. It also followed that the space charge produced during the negative half-cycle had a negligible effect on the stabilization phenomenon.

Liao and Plump (5) concluded that the breakdown of air in a non-uniform field was always at a lower voltage than in a uniform field. For moderate non-uniform field electrodes such as coaxial cylinders, the breakdown voltages increased nearly with increasing spacing as in a uniform field. As the spacing between electrodes became comparable to and greater than the diameter of either electrode, the breakdown value increased more slowly with increasing spacing. If the spacing further increased, local breakdown near the smaller electrode, or that producing higher surface gradient, was practically independent of spacing. For very non-uniform field electrodes, such as a wire electrode, the breakdown characteristics were not so regular. Maxfield and Benedict (4) pointed out that for small spacings of the electrodes compared with their radius of curvature, a complete breakdown in the gap occurred.

Liao and Plump (5) also found that the irregular breakdown of very non-uniform fields was attributed to space charges produced by local ionization prior to breakdown in the gap. For some gases, such as nitrogen, only positive-ion space charges could be produced. For air, negative-ion space charges due to oxygen were also present which, even in a relatively small quantity, tended to complicate the breakdown in an air gap. However, for electronegative gases, which could produce a large amount of negative-ion space charges upon ionization, the breakdown characteristics were found to be very irregular.

Peek (2) investigated the corona inception stress of air for a wire in the center of a metal tube and derived the following formula:

$$E_i = 31\delta \left(1 + \frac{0.308}{(\delta r)^{\frac{1}{2}}}\right) \qquad (2.1)$$

where δ = relative density (=1 at 760 mm Hg and 25 °C)

r = radius of cylinder, cm

E_i = inception stress, kV/cm

Further tests showed that the effect of humidity and frequency on the starting point of the visual corona was not obvious. As the visual critical voltage was the voltage at the breakdown of the air, the breakdown gradient was shown to be independent of the spacing. The gradient was not affected by the material or density of the wire. Alston (1) indicated that electrode materials did not affect breakdown at atmospheric pressure, but became important if the pressure was increased sufficiently. Penning (11) indicated that in air at atmospheric pressure, a space-charge breakdown might occur when the electrodes were more than about 1.5 cm apart.

Giao and Jordan (33) concluded that for coaxial cylinder geometry the critical distance, d_o, at corona threshold should satisfy the following expression:

$$(d_o + r)^2 - r^2 = \frac{rkE_i}{f} \qquad (2.2)$$

where r = inner conductor radius, cm

f = frequency, Hz

k = ion mobility, cm^2/Vs

Thornton (44) measured the corona starting gradients in wire-cylinder gaps. A 50 Hz alternating voltage was used in the experiments. The gradients are shown in Table I for a number of gases at 760 mm Hg and 0 °C.

For concentric cylindrical electrodes with two dielectric layers, the total voltage, V_b, necessary to initiate the corona in the gas gap could be expressed as (31)

$$V_b = 0.5 E D_2 K_g \delta \left(\frac{\ln(D_2/D_1)}{K_d} + \frac{\ln(D_3/D_2)}{K_g} + \frac{\ln(D_4/D_3)}{K_d} \right) \quad (2.3)$$

where K_d = dielectric constant of barrier

K_g = dielectric constant of gas

D_1 = inner diameter of the inner tube, cm

D_2 = outer diameter of the inner tube, cm

D_3 = inner diameter of the outer tube, cm

D_4 = outer diameter of the outer tube, cm

Manley (34) presents a comparison of the breakdown voltage of ozonizers with that of parallel plates and found that the discharge occurred at a lower voltage. His explanation was that the glass surface was covered with ions. This was supported by Honda and Naito (42) that the electrical charges produced by breakdown accumulated on the glass surfaces and reduced the field intensity of the gap.

TABLE I

CORONA STARTING GRADIENT FOR VARIOUS GASES

Gas	Corona Starting Gradient Voltage (kV/cm)
Air	35.5
H_2	15.5
He	4.0
O_2	29.1
N_2	38.0
Cl_2	85.0
CO	45.5
CO_2	26.2
NH_3	56.7
N_2O	55.3
H_2S	52.1
SO_2	67.2
CS_2	64.2
CH_4	22.3
CH_2Cl_2	126.0
$CHCl_3$	162.0
CCl_4	204.0
CH_3Cl	45.6
CH_3I	75.0
CH_3Br	97.0

Types of Electrical Discharge

Electrical discharges can be divided into three classifications: corona, glow and arc discharge. As shown in Figure 1, the various types of discharge can be characterized by the relation of current density and ratio of pressure to electric field strength (7). Although this general way of classifying electrical discharges is not absolute, it is useful as a first step in understanding the interrelationships and differences among the various types. The discharges mentioned are self-sustained and can be maintained without the support of an external ionizing agency. In other words, excitation and thermal ionization of an isolated gas at a given reduced pressure can be obtained by application of an external source of energy. Corona and glow discharge are sometimes called silent discharges.

Corona discharge

A corona discharge results from the incomplete breakdown of a gas and is soft and bluish (27). Dibelius et al. (31) described a corona discharge and characterized it as a low current carrying column with a voltage gradient on the order of the electrical breakdown strength of the gas. The gas is only slightly ionized and a soft bluish glow is observed. In a corona discharge at atmospheric pressure the electrons have an energy distribution from zero to somewhat

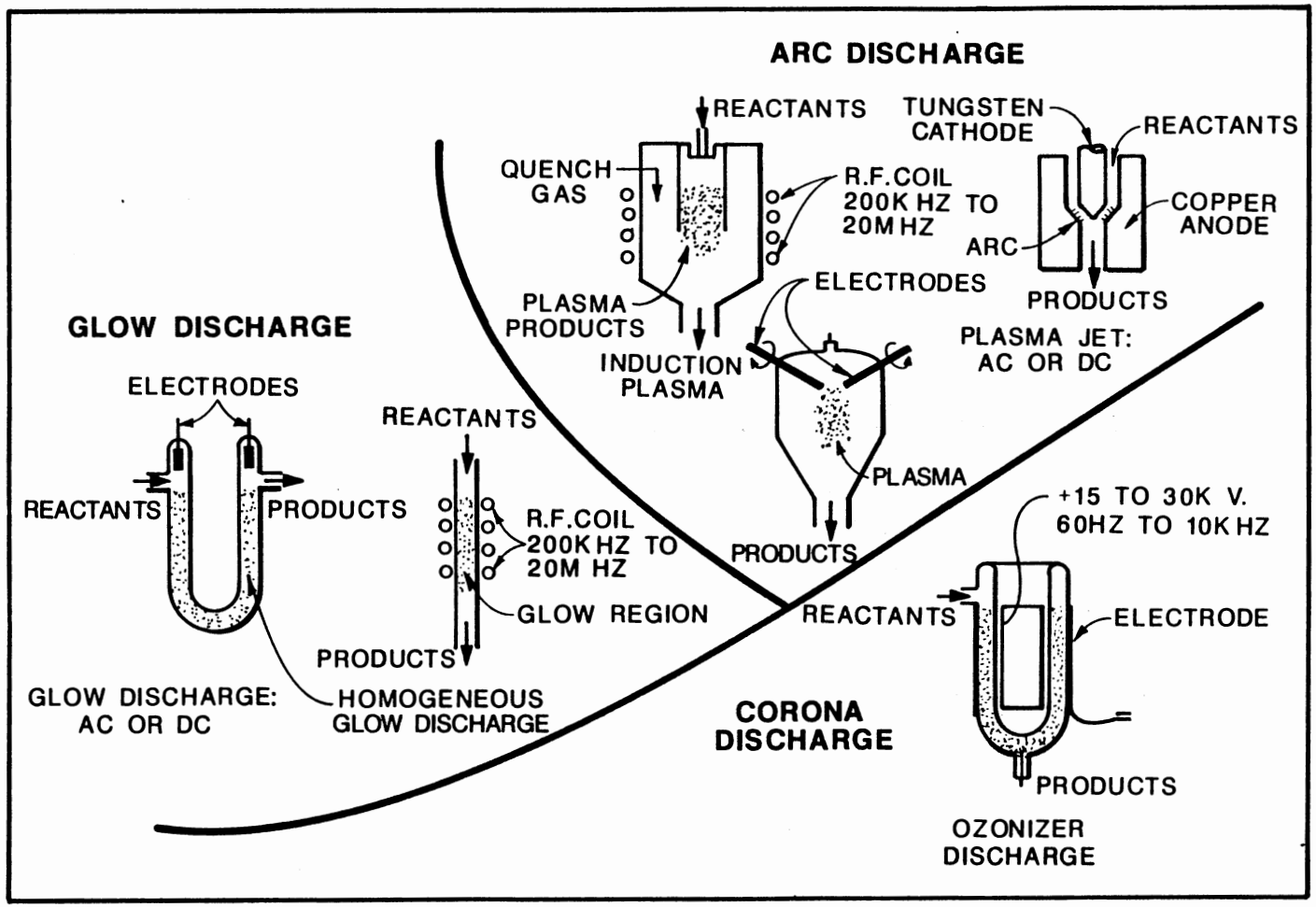

Figure 1. Plasma Operating Regions.

above the ionization potential of the gas in which the corona occurs. Since the electron energy necessary to produce excited states and free radicals is lower than that necessary to produce a positive ion and an electron, there are many more free radicals produced than positive ions

Giao and Jordan (33) concluded that three conditions must be satisfied to initiate a corona discharge: (1) field intensity must be high enough; (2) field nonuniformity must be high enough; (3) free electrons must be available in the overstressed field regions.

Glow Discharge

A glow discharge is generated when sufficient voltage is applied to two electrodes with a gas gap at a much lower pressure. The discharge is maintained by electrons produced at the cathode by bombardment of particles and light quanta from the gas. The luminosity is probable due to excitation of molecules by positive collision (23). Glows are generally limited to low degrees of ionization and operate most readily at low gas density (12). Glow discharges are nonequilibrium gas discharges and are largely or completely self-sustained (41). Klyarfel'd (12) states that a self-sustaining glow discharge can exist before changing into an arc at comparatively large current (> 1 A) and at voltages of the order of tens of kilovolts between the electrodes. The change from glow to arc discharge depends on a number of factors, such as the presence of a high

local field and occlusions in electrodes with a low-work function.

When glow discharge is generated by an alternating current instead of a direct current, each electrode alternately acts as the cathode. Chapman (3) indicated that conventional frequency was found not to be very effective because the time during which the insulator charged up was much less than half the period of the applied frequency. Therefore most of the time the discharge would be off.

The development of efficient high-frequency power sources has resulted in the wide use of electrodeless radiofrequency and microwave discharges and decreased interest in discharges between electrodes. Typically, a glass tube is placed in a solenoid through which an alternating current of high frequency passes. Corona discharges are produced by the discharge of a condenser via a spark gap (35). In most respects, high frequency discharge resembles glow discharge, except that it operates only at high frequency.

Arc Discharge

Arc discharge is characterized by exceptionally low cathode fall of potential and high current density (15). In other words, the discharge is characterized by a voltage necessary for maintaining the discharge which is less than the minimum sparking voltage (4). The arc has a high temperature and the current is carried almost entirely by

mobile electrons of negligible mass. The free electron temperature is relatively close to that of the discharge gas. Arc discharge is also called hot discharge.

Chemical Reactions in Electrical Discharges

Chemical reactions in silent discharges are reviewed briefly to understand the possible reactions for evaluating the discharge as an alternate method for toxic vapor disposal. This review also covers the effects of discharge and operational variables.

There are major differences between thermal activation and electrical activation. Thomas et al. (15) states that in thermal activation, energy would be concentrated in a given bond and causes chemical reaction. In electronic activation, the collision with an electron produces activation directly without adding to the translational or rotational energy of the molecule. Lunt and Emeleus (32) indicates that it is not necessary for a molecule to become ionized to react chemically in the discharge. At atmospheric pressure the electron can be regarded as the primary activating agent (15).

Discharge reactions are highly sensitive to the chemistry and geometry of the reaction system as well as to electricity. Clothiaux et al. (19) investigated the oxidation of phosphorofluric acid methyl-1, 2,2-trimethyl-propyl ester (PFA) vapor in air passed through a silent discharge. A coaxial discharge reactor with a coil wound on

the outer tube was powered by an autotransformer. The discharge was initiated in air, then switched to the flowing PFA-air mixture. The frequency was held constant at 60 Hz. The decomposition efficiencies of PFA are given in Table II.

The decomposition of gas phase formaldehyde by plasma discharge was investigated by Neely et al. (26). Oxygen at atmospheric pressure was used as the carrier. The experiment was conducted at a flow rate of 400 ml/min. Direct oxidation of formaldehyde by ozone at this concentration and contact time was shown to be insignificant. However, reaction with triplet-p oxygen could easily occur. The decomposition of the formaldehyde was as high as 40 %.

Fraser and Sheinson (21) examined oxidation of trace levels of hydrogen cyanide in an ozonizer discharge operating at atmospheric pressure and at 60 Hz. The

TABLE II

DECOMPOSITION EFFICIENCY OF PFA

Flow Rate (ml/min)	PFA Concentration (gm/l)	Decomposition Efficiency (%)
100	1900	> 99.6
200	1850	> 99.8
800	1950	81.5

Source: reference (19)

discharge current was 1.3-1.5 mA at 19.6 kV and the residence time was less than 10 seconds. The principal products observed from the discharge of hydrogen cyanide with added oxygen were CO, CO_2, N_2, and unreacted HCN.

Fraser et al. (14) investigated the destruction efficiency of dimethyl methyl-phosphonate (DDM) in a helium/air discharge. A capacitive ozonizer discharge was powered by a 16 kV, 50 Hz transformer. The reactor had a 35 cm effective length. The current was 1 mA and no detectable temperature rise was observed. The results showed that a higher DDM concentration decreased the destruction efficiency and oxygen had a slightly enhancing effect on DDM destruction.

Sulfur-containing hydrocarbons are common pollutants and often noxious. Discharge destruction of dimethylsulfide (DMS) has been studied by Davis and Tevault (24). In the absence of oxygen, DMS decomposition in N_2 produced NH_3, HCN, CS_2, and a trace of H_2S. As oxygen was added, the above products decreased in favor of the oxidation products CO, CO_2, H_2O, NO, N_2O, NO_2, SO_2, and O_3. DMS was completely destroyed in the discharges.

Air or oxygen in a silent discharge has long been studied in the formation of ozone. According to My and Sahgal (28), the performance of the ozonizer is adversely affected by the presence of water vapor. The concentration of ozone decreases drastically by varying the relative humidity from 40 % to 50 %. Inoue (13) reported that ozone

formation was completely inhibited by adding hydrocarbons to air. Further tests were carried out by Inoue and Sugino (13) to clarify the inhibiting action of hydrocarbons. Three hydrocarbons were used: n-hexane, cyclohexane, and n-heptane. No marked difference in inhibiting action was observed on changing the type of hydrocarbons.

McEachron (43) found that in air the corona discharge favored the product ozone, while sparks tended to produce oxides of nitrogen. Increase in current raised the yield of both ozone and oxides of nitrogen to a maximum and the yield of ozone tended to be constant at the higher rates. McInally (23) observed that for a given gap the rate of ozone formation was roughly proportional to the current. When the same current was used for oxygen and air, the voltage for oxygen was 50 % less than for air and the rate of ozone production for air was approximately 40 % of that for oxygen.

Tevault et al. (18) studied NO_x production in a silent discharge as a function of frequency, power, and humidity. Power was applied to the capacitive-inductive discharge reactor by a variable frequency power supply coupled to a high voltage transformer. Humid air was used at a flow rate of 1 l/min. The results showed that at a fixed primary voltage NO_x levels went through a maximum as frequency increased. The frequeny where the peak NO_x level occurred shifted to a lower one at a higher primary voltage. NO_x in the effluent was suppressed and undetected as air was

humidified to 100 %. Moore et al. (22) conducted an investigation on the decomposition of cyanide compounds in a silent discharge. The destruction of methyl cyanide was not affected by humidifying the air streams.

Sheinson (25) examined the effect of discharge voltage on the conversion of methane in a capacitive-inductive helium discharge. Methane destruction increased as discharge voltage increased and the maximum efficiency was about 90 %. Piatt (29) used the same types of reactors. Methane destruction in O_2/He discharge was clearly maximum at an optimum frequency but was relatively low (< 35 %). Increases in flow rate decreased the efficiency. Apparent power inputs to the discharge reactors were measured and used to develop a kinetic model which resulted in erroneous analysis.

Hosselft (30) attempted to improve the efficiency of an ozonizer by analyzing the effect of the discharge circuit. Experiments showed that efficiencies increased up to 28.7 % compared with conventional ozonizers with efficiencies from 4 to 8 %. Moore and Birmingham (20) studied the destruction of cyanogen chloride in a packed alternating current plasma reactor. Flow rates of air containing cyanogen chloride were in the range of 1 to 5 CFM. Destruction efficiencies of 99 % or greater were achieved as shown in Table III. It was suggested that a threshold power level existed for the reactor, below which changes in applied power had a marked

TABLE III

DECOMPOSITION OF CYANOGEN CHLORIDE

Flow Rate (ft^3/min)	Power (kW)	Residence Time (s)	Decomposition Efficiency (%)
1.0	1.0	10.6	> 99.6
2.59	1.0	7.3	> 99.6
5.00	1.3	2.3	> 99.8

Source: reference (20)

influence on destruction efficiency. From gas analysis, the products were CO_2 and a solid precipitate mixture containing N and Cl atoms. Cyanic acid was observed as a minor reaction product at low ppm concentrations.

Lind and Glockler (38) examined reactions of gaseous hydrocarbons in semi-corona discharges at atmospheric pressure. Eleven semi-corona tubes of pyrex glass (rod-type ozonizer) were connected in series as to gas flow but in parallel as to electrical flow. The discharge took place across an annular space of 0.5 inch with an AC voltage of 18,000. In series gas flow through a number of discharge tubes, the amount of liquid condensate increased in successive tubes. Maximum liquid yield was attained in an intermediate tube as the rate of flow was low enough to deplete the reactant. Since the type of discharge employed might influence the reaction, Lind and Glockler (39) also

considered all-glass ozonizers to examine chemical reaction of butane in the discharge. Twelve ozonizers were connected in parallel. A secondary voltage of 20,000 volts resulted from a transformer using a primary current of about 12 A and a primary voltage of about 110 V. The tubes were arranged in parallel as to gas flow. Butane flow rate was 3.46 l/hr. Result showed that 15.37 % by weight of the butane was converted into condensate.

CHAPTER III

EXPERIMENTAL APPARATUS AND PROCEDURE

Apparatus

A schematic of the discharge system is shown in Figure 2. The system is designed to run at about atmospheric pressure and at room temperature. Three main parts of the system are: power source, voltage transformer and discharge reactor. The discharge reactors were fabricated using pyrex glass and consist of coaxial glass tubes similar to an ozonizer (Figure 3). The inside of the inner tube and the outside of the outer tube were coated with inorganic silver. The pyrex glass is Corning code 7740 chemical-resistant borosilicate glass with a dielectric constant of 4.6 at 25 °C (6). To change the gap distance, several reactors with different tube diameters were used. Geometries of the reactors are given in Table IV. The length of all the reactors is 37.5 cm with a 20.2 cm long effective discharge zone.

The electrical system is an impedance-changing circuit. Power is supplied through a voltage transformer to a discharge reactor using a power amplifier (California Instruments Model 161T with a plug-in oscillator). In such a system, the secondary voltage of the transformer can be

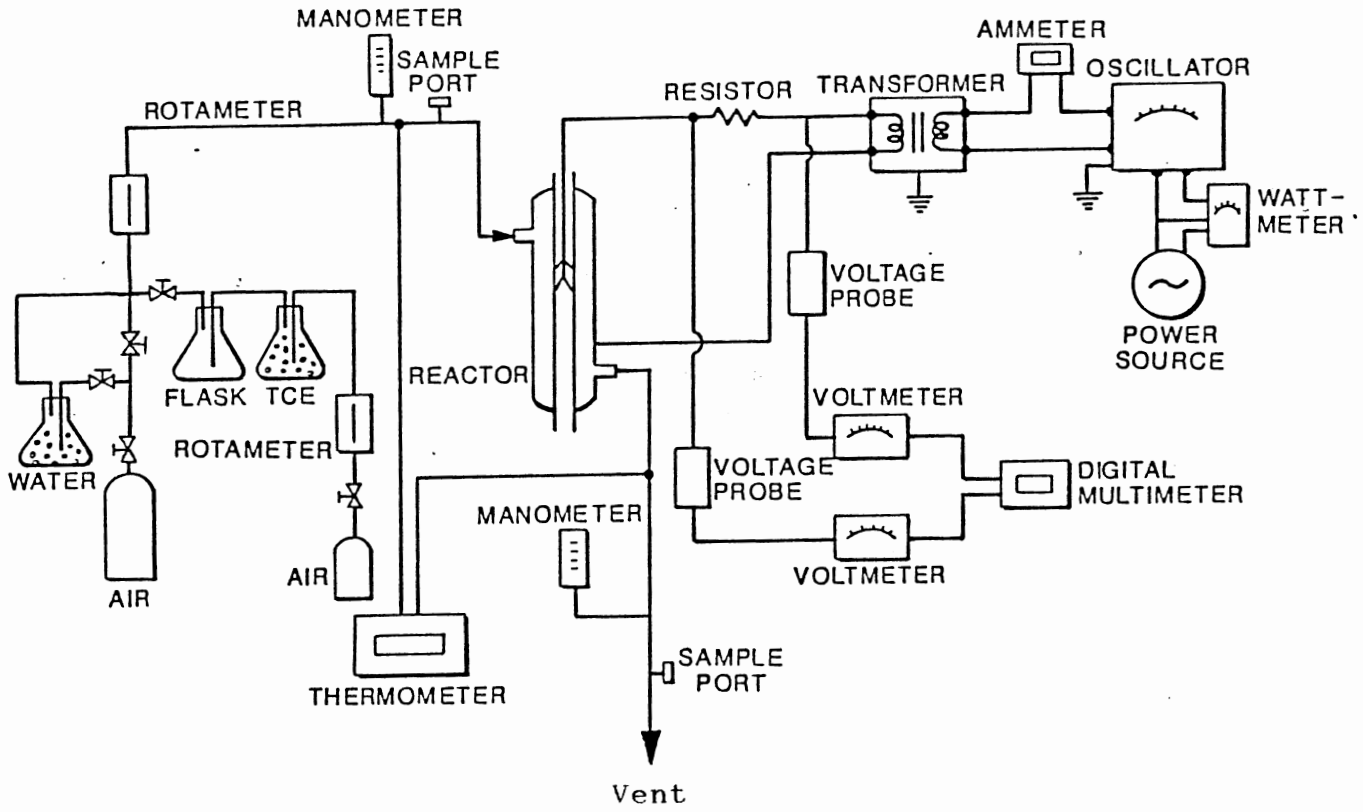

Figure 2. Schematic of Discharge Reactor System.

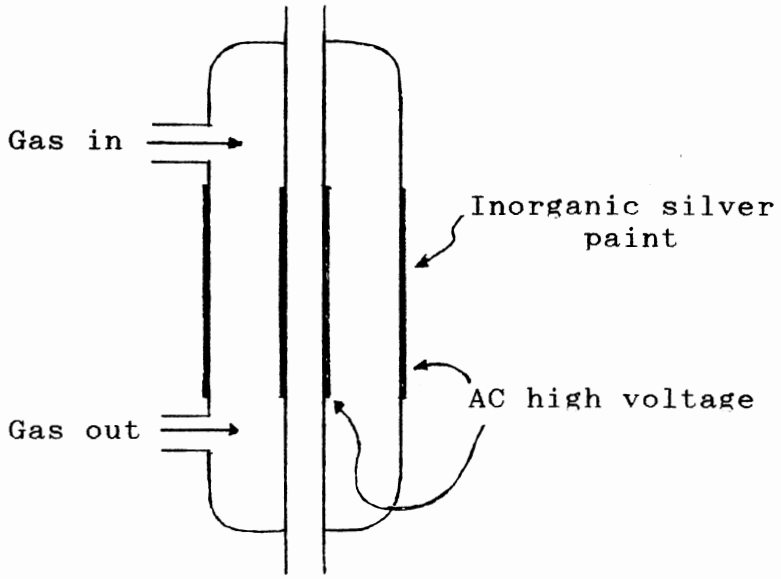

Figure 3. Capacitive Discharge Reactor

TABLE IV

DETAILED GEOMETRIES OF THE DISCHARGE REACTORS

Reactor	Diameter				Gap	Diameter Ratio
	Inner Tube		Outer Tube			
	D_1 (cm)	D_2 (cm)	D_3 (cm)	D_4 (cm)	(cm)	(D_3/D_2)
A	1.27	1.50	2.19	2.50	0.345	1.460
B	1.55	1.80	2.19	2.50	0.195	1.217
C	1.55	1.80	2.64	3.00	0.420	1.467
D	1.77	2.00	2.64	3.00	0.320	1.320

tuned by an oscillator. The oscillator is a type of Wien-bridge and produces a nearly perfect sine wave with less than 1 % distortion from 20 to 200 Hz. The output range of the oscillator is from 40 to 5,000 Hz. The iron-core transformer (Jefferson Electric Co.) which was used is a luminous tube, high power factor transformer with a midpoint grounded secondary. The output from one winding is positive-going with respect to ground, while the output from the other is negative-going, and vice versa. The total output voltage from the windings is the sum of the outputs from each. The capacitor (rated at 600 V) in the primary of the transformer was disconnected due to overload of the power amplifier. The rating of the transformer is 15 kV and 60 mA for a primary voltage of 120 at 60 Hz.

The power amplifier is a solid state, high performance, low distortion power source that provides up to 160 VA output. The normal input of the power amplifier, at 160 VA, is between 360 and 550 W, depending on line and load conditions. The power amplifier can automatically adjust to changes in load. Under a no load condition, the amplifier draws less than 60 W at mid-line voltage (tested by a connecting 1 kV wattmeter and a 1 KV Variac in series with the alternating current line).

For the measurement of the secondary voltage, Simpson AC high voltage probes were used in conjunction with Simpson 620 multimeters (with the outputs fed to a digital multimeter to measure the voltage across the reactor).

Current in the discharge was measured by the voltage drop across a resistor of 14650 ohm in series with the circuit. The primary current and total system power input were measured by Simpson autoranging multimeter and GE wattmeter, respectively. Gas flow rate to the reactor was measured using a calibrated rotameter. Gas analysis was performed on a gas chromatograph (Perkin-Elmer Sigma 3B) with a flame ionization detector. The output signal was evaluated using an integrator (Perkin-Elmer Sigma 15). Gas temperature and reactor pressure were measured by a type R thermocouple and water manometers which were placed 4 cm away from the entrance and exit of the discharge reactor.

Procedure

Air was used as the carrier for simulating environmental conditions which might be contaminanted with toxic agents. Unless otherwise stated, gas flowed into the top port of the reactor and exited from the bottom. After the reactor, the gas effluent was vented to a hood.

Transformer Open-circuit Tests

The influence of frequency on the power loss, voltage and current of the transformer can be evaluated by means of open-circuit tests. Through these tests, the operating frequency range of the system also can be determined.

The experimental procedures are shown below:

1. The secondary of the transformer was disconnected.

2. The primary voltage was set.
3. The frequency was varied from 60 Hz until the rated voltage of the transformer was reached. The electrical data were collected.
4. The step (3) was repeated for the different primary voltages.

When the primary power was required to be measured, the wattmeter was placed between power source and transformer. Owing to the limitation of the effective frequency, power data were collected only from 60 to 130 Hz.

Breakdown Tests

Breakdown tests for each reactor and the two reactors in parallel with series gas flow were performed in order to provide some insight on the design problems of discharge reactors. The measured breakdown voltage is the total applied voltage to the discharge reactor. It is different from the gas breakdown voltage, which is the voltage in the gas gap.

The following are the experimental procedures to measure breakdown voltage and frequency:

1. The supply power was turned on and the primary voltage was set. The dry air was passed through the reactor at a specific flow rate.
2. The secondary voltage of the transformer was quickly raised to about 90 % of the expected breakdown value by varing frequency.

3. Small adjustments were made until the discharge occurred. It could be identified because of an audiable noise made. The voltage and frequency were then recorded.
4. The same procedures were repeated for the different primary voltages and reactors.

Non-destructive Tests

To understand the electrical characteristics of this system, non-destructive tests (dry air discharges) were undertaken under unsteady and steady state conditions. For unsteady state tests, the measurements were instantaneous. This was observed for the case where discharge took place. The readings depended on the elapsed time after the applied frequency was tuned.

The unsteady state, experimental procedures are detailed as follows:

1. The start-up procedure was the same as shown in the step (1) of the breakdown tests.
2. Data were taken by increasing the frequency from 60 to 1,000 Hz with a 100 Hz increment. When the voltage approached the breakdown voltage, the frequency was tuned smoothly until the discharge took place.
3. With the same reactor, the step (2) was repeated for the different primary voltages.
4. Following the steps (2) and (3), the tests were continued for another reactor

Steady state tests were performed only for a specific

primary voltage. The procedures were completely the same as the unsteady state tests except that after gas breakdown occurred, at least 30 min. was allowed to pass to establish steady state conditions.

Destructive Tests

Destructive tests were conducted using both dry air and wet air under steady state conditions. The TCE-rich dry air was prepared by passing dry air over the surface of pure liquid TCE. This stream was mixed with another dry air stream or wet air stream in a T-connection to obtain an approximately constant concentration of TCE in the feed gas. Dry air in the presence of gaseous TCE was first considered to investigate the effect of frequency on destruction efficiencies of TCE in each discharge reactor. The effect of concentration was conducted only for specific reactor.

Destructive tests in wet air discharges were first performed with a single reactor and specific two reactors in parallell to examine the effects of concentration and flow rate. The effect of the flow direction of the gas was tested only for the two reactors in parallel. In these tests, except in a test where the effects of frequency and concentration were examined for specific two reactors in parallel. The tests were conducted at a frequency, resulting in a more uniform breakdown.

Gas samples were extracted from the sample ports of the gas influent and effluent lines. A gas sampling valve was

employed to inject a 1 ml sample into the GC. Only the TCE peak was measured and TCE concentration was determined by comparison with a standard.

The experimental procedures are generalized and summaried as follows:

1. The start-up procedure was the same as shown in the step (1) of the breakdown tests.
2. The frequency was tuned to generate the discharge. At least 30 min. was allowed to pass to stabilize the discharge.
3. Dry air or wet air stream mixed with the TCE-rich dry air was then passed through the reactor.
4. Gas examples were collected to check TCE concentration.
5. When the readings were stable and the specified, TCE concentration in the feed was reached, the feed and gas product samples were collected and analyzed by the GC. The concentration and electrical data were recorded.
6. When the effects of frequency, concentration and flow rate were examined, the steps (4) and (5) were repeated during the tests.

CHAPTER IV

MODEL DEVELOPMENT

A frequency-tuned discharge system is a double tuned impedance-changing circuit. The effects of the applied frequency and voltage on the behavior of the discharge system deserve particular attention. As the literature survey in chapter II has shown, the interaction of operational parameters of the discharge system and the chemical reactions in the discharge is complex so that detailed electrical circuit simulation and kinetic modeling are extremely difficult. The development of experimentally-based models was therefore the approach taken for model development.

Electrical Behavior of System Devices

Voltage Transformer

Generally, a transformer consists of two coils of wire that are magnetically coupled to each other. The transfer of energy from the primary to the secondary winding of the transformer depends on the magnetic lines of force around the primary winding cutting the turns of the secondary winding. Copper and iron-core are the major places of power loss in a transformer. The copper loss is

due to the resistance of the wires making up the turns of the windings. The iron loss can be divided into two parts. Since the flux in a transformer core is alternating, power is required for the continual reversal of the elementary magnets of which the iron is composed. This is called the hysteresis loss. The hysteresis loss in a transformer varies directly with the frequency. The other iron loss is due to an electrical current that is induced in the core by the changing magnetic fields of the coils wound on it. This induced current is called the eddy current which results in the so-called eddy loss. Total iron loss is proportional to the square of the induced voltage.

Typically, when the load on a transformer increases (its impedance is reduced), more current is drawn from the source through the secondary circuit. This shows that the transformer automatically adjusts itself to changes in load.

Capacitive Discharge Reactor

The behavior of a capacitive discharge reactor operating with alternating current can be determined by the breakdown voltage (threshold voltage) of the gas gap. When the applied voltage is lower than the breakdown voltage of the gas gap, no discharge occurs. The discharge reactor can be viewed as a perfect capacitor. The total reactor capacitance consists of a combination of two glass capacitances and a gas gap capacitance connected in series.

The charging current is proportional to the applied voltage, frequency, and reactor capacitance. The variation of the current is sinusoidal and leads the voltage by 90° provided that a sinusoidal voltage is applied.

Discharge takes place as soon as the applied voltage reaches the breakdown voltage. During each cycle of the alternating current there are discharge periods and alternating two dark periods. The discharge periods correspond to the two high peaks in the current wave. The ending of the discharge coincides with the maximum of the applied voltage, but the time of its beginning will depend on the interior surface charges accumulated during previous discharges. The resulting impedance of the discharge reactor therefore is no longer constant for the time interval of a cycle. Thus the equivalent circuit is better approximated by a capacitor connected in series with a resistor of varying resistance.

Breakdown Model

The transformer plays an important role in the operation of discharge reactors. This is true since for a given applied voltage, the transformer is a matching device and by changing the applied frequency a maximum secondary or energy transfer results.

Generally, the voltage of a transformer is proportional to the frequency. However, owing to transformer losses, the proportionality between primary and secondary voltages does

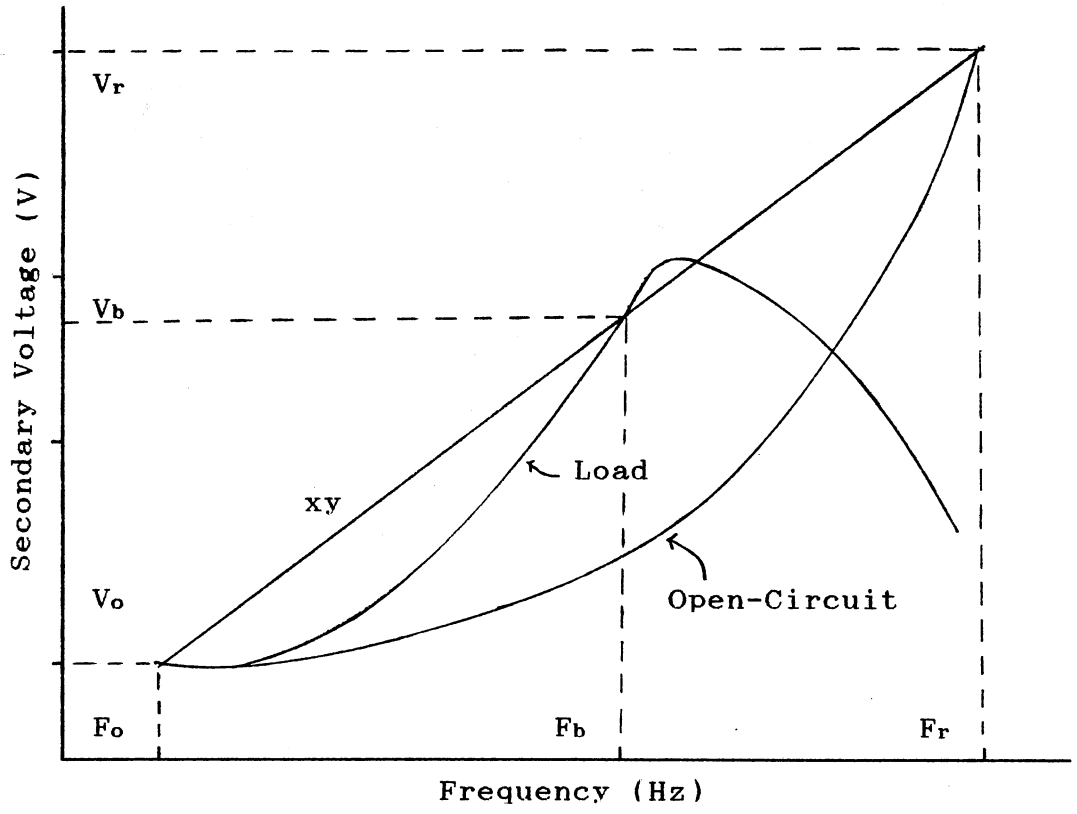

Figure 4. Relation of Secondary Voltage and Frequency of Voltage Transformer.

not hold true. As shown in Figure 4, the shape of the open-circuit curve is found to be concave upward and the transformer is in resonance with the secondary. This resonance occurs only when a transformer with a high secondary load resistance (high open-circuit impedance) is fed from a low-resistance source.

Before the start of a glow, a discharge reactor can be treated as a perfect capacitor (no dielectric loss), with power being drawn from the transformer. The impedance of the capacitor decreases as the frequency increases. This results in more current being available to the transformer and generates a higher voltage. When the voltage increases to a value close to the breakdown voltage, the power withdrawn from the power source almost overcomes the saturated transformer loss.

At this point, the breakdown voltages may lie in a straight line, xy, obtained by connecting the starting and rated voltages of the transformer under open-circuit conditions for a resonance frequency range of the oscillator. The frequency corresponding to the breakdown voltage is called the breakdown frequency. This behavior is expected if the capacitance of the reactor is small so that the starting voltage of the reactor is close to the specific open-circuit voltage. Using open-circuit data, a general equation was formulated to predict the breakdown frequency and is expressed as

$$f = f_o + (V_b - V_o)\frac{(f_r - f_o)}{(V_r - V_o)} \qquad (4.1)$$

where f_o = starting frequency for a resonance frequency range of the oscillator, Hz

V_b = breakdown voltage, V

V_o = voltage at starting frequency, V

V_r = rated voltage of transformer, V

f_r = frequency at rated voltage, Hz

From equations (2.2) and (2.3), the breakdown voltage also can be expressed in terms of frequency and ion mobility

$$V_b = \frac{\mu f}{k} \qquad (4.2)$$

where μ is constant for a particular reactor. It must be noted that the ion mobility is a function of P/E. Equation (4.2) shows that the breakdown voltage is not linear with breakdown frequency. In spite of these effects, the static breakdown voltage can be approximated by substituting the value of Ei from equation (2.1) in equation (2.3), there results:

$$V_b = 10.96 D_2 \delta \left(1 + \frac{0.308}{(\delta D_2)^{\frac{1}{2}}}\right)\left(\frac{\ln(D_2/D_1)}{K_g} + \frac{\ln(D_3/D_2)}{K_a} + \frac{\ln(D_4/D_3)}{K_g}\right), Kv \qquad (4.3)$$

where k_g = dielectric constant of glass

K_a = dielectric constant of air

This is the equation for the effective value of the voltage required to start visual corona. The relative air density , δ, for any temperature and pressure can be expressed as

$$\delta = \frac{3.921PZ}{273 + T} \qquad (4.4)$$

where P = pressure, cm Hg

Z = compressibility factor

T = temperature, °C

Power Model

Discharge power is a major parameter in understanding the overall performance of this reactor system. However, the experimental technique is limited to measure current and voltage of the circuit. In such cases, a power model may be a useful means for approximately predicting the power input.

The electrical circuit of an ozonizer is generally treated as pure capacitive reactance. The capacitance in the circuit is not variable. Some investigators (13, 34, 40) have used this circuit to develop a mathematical theory of an ozonizer. However, no experimental data support the validity of these theories for air discharges.

Faes (40) presented a detailed theory for a wire-type ozonizer. In the current research, discharge reactors consist of two coaxial glass tubes. The midpoint grounded transformer is quite different from conventional one-

end grounded transformers. On the basis of Faes' theory, a power model is developed to specially fit to the present discharge reactor system by including these effects.

In deriving the model equations, the following assumptions are made:

1. The breakdown voltage in the gas gap is assumed to be constant during the time interval of the discharge;
2. The capacitance of the discharge reactor is constant.

The equivalent circuit is shown in Figure 5. C_a is capacitance of the air gap and $C_d = C_o C_i/(C_o + C_i)$, where C_i and C_o are the capacitance of the inner tube and outer tube, respectively. The capacitances of glass tubes and air gap can be calculated as (2)

$$C_i = \frac{55.63\ k_g L}{\ln(D_2/D_1)} \qquad C_o = \frac{55.63\ k_g L}{\ln(D_4/D_3)} \qquad C_a = \frac{55.63 k_a L}{\ln(D_3/D_2)}, \text{ pf} \qquad (4.5)$$

where L = length of the discharge zone, m.

The applied voltage can be described by $U = V_m \sin wt$.

According to Kirchhoff's voltage law, the instantaneous voltage across C_d and C_a can be expressed as

$$U_a = \frac{C_d}{C_d + C_a} V_m \sin wt \qquad U_d = \frac{C_a}{C_d + C_a} V_m \sin wt \qquad (4.6)$$

where U_a = instantaneous voltage across C_a, V

U_b = instantaneous voltage across C_b, V

V_m = amplitude of the alternating current, V

$w = 2\pi f$, rad/s

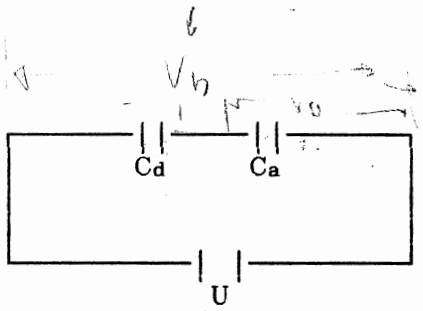

Figure 5 The Equivalent Capacitive Circuit of a Discharge Reactor.

The instantaneous charging current, j, is described by

$$j = C_d \frac{dU_d}{dt} = \frac{C_a C_d}{C_a + C_d} w V_m \cos wt \qquad (4.7)$$

As soon as the voltage across C_a reaches the value of gas breakdown, a discharge occurs. The instantaneous discharge current, i, is

$$i = C_d \frac{d(U - V_a)}{dt} C_d V_m w \cos wt \qquad (4.8)$$

The effective current drawn by the discharge reactor consists of charging and discharge currents and can be calculated as (40)

$$I_s = \{ \frac{w}{\pi} (\int_{t_o}^{\pi/2w} i^2 dt + \int_{\pi/2w}^{\pi/w+t_o} j^2 dt) \}^{\frac{1}{2}}$$

$$= \frac{1}{\pi^{\frac{1}{2}}} C_d w V_m \left[\left(\frac{\pi}{4} - \alpha + \left(\frac{C_a}{C_a + C_d} \right)^2 \left(\frac{\pi}{4} + \alpha \right) \right] \right]^{\frac{1}{2}} \qquad (4.9)$$

where $\alpha = \frac{wt_o}{2} + \frac{\sin wt_o}{4}$

t_o = discharge time, s

Note that the effective value of current leads to an average (not effective) value of power. The power input in the discharge is determined by the following equation (40)

$$W_s = \frac{w}{\pi} \int_{t_o}^{\pi/2w} i V_a \, dt$$

$$= \frac{w}{\pi} V_a V_m C_d (1 - \sin wt_o) \qquad (4.10)$$

Since the available discharge voltage is symmetric with respect to the breakdown voltage, the discharge time can be obtained by

$$V_m - V_a \left(1 + \frac{C_a}{C_d}\right) = V_a \left(1 + \frac{C_a}{C_d}\right) - V_m \sin wt_o \qquad (4.11)$$

From equations (4.10) and (4.11), the power input can be rewritten as

$$W_s = 4 f V_a V_m C_d \left(1 - \frac{V_a}{V_s} \left(1 + \frac{C_a}{C_d}\right)\right) \qquad (4.12)$$

Dielectric losses resulting from polarization effect are

very low and can be neglected. By considering the relative effect of frequency, the breakdown voltage can be approximated as

$$V_b' = V_b \left(\frac{f_u}{f}\right)^{1/8} \qquad (4.13)$$

where V_b' = modified breakdown voltage, V

f_u = uniform breakdown frequency, Hz

Since the gas heating in the discharge occurs, the initial breakdown voltage of the gas gap is reduced. Assume that the reactor has a plug flow. The actual breakdown voltage can be evaluated at the average gas temperature. The effluent gas temperature, T_e, is obtained by an energy balance, as

$$T_e = \beta_1 + (T_o - \beta_1) \exp(-\beta_2 L) \qquad (4.14)$$

where $\beta_1 = \dfrac{\pi h(D_1 + D_4)}{Mc}$

$$\beta_2 = T_w + \frac{\epsilon W_s}{hA_s}$$

T_o = inlet gas temperature, °C

T_w = wall temperature, °C

A_s = heat transfer area, cm^2

h = overal heat transfer coefficient, $w/cm^2\,°C$

$Mc = MC_p$, w/°C

M = mass flow rate, g/s

C_p = heat capacity of the gas, J/g°C

ϵ = heating factor

Dynamic Model

Hydrocarbons in a discharge has been shown to conduct more current (15). Masuda and Kiss (37) showed that dynamic capacitance of an ozonizer was much higher than its static capacitance. In order to evaluate dynamic capacitance and resistance in discharge reactors, a dynamic model must be developed. The circuit used for the dynamic model has a dynamic capacitance in series with a finite resistance. The model is developed on the basis of the equivalent circuit as shown in Figure 6.

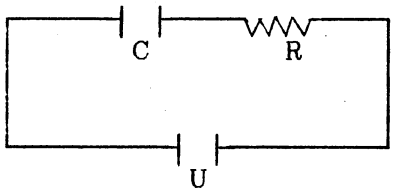

Figure 6 The Equivalent Dynamic Circuit of a Discharge Reactor.

C and R are dynamic capacitance and resistance of the reactor, respectively. The apparent and true powers are expressed as

discharge power

$$W_s = I_s^2 R \qquad (4.15)$$

$$W_a = I_s^2 (R^2 + (1/2\pi fC)^2)^{\frac{1}{2}} \qquad (4.16)$$

From equations (4.15) and (4.16), the dynamic capacitance is

$$C = \frac{I_s^2}{2\pi f (W_a^2 - W_s^2)^{\frac{1}{2}}} \qquad (4.17)$$

CHAPTER VII

RESULTS AND DISCUSSIONS

Open-Circuit Characteristics of the Transformer

Figures 7 and 8 show secondary voltage and primary current as a function of frequency under open-circuit conditions, respectively. The primary current is found to reach a minimum and then increase with increased frequency while the secondary voltage always increases as frequency increases. With an open-circuit, the primary current is very small. This indicates the effect of very high inductance and some resistance. The no-load current is used to overcome core losses and to produce an emf to force the flux through the core. Since the flux which produces the counter emf in the primary does not all link with the secondary, the nonlinking flux causes voltage loss. As expected, the primary current increases more rapidly than the secondary voltage. The decreasing current in Figure 8 is due to a great decrease in inductance.

At higher frequency, the capacitive effect of a transformer can be important. Higher frequency leads to higher hysterises loss. It was observed that the no-load power factor of the transformer increases as frequency increases. Since the measurements were made below 130 Hz,

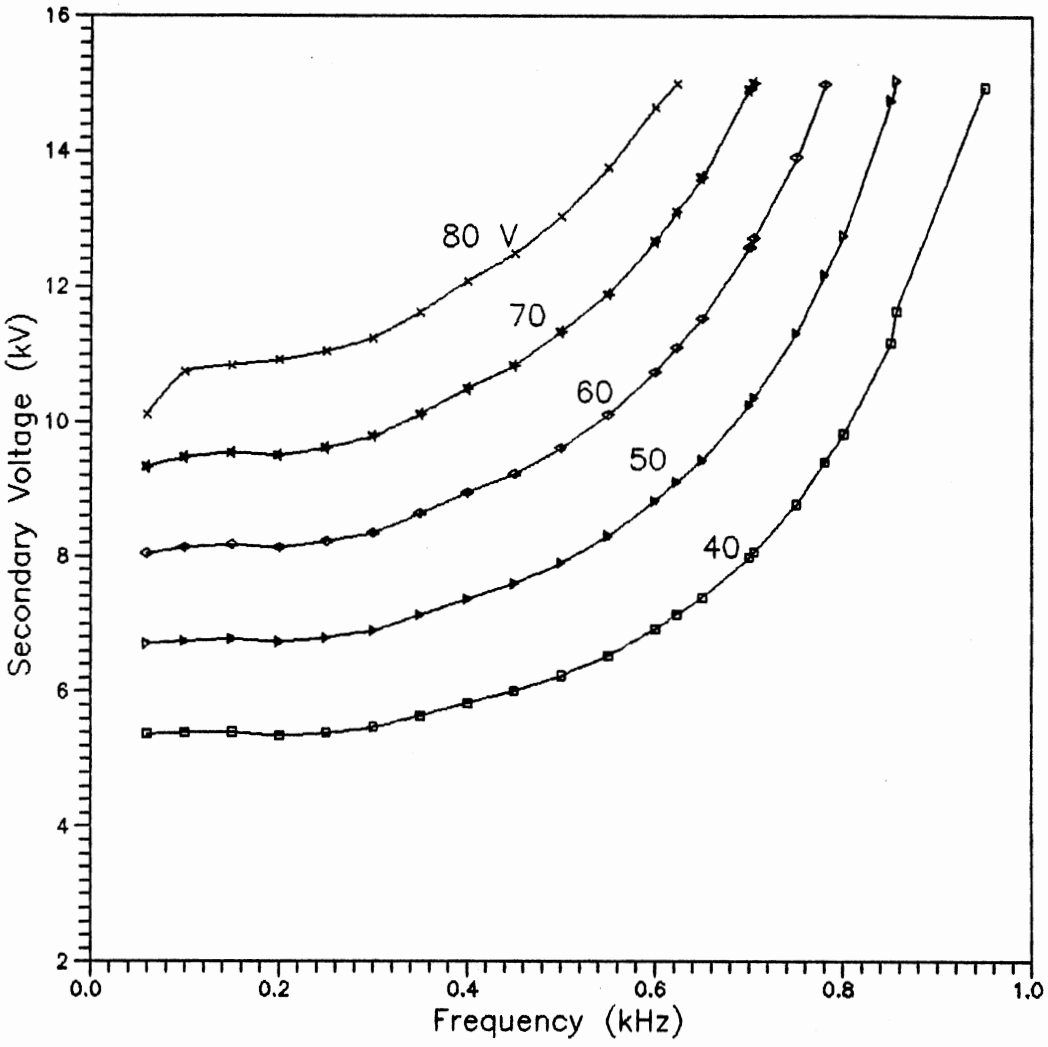

Figure 7. Effect of Frequency on Open-Circuit Secondary Voltage for Various Primary Voltages.

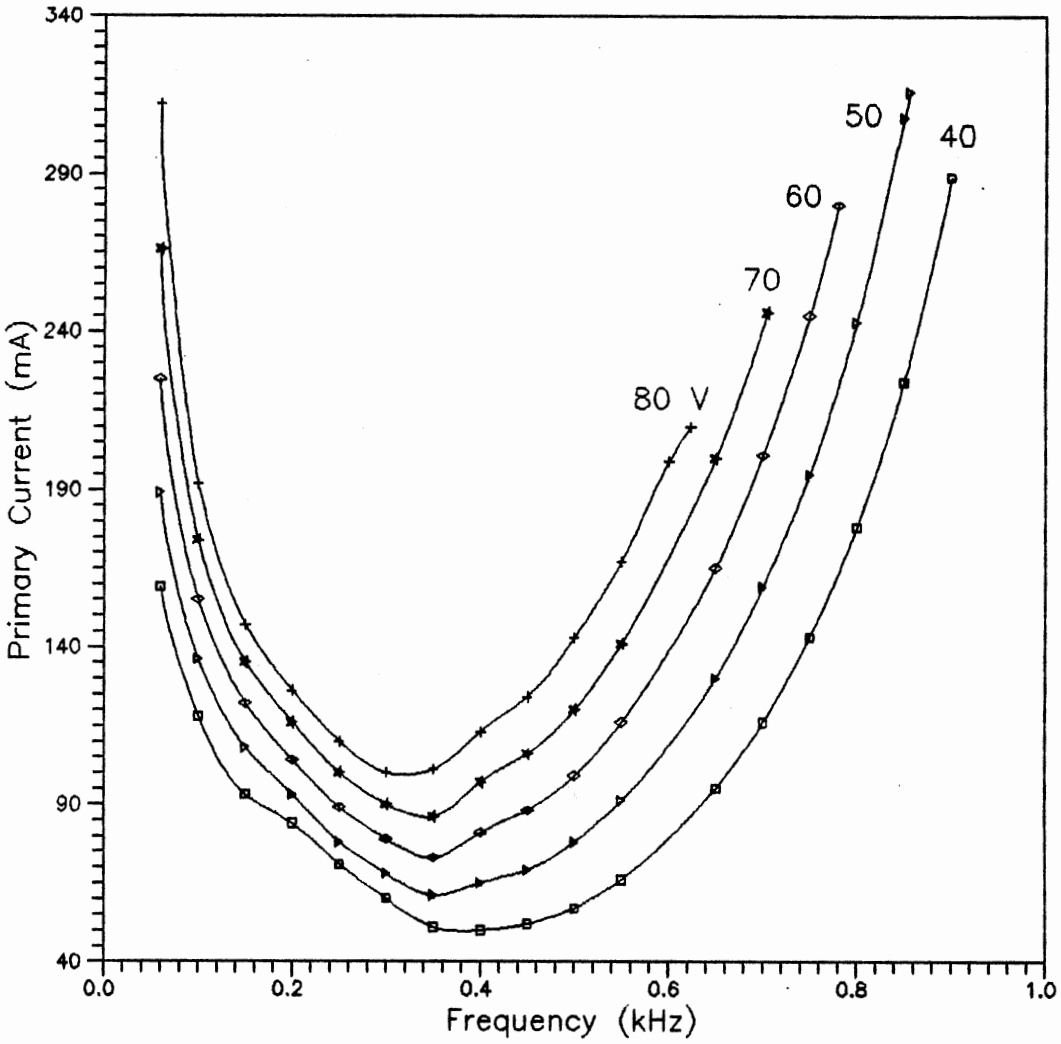

Figure 8. Effect of Frequency on Open-Circuit Primary Current for Various Primary Voltages.

the behaviors of power factor and transformer loss at higher frequencies are still unknown. It is evident from Figure 8 that the transformer is in resonance. When the secondary voltage is tuned to the rated voltage of the transformer, further increases in frequency result in a considerable increase in voltage and current. Resonance frequency is shown to be a function of the primary voltage. The higher the primary voltage, the lower the corresponding resonance frequency. Resonance frequency reveals the frequency range to be expected for operation of a particular capacitive discharge reactor system.

Breakdown Voltage and Frequency of the Discharge Reactors

A series of breakdown tests were performed at atmospheric pressure and room temperature to determine the breakdown voltages and frequencies of the discharge reactors. The flow rate of dry air used in the tests was 2910 ml/min. The measured breakdown voltage is the effective value of the voltage. Tables V-VIII show the breakdown voltages and frequencies of the different reactors as a function of primary voltage. The breakdown voltage increases with increasing primary voltage. Increases in primary voltage also decrease the breakdown frequency. A comparison of the calculated breakdown voltages from equation (4.3) with experimental data shows reasonable agreement.

Experimental observations show that if the applied voltage on a discharge reactor is rapidly increased the breakdown frequency is lower than that obtained with a very slow increase in voltage. The magnitude of this effect depends on the sources of initial ionization which are present and on the rate of rise of the voltage with frequency. When calculating breakdown voltage, equation (4.3) does not account for the effect of space charge and frequency. Although equation (4.2) takes into account ion mobility and frequency, the complexity of the discharge system does not allow for accurate prediction of the breakdown frequency and voltage.

In the general case of a nonuniform field gap, the self-sustained discharge is of the corona type, which in a uniform or quasi-uniform field gap, may immediately lead to breakdown in the gap. The experimental results show evidence of the existence of a critical diameter ratio (D_3/D_2). For a reactor with diameter ratio greater than the critical, the breakdown occurs immediately after the corona starts, leading to a direct breakdown. This is reflected in the fact that for discharge reactors A and C, the complete breakdowns in the gaps occur when the applied voltages reach the breakdown voltages. As shown in Table IV , the geometries of reactors A and C are more non-uniform than the other two reactors. The diameter ratio, 1.46, can be seen as a critical one, above which a direct discharge results.

The breakdown measurement for two reactors in parallel

TABLE V

EXPERIMENTAL AND CALCULATED BREAKDOWN VOLTAGE AND FREQUENCY FOR REACTOR A

V_p (V)	f_{bexp} (Hz)	f_{bcal} (Hz)	Dev (%)	V_{bexp} (V)	Dev (%)
20	670	NA	NA	9060	1.5
25	632	NA	NA	9080	1.3
30	597	582	2.5	9160	0.4
35	558	533	4.5	9180	0.2
40	518	497	4.1	9280	0.9
45	476	449	5.7	9340	1.5
50	432	407	5.8	9380	2.0
55	383	365	4.7	9480	3.0
60	329	322	2.1	9580	4.1

V_{bcal} = 9200 V @ 76.2 cm Hg, 21.2 °C

TABLE VI

EXPERIMENTAL AND CALCULATED BREAKDOWN VOLTAGE AND FREQUENCY FOR REACTOR B

V_p (V)	f_{bexp} (Hz)	f_{bcal} (Hz)	Dev (%)	V_{bexp} (V)	Dev (%)
20	526	NA	NA	6260	1.5
25	478	NA	NA	6300	0.9
30	425	371	14.3	6320	0.6
35	362	321	11.3	6360	0.1
40	297	282	5.0	6440	1.3
45	200	225	12.5	6440	1.3

V_{bcal} = 6355 V @ 76.2 cm Hg, 20 °C

TABLE VI

EXPERIMENTAL AND CALCULATED BREAKDOWN VOLTAGE AND FREQUENCY FOR REACTOR C

V_p (V)	f_{bexp} (Hz)	f_{bcal} (Hz)	Dev (%)	V_{bexp} (V)	Dev (%)
20	683	NA	NA	9900	9.2
25	650	NA	NA	10000	9.1
30	620	668	7.7	10300	6.0
35	580	614	5.9	10380	4.8
40	550	589	7.1	10500	3.7
45	525	548	4.4	10620	2.6
50	484	513	6.0	10700	1.9
55	444	471	6.1	10750	1.4
60	407	430	5.7	10860	0.4

V_{bcal} = 10905 V @ 76.2 cm Hg, 21.2 °C

TABLE VIII

EXPERIMENTAL AND CALCULATED BREAKDOWN VOLTAGE AND FREQUENCY FOR REACTOR D

V_p (V)	f_{bexp} (Hz)	f_{bcal} (Hz)	Dev (%)	V_{bexp} (V)	Dev (%)
20	615	NA	NA	8620	4.3
25	579	NA	NA	8660	3.9
30	541	546	0.9	8660	3.9
35	502	498	0.8	8720	3.2
40	463	458	1.1	8760	2.8
45	421	409	2.9	8820	2.1
50	372	368	1.1	8860	1.7
55	319	320	0.3	8940	0.8

V_{bcal} = 9010 V @ 76.2 cm Hg, 20 °C

is referred to the discharge reactor with a lower breakdown voltage. Initially, model equation (4.1) fails to predict breakdown frequency due to the additional effect of current caused by a great increase in capacitance. The breakdown frequency is found to be lower than that of a single discharge reactor, while the breakdown voltage becomes higher due to the effect of lower frequency. The model can be modified to include this effect. The additional model equations are expressed as

$$f_b = \Phi f_{bi} \tag{5.1}$$

$$V_b = \Phi^{\frac{1}{4}} V_{bi} \tag{5.2}$$

where $\Phi = \left(\frac{C_{ti}}{C_{ti} + C_{tj}}\right)^{1/3}$

C_{ti} = capacitance of reactor i, pf

C_{tj} = capacitance of reactor j, pf

V_{bi} = measured breakdown voltage of reactor i, V

f_{bi} = measured breakdown frequency of reactor i, Hz

V_b = breakdown voltage, V

f_b = breakdown frequency, Hz

For given tube diameters and primary voltages, measured breakdown data of small reactors can be used as a basis to evaluate breakdown voltage and frequency for either multi-reactors in parallel or for a single large reactor.

Tables IX and X list the calculated breakdown voltages and frequencies for two reactors in parallel. The predicted

TABLE IX

EXPERIMENTAL AND CALCULATED BREAKDOWN FREQUENCY AND VOLTAGE FOR TWO REACTORS IN PARALLEL FOR A PRIMARY VOLTAGE OF 40 V

Reactor	f_{bexp} (Hz)	f_{bcal} (Hz)	Dev (%)	V_{bexp} (V)	V_{bcal} (V)	Dev (%)
A-D	387	384	0.8	9140	9111	0.3
B-A	246	254	3.3	6740	6696	0.7
C-A	413	411	0.5	9960	9830	1.3
C-B	246	254	3.3	6700	6696	0.1
C-D	373	382	2.4	8980	9191	2.4

TABLE X

EXPERIMENTAL AND CALCULATED BREAKDOWN FREQUENCY AND VOLTAGE FOR TWO REACTORS IN PARALLEL FOR A PRIMARY VOLTAGE OF 30 V

Reactor	f_{bexp} (Hz)	f_{bcal} (Hz)	Dev (%)	V_{bexp} (V)	V_{bcal} (V)	Dev (%)
A-D	436	448	2.8	9060	9075	0.2
B-A	351	363	3.4	6500	6572	1.1
C-A	473	473	0.0	9800	9750	0.5
C-B	352	363	3.1	6540	6572	0.5
C-D	440	446	1.4	8940	9086	1.6

results are in good agreement with the experimental data. Although equations (5.1) and (5.2) give a good prediction of breakdown for two reactors in parallel, breakdown tests with large reactors, which have much higher capacitance, would be useful in evaluating this model.

Dry Air Discharges and System Characteristics

Figures 9-12 give the instantaneous variations of secondary voltage with frequency at different primary voltages for the various reactors. The voltage increases smoothly with frequency from a low, initial value. At breakdown or corona starting voltage, however, a sudden or jump continuous increase of voltage is observed. Further increases in frequency are accompanied by a decrease in the voltage. The curves are concave downwards This is a typical characteristic of an impedance-changing circuit.

In this system, the primary voltage (gain) represents possible maximum power transferred to the transformer provided that the power factor is assumed to be one. For higher values of primary voltage, higher power input and secondary voltage result. The data indicate that at a primary voltage of 50 V the curves for reactors A and C are seen to be flat as compared to reactors B and D. As indicated by comparing the gas gap in Table IV, a short gas gap results in an intense glow due to a higher voltage available for the discharge.

At breakdown voltage the non-self-sustaining discharge

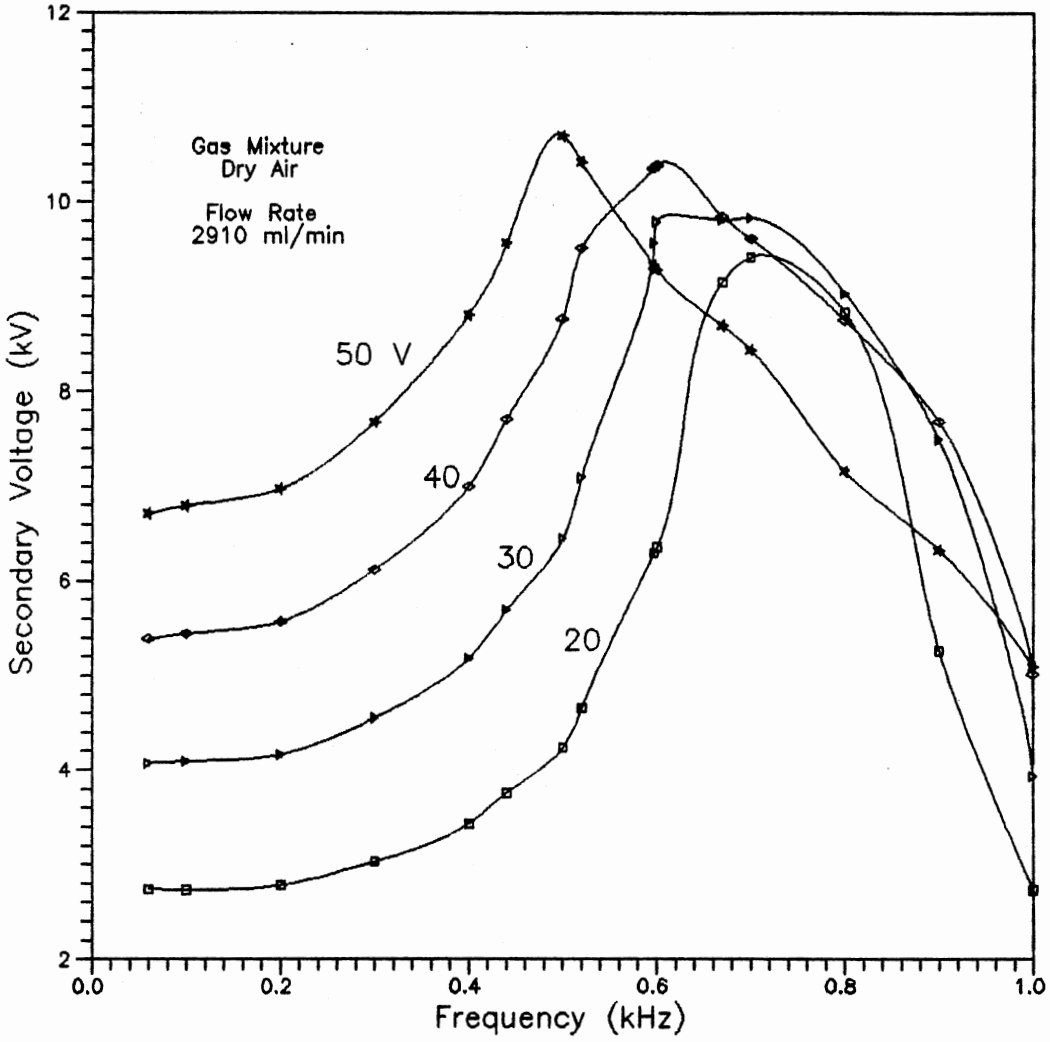

Figure 9. Effect of Frequency and Primary Voltage on Secondary Voltage for Reactor A Under Unsteady State Conditions.

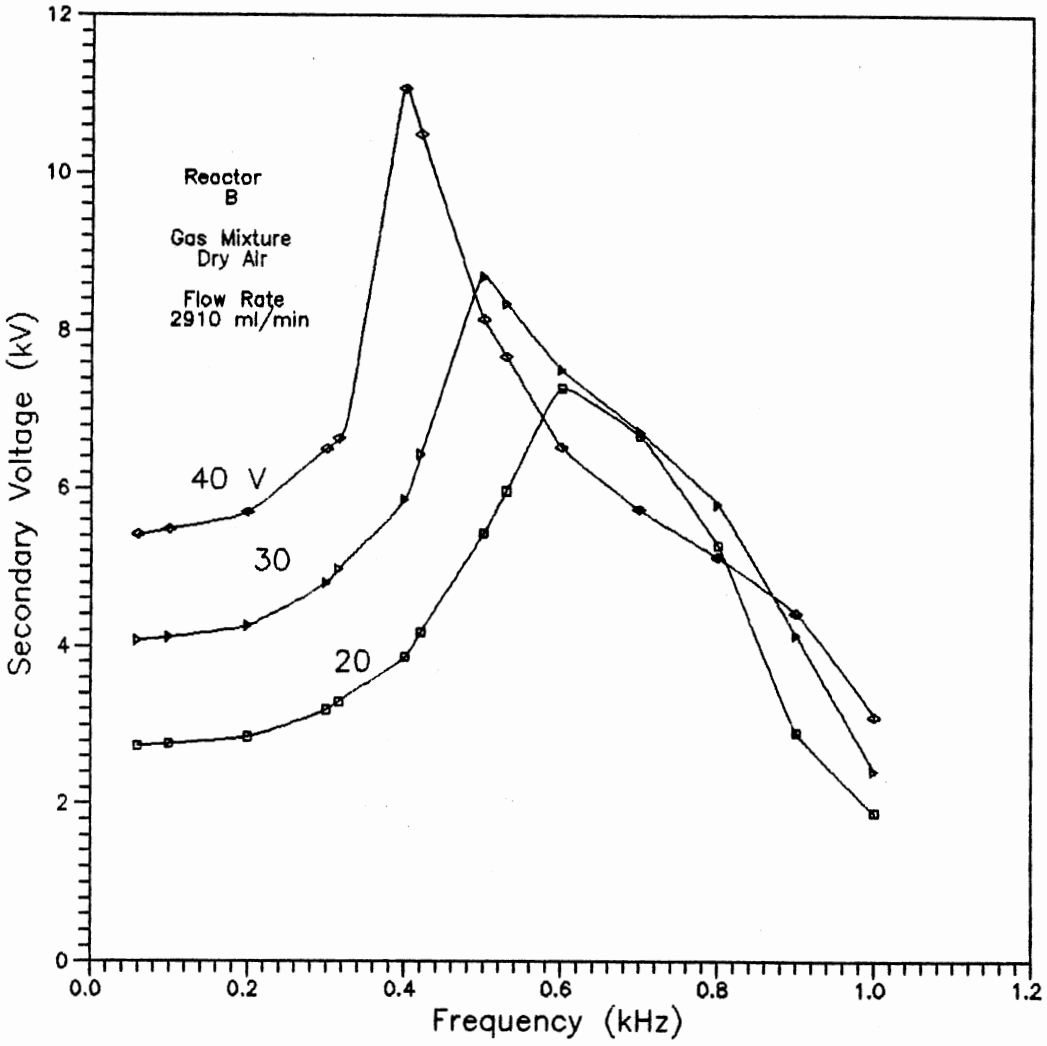

Figure 10. Effect of Frequency and Primary Voltage on Secondary Voltage for Reactor B Under Unsteady Steady Conditions.

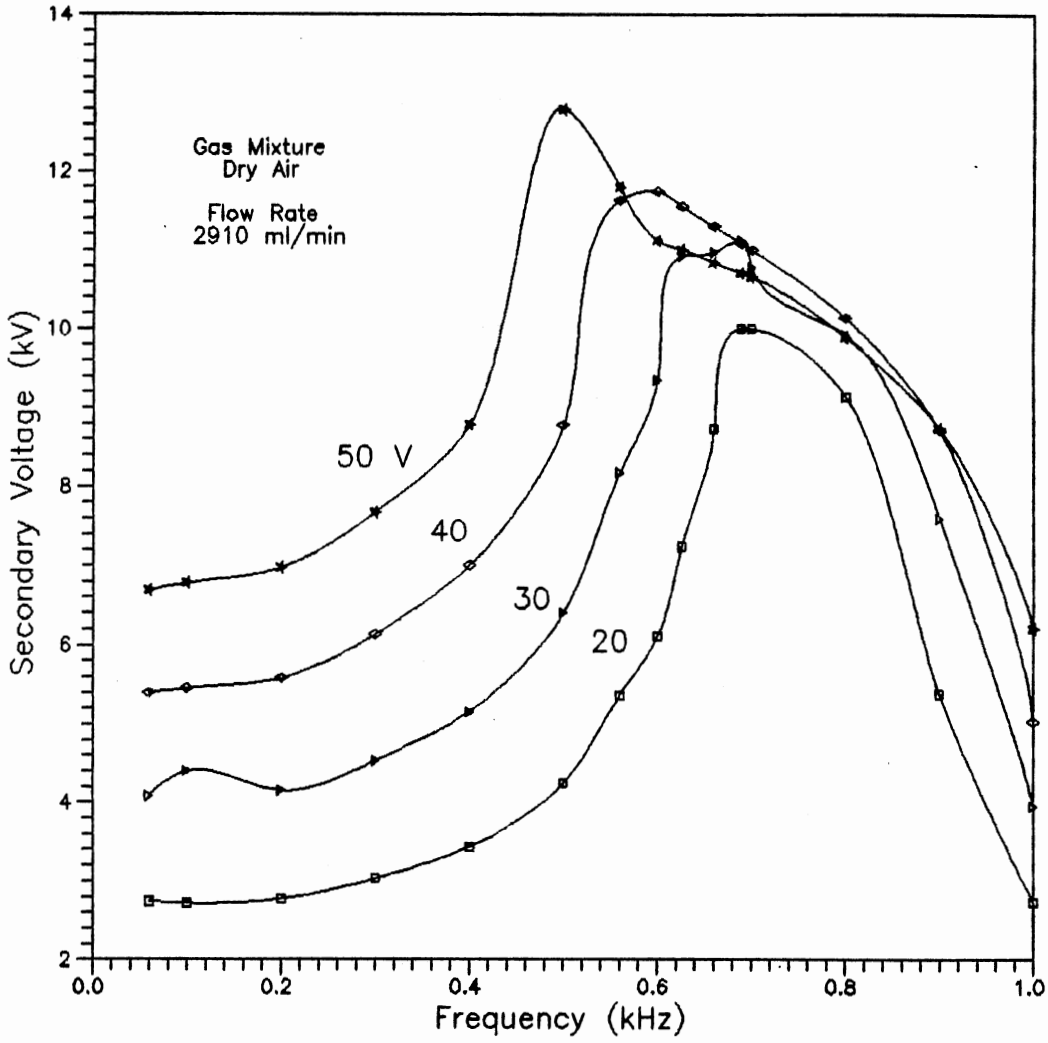

Figure 11. Effect of Frequency and Primary Voltage on Secondary Voltage for Reactor C Under Unsteady State Conditions.

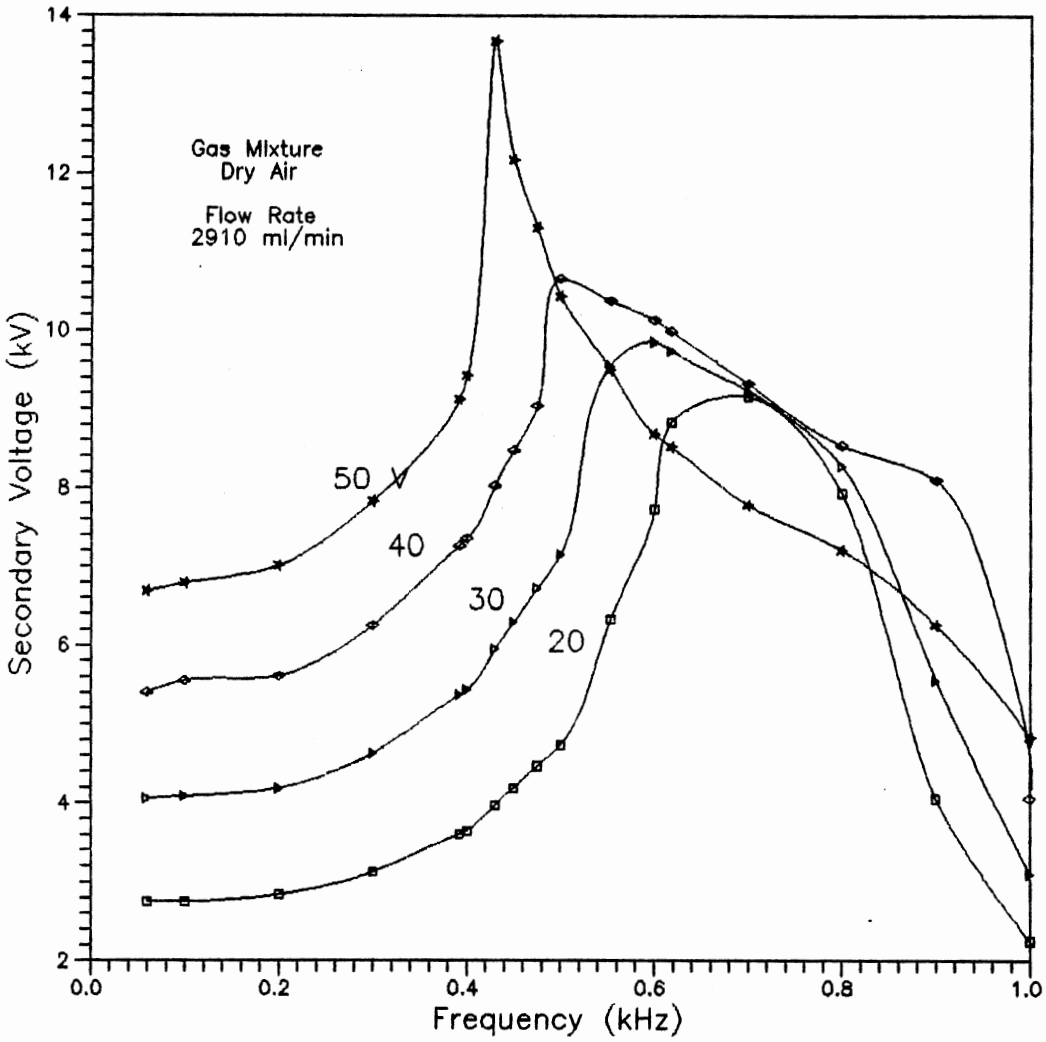

Figure 12. Effect of Frequency and Primary Voltage on Secondary Voltage for Reactor D Under Unsteady State Conditions.

(Townsend discharge) changes to a self-sustaining discharge. Ionization occurs rapidly in the gas gap and produces surface-bound space charges. A space-charge field is developed as a result of the low mobility of positive ions formed in the discharge. The existence of a space-charge distortion results in the lowering of the applied voltage required to maintain a discharge.

Theoretically, the breakdown voltage can be located by reducing the voltage until the discharge ceases. For a double frequency-tuned discharge system, this method is not reliable because breakdown voltage also varies with the applied frequency and primary voltage.

Instantaneous power input for reactor A is shown in Figure 13. The power input reaches a maximum immediately after the gas breaks down. A drastic increase in power input is caused by the build-up of the current flowing in the gap. The energy absorbed in the discharge is drawn from the power source. For a primary voltage of 50 V the instantaneous total power input is observed to increase from 44.5 to 123.5 W as soon as the breakdown occurs. Since the power transferred to the transformer never exceeds 50 W, it appears that more energy dissipates in the power amplifier in order to balance the output. Figure 14 shows that a similar trend is followed by the primary current. The current is approximately proportional to the total power input.

From the above-mentioned considerations, a higher

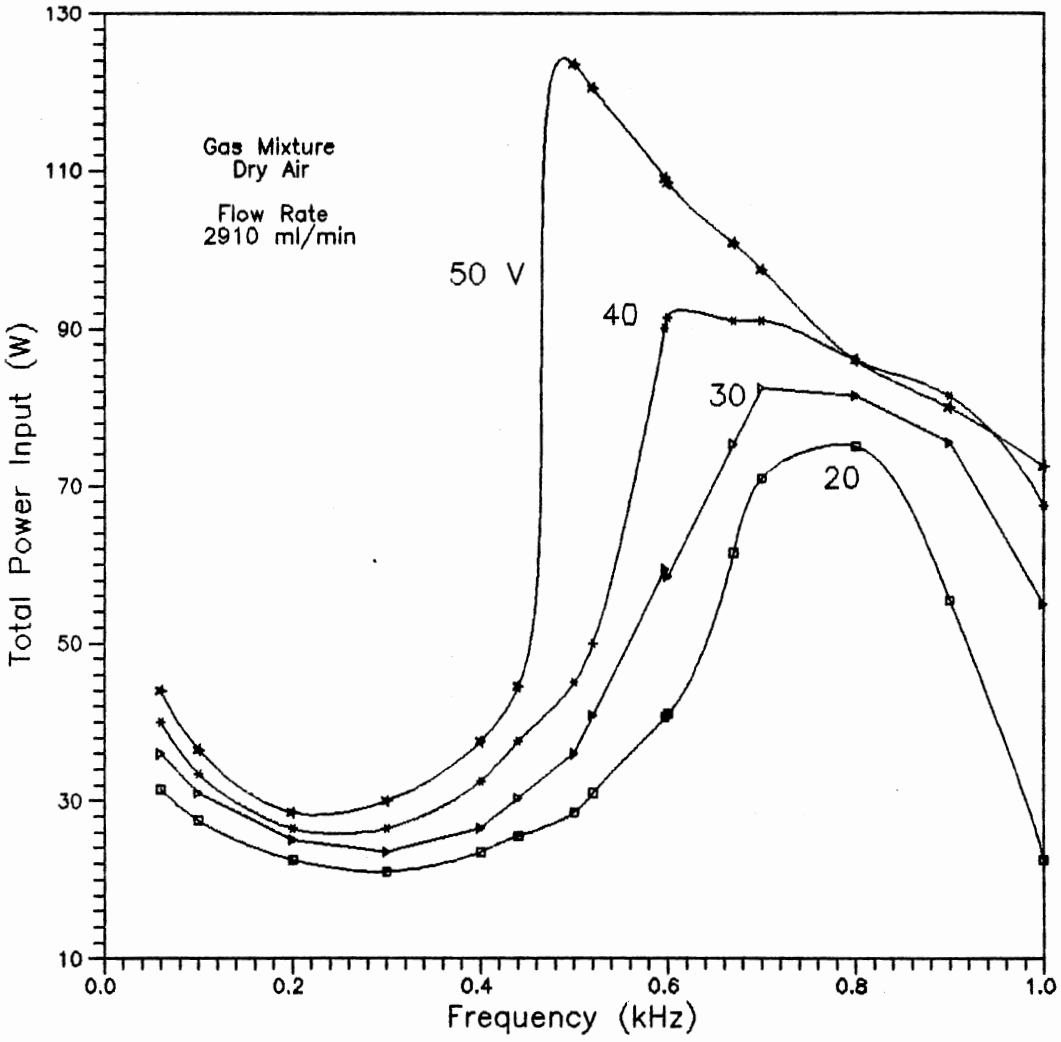

Figure 13. Effect of Frequency and Primary Voltage on Total Power Input for Reactor A Under Unsteady State Conditions.

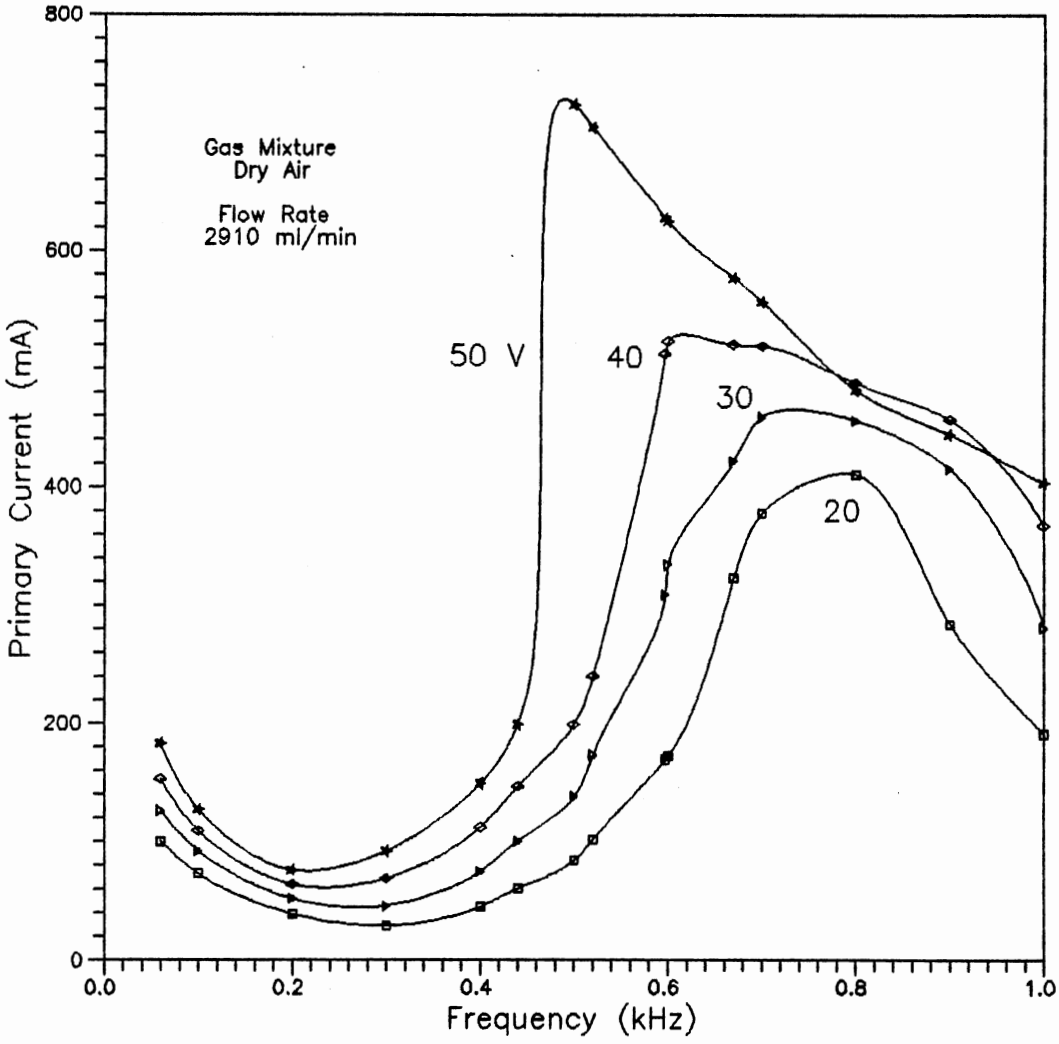

Figure 14. Variation of Primary Current with Frequency and Primary Voltage for Reactor A Under Unsteady State Conditions.

primary voltage increases the discharge power but also leads to a relatively high total power input. When the primary voltage is made too high, the discharge becomes very intense so that the surface of the tube wall is conductive. Under such conditions, the arc is formed and enough current flows through the secondary circuit to burn the transformer. To protect the circuit, discharge reactor tests should start from a low value of primary voltage.

Steady state secondary voltage profiles for the various reactors are shown in Figure 15. Compared to breakdown voltages, the maximum voltage increases for the four different reactors are : 9 (A), 69 (B), 5.5 (C) and 17.8 % (D). As shown in equation (4.12), discharge power is related to voltage difference between the applied voltage and gas breakdown voltage. Thus reactor B should have the highest power input of all the reactors. For reactor B with a short gap, the maximum secondary voltage is much higher and the secondary voltage decreases rapidly as the frequency increases past the maximum.

The load of a discharge reactor and the heat loss to the environment determine the maximum secondary voltage. As shown in equation (4.3), gas breakdown voltage is directly affected by gas temperature. Higher gas temperature has the effect of enabling the discharge to be self-sustaining at a lower gap voltage. Referring to Figure 15 and Table V-VIII, however, the applied voltage is still higher than the initial breakdown voltage. This is attributed to more

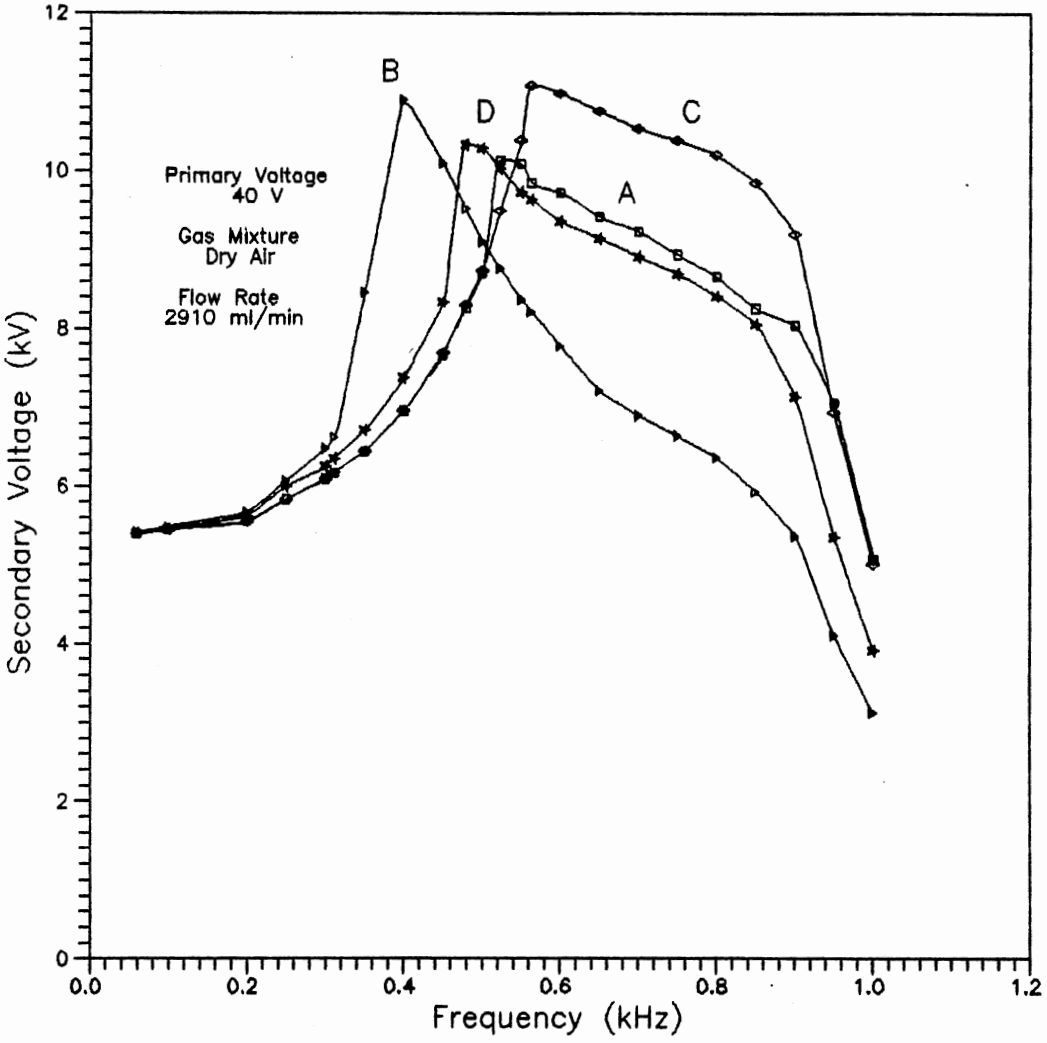

Figure 15. Effect of Frequency on Secondary Voltage for Various Reactors Under Steady State Conditions.

current in the primary available for generating higher voltage.

Figure 16 shows the effect of frequency on the total power input for various reactors under steady state conditions. With the exception of reactor B, after the breakdown, the total power input slightly increases with frequency before decreasing. A qualitative comparison of Figures 15 and 16 shows that a decrease in secondary voltage does not conform with an decrease in total power input. This may arise from the correction of the power factor for a discharge reactor.

Figure 17 shows the exit gas temperature as a function of frequency. Before discharge, gas temperatures are at room temperature. The rise of gas temperature indicates the part of discharge power is used for gas heating. Compared to reactors B and D, reactors A and C were observed to maintain approximately constant gas temperatures over a wide range of frequency. This suggests that the gas temperature of a reactor with a direct breakdown is less sensitive to frequency.

It is noted that gas temperature is a function of discharge power, heat of reaction and heat loss. A heating factor is considered to include theses effects. This factor indirectly represent the fraction of discharge power available for gas heating and heat loss to the environment. Since the natural convection at the wall is controlling, the overall heat transfer coefficient can be assumed to be 1

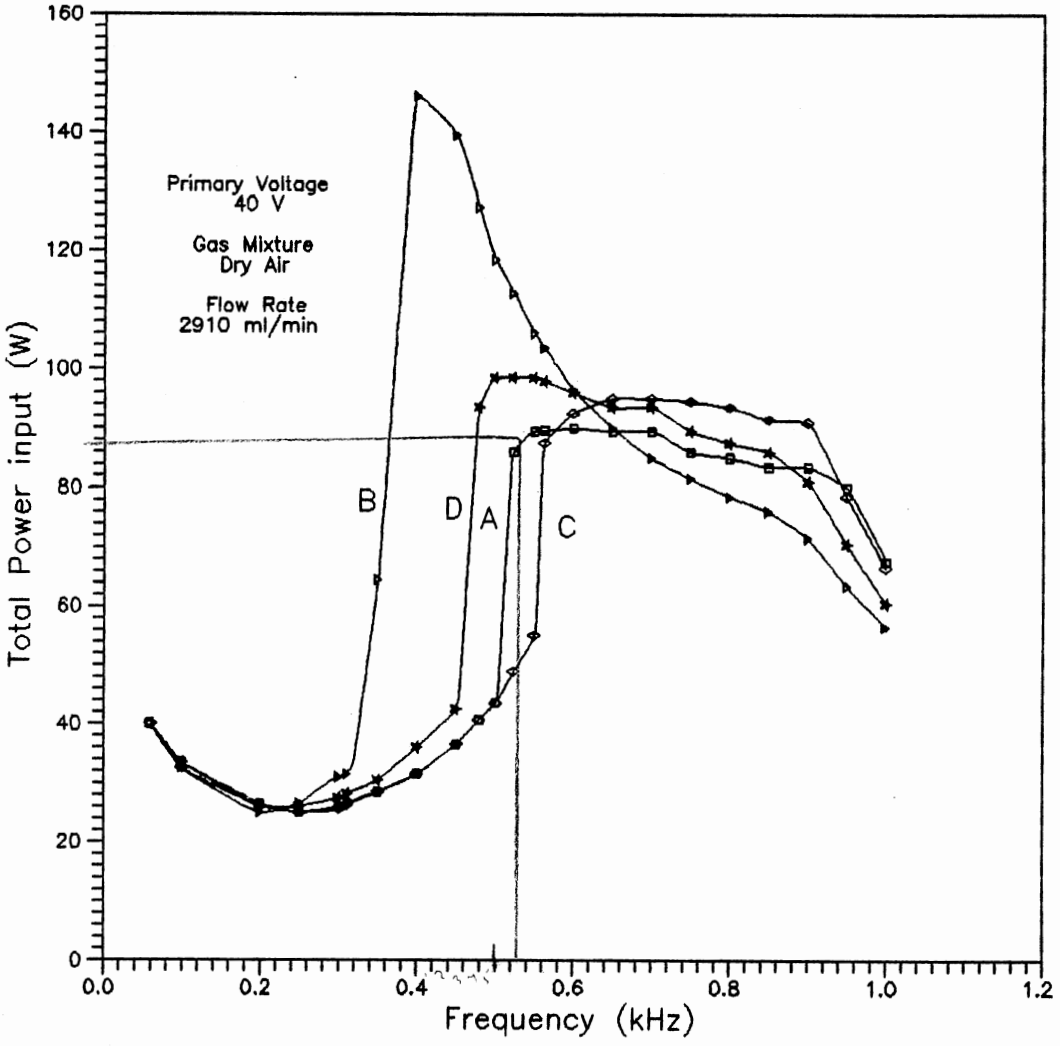

Figure 16. Effect of Frequency on Total Power Input for Various Reactors Under Steady State Conditions.

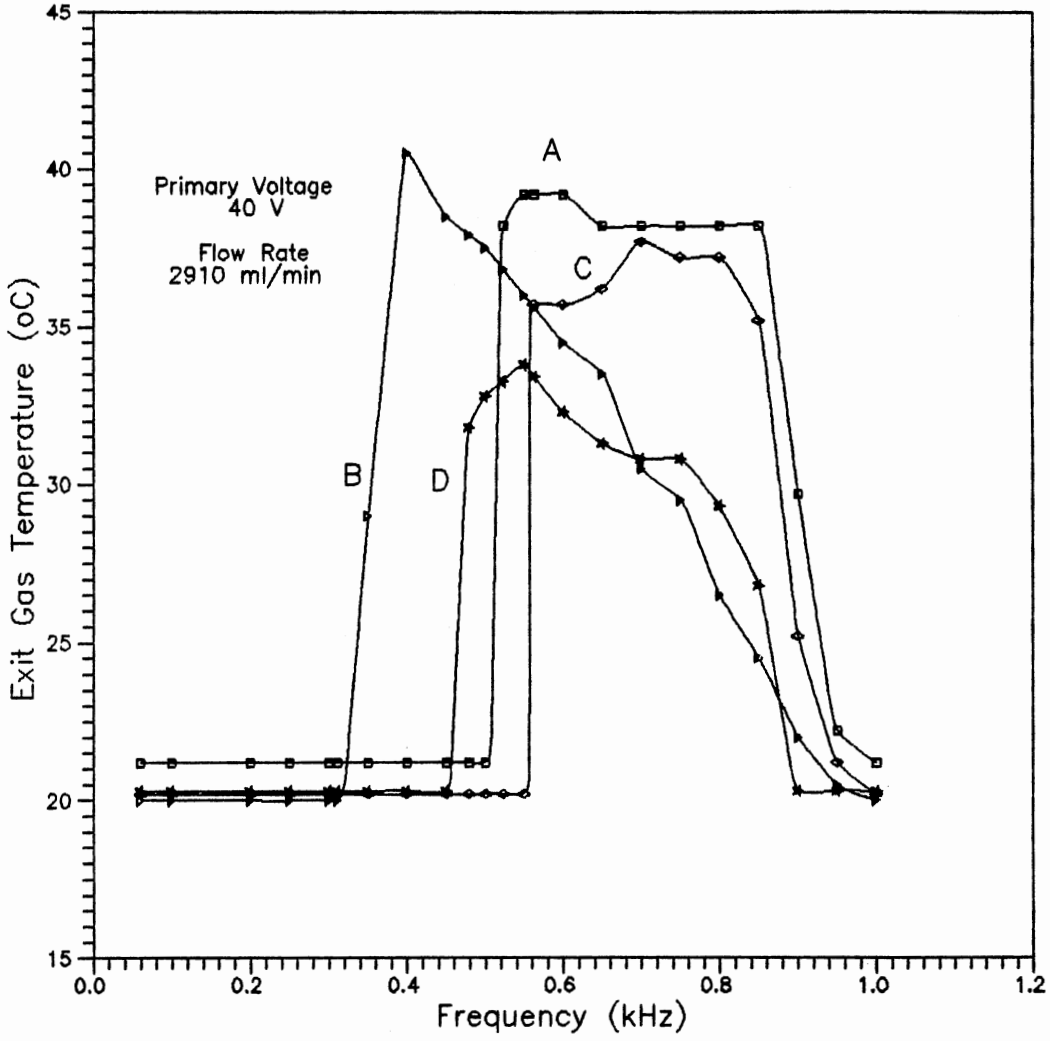

Figure 17. Effect of Frequency on Effient Gas Temperature for Various Reactors Under Steady State Conditions.

W/m°C. As shown in Figure 18, the reactors A and C have a higher heating factor. Further, as can be seen, for more uniform discharges, the heating factor is about 0.2, which can be used as a design factor of the reactor. Figure 19 shows that for all reactors, the power factors are below 0.5, which is reasonable because of the inherently low power factor of a capacitive reactor. Experimental and calculated secondary current are shown in Table XI. Since the measured maximum error is ± 0.6 mA, equation (4.9) is shown to give a good approximation for the effective current of the discharge reactor with dry air discharges. The results further show that the power model can be used to make reliable predictions of discharge power.

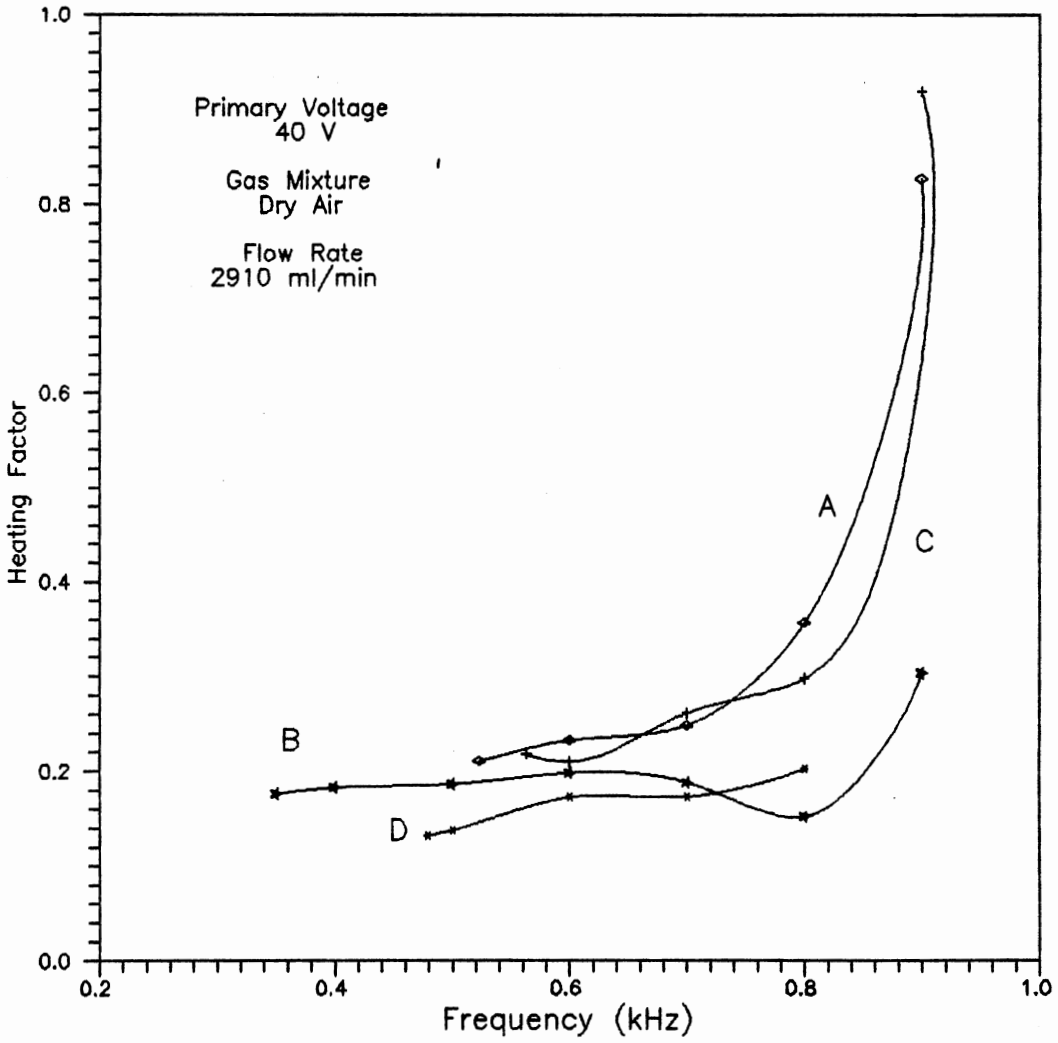

Figure 18. Heating Factor as a Function of Frequency.

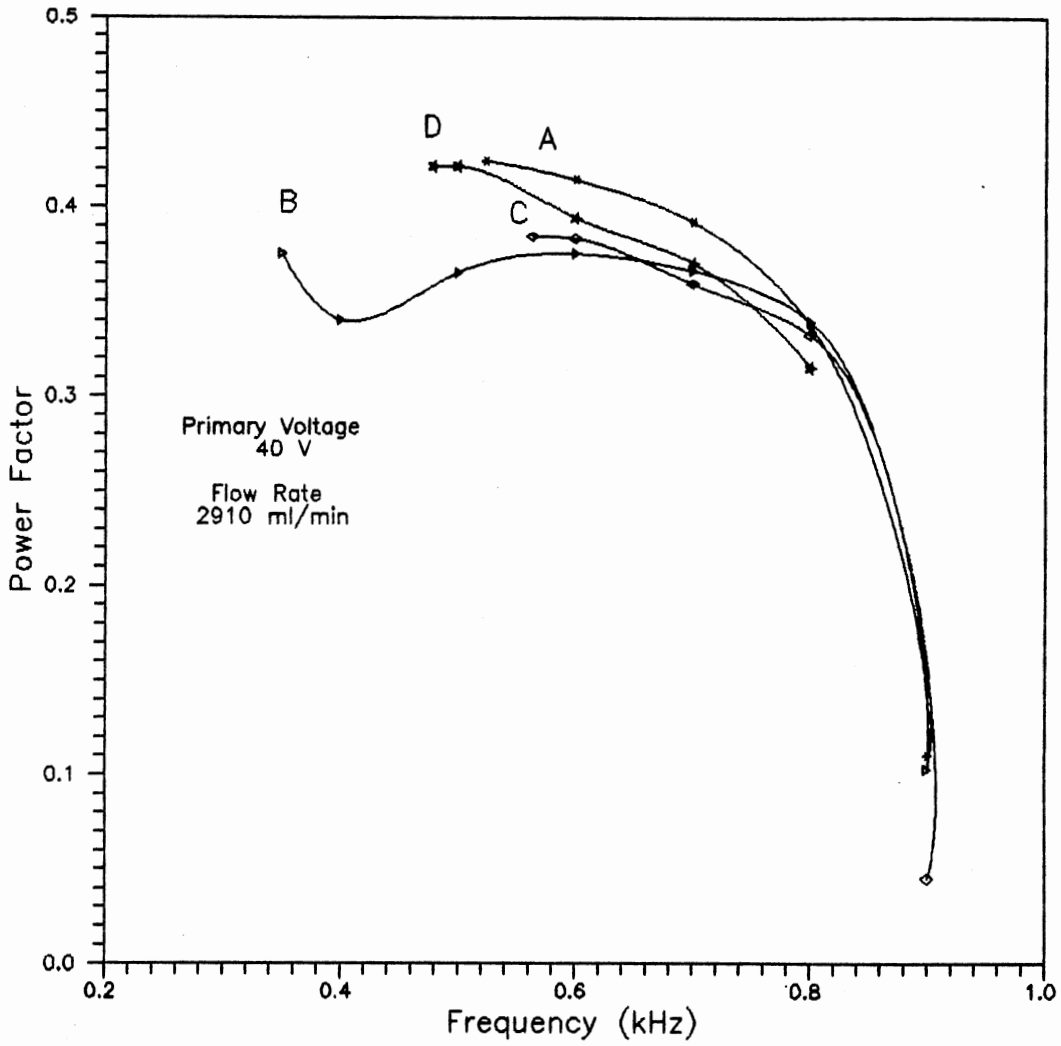

Figure 19. Calculated Power Factor as a Function of Frequency for Various Reactors with Dry Air Discharges.

TABLE XI

EXPERIMENTAL AND CALCULATED EFFECTIVE CURRENTS FOR FOUR DIFFERENT REACTORS AT A PRIMARY VOLTAGE OF 40 V

Reactor	f (Hz)	I_{sexp} (mA)	I_{scal} (mA)
A	523	2.7	2.0
	600	2.4	2.1
	700	2.4	2.0
	800	2.0	1.7
	900	1.4	1.2
B	350	2.7	1.9
	400	3.4	3.5
	500	3.8	3.3
	600	2.7	2.9
	700	2.7	2.5
	800	2.0	2.3
	900	1.4	1.4
C	563	2.4	1.9
	600	2.4	2.0
	700	2.0	2.0
	800	1.7	2.0
	900	1.4	1.3
D	479	3.1	2.6
	500	3.0	2.7
	600	2.7	2.4
	700	2.0	2.3
	800	2.0	2.1

Destruction of Trichloroethylene in Dry Air Discharges

In previous sections the electrical characteristics of discharge reactors were discussed. In the following sections TCE destruction data are used to provide a basis for the assessment of electrical parameters and operational variables of discharge reactors.

Figures 20-23 show the TCE conversions obtained from dry air/TCE discharges as a function of frequency at constant flow rate. For all reactors, the conversion curves have the same general shape. High conversion is maintained to some extent and then falls off rapidly at a certain frequency limit. The only difference is for reactor B where conversion increases from a low value. This is due to the fact that reactor B has an evident, partial discharge at low frequency.

The drastic decline in conversion gives an indication of the threshold power. Consideration of the effect of discharge power should assist in determining the true cause for the phenomenon. Since the measured power inputs are not available, the power model is used to predict the power in the discharge. Note that the discharge powers are obtained from the non-destructive data. The reason for this is that for both dry air discharge and dry air/TCE discharge, primary current and total power input are quite similar (as shown in Appendix D) despite the fact that secondary voltage

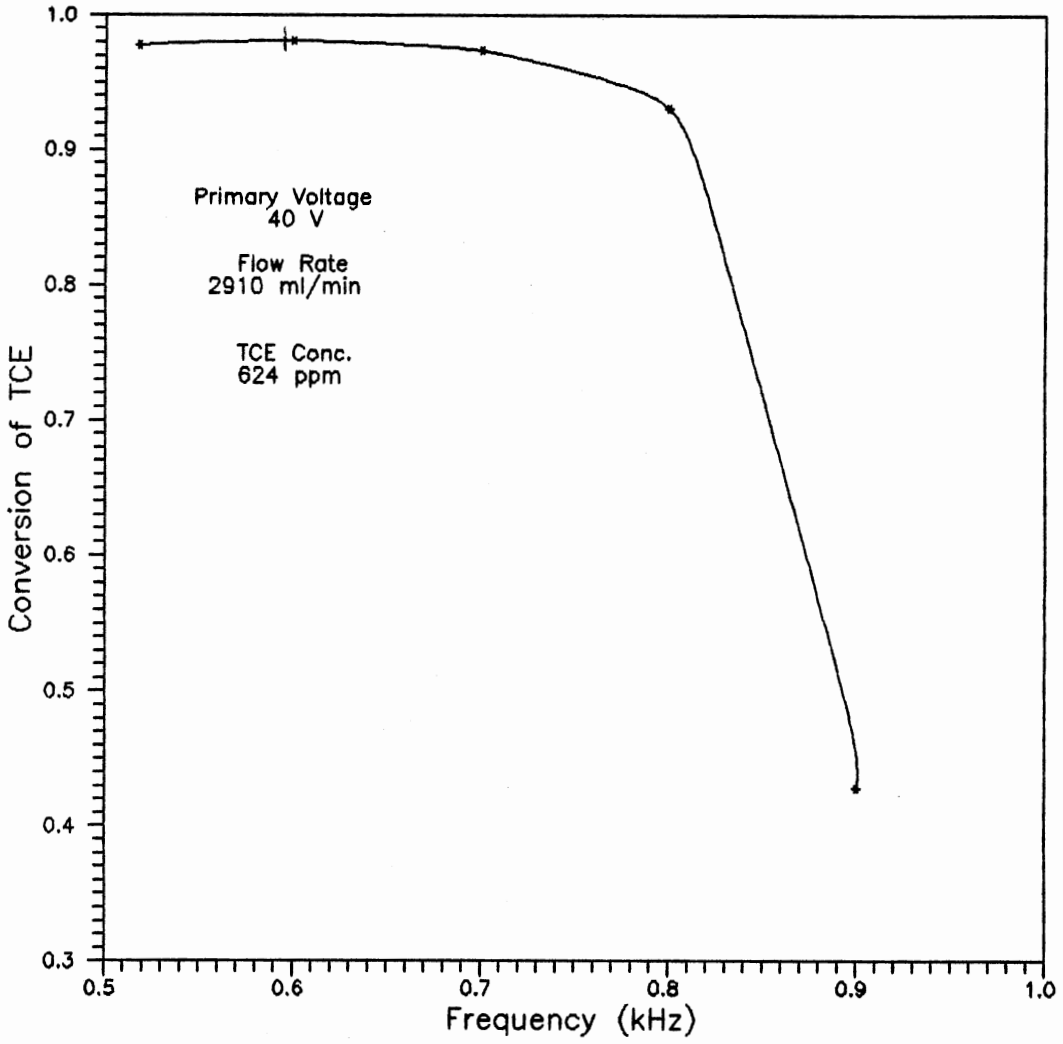

Figure 20. Effect of Frequency on Conversion of TCE in Dry Air Discharges for Reactor A.

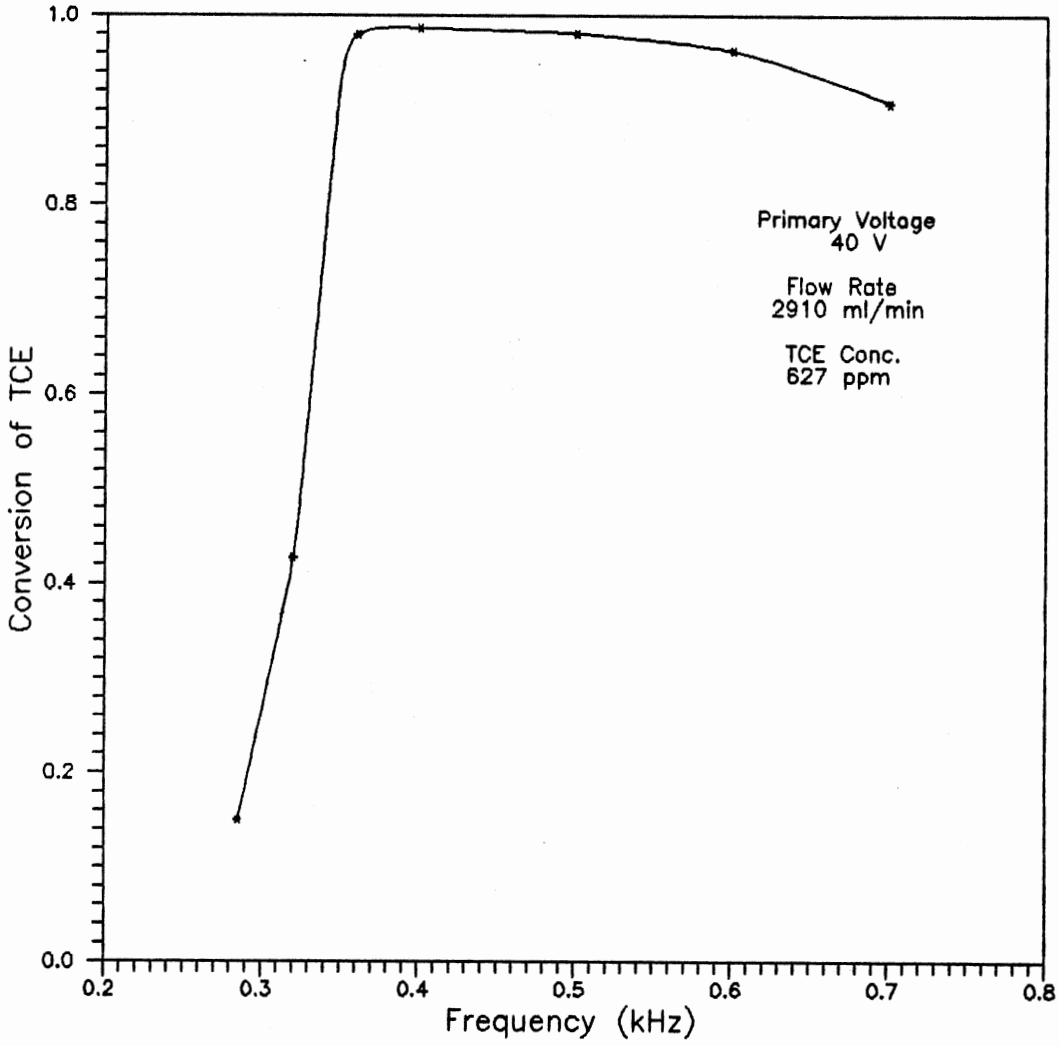

Figure 21. Effect of Frequency on Conversion of TCE in Dry Air Discharges for Reactor B.

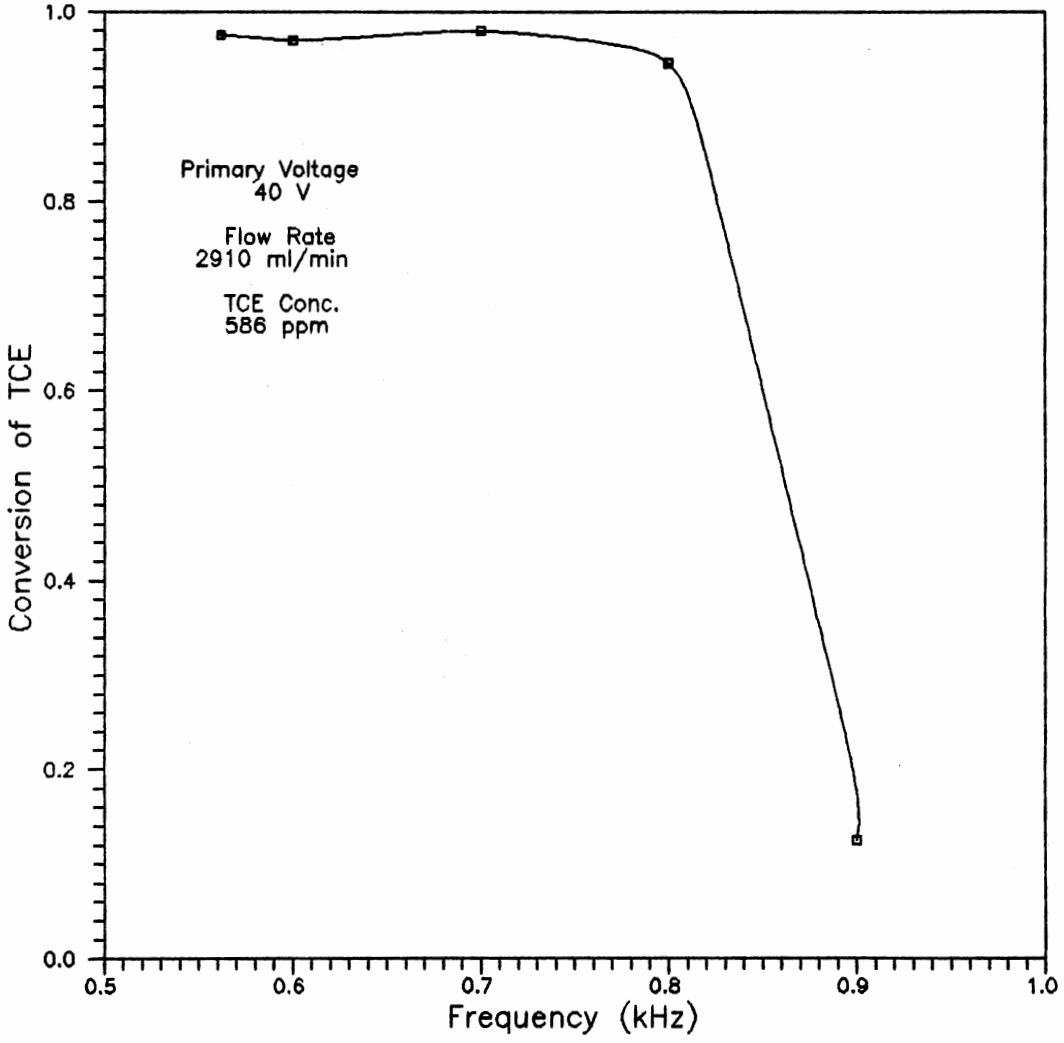

Figure 22. Effect of Frequency on Conversion of TCE in Dry Air Discharges for Reactor C.

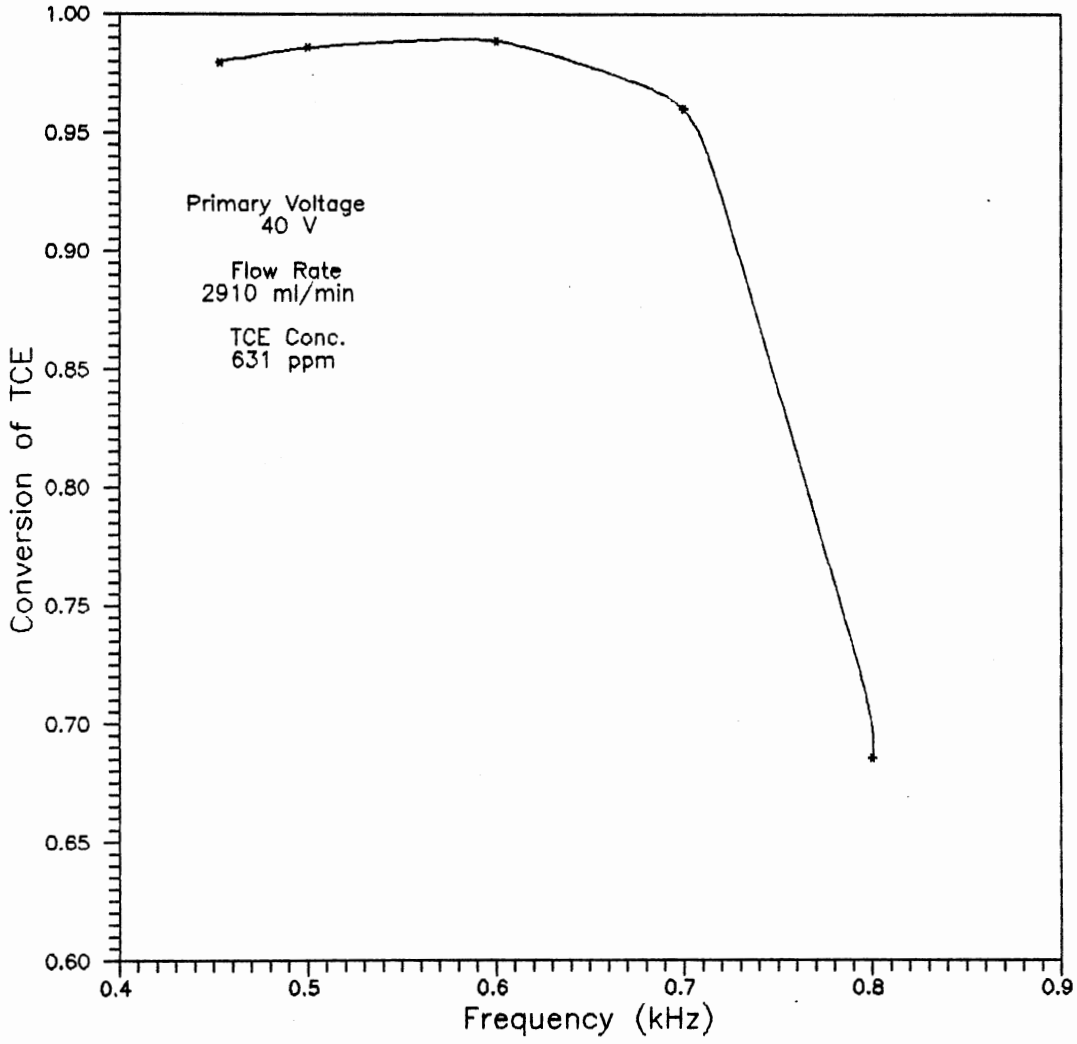

Figure 23. Effect of Frequency on Conversion of TCE in Dry Air Discharges for Reactor D.

and current are different. Further, there is always a corresponding current output from the power source to match the load.

Discharge powers of the four different reactors at different frequencies were evaluated using the power model and are shown in Figures 24-27. The sharp declines in conversion observed in Figures 20-23 correspond to lower power inputs. Obviously, there exists a threshold power level, below which a further increase in power causes conversion to decrease rapidly. The discharge power data further illustrate that a certain electron density level must be reached in order to maintain an approximately constant level of conversion. Since the threshold power level is dependent on the geometry of the reactor, system characteristics and operating conditions, no general formula is available to predict the possible level of threshold power.

Physically, the discharge process is most efficient when the energy supplied to the electrons from the electrical field is just efficient to sustain the discharge. This is true for a reactor with direct breakdown. However, when the reactor has a partial discharge, such as reactor B, conversion is low at low frequency, as shown in Figure 21. Table XII shows the total power inputs and conversions for the four different reactors. Reactors B and D require higher total power inputs to have slight increases in conversion as compared to reactors A and C.

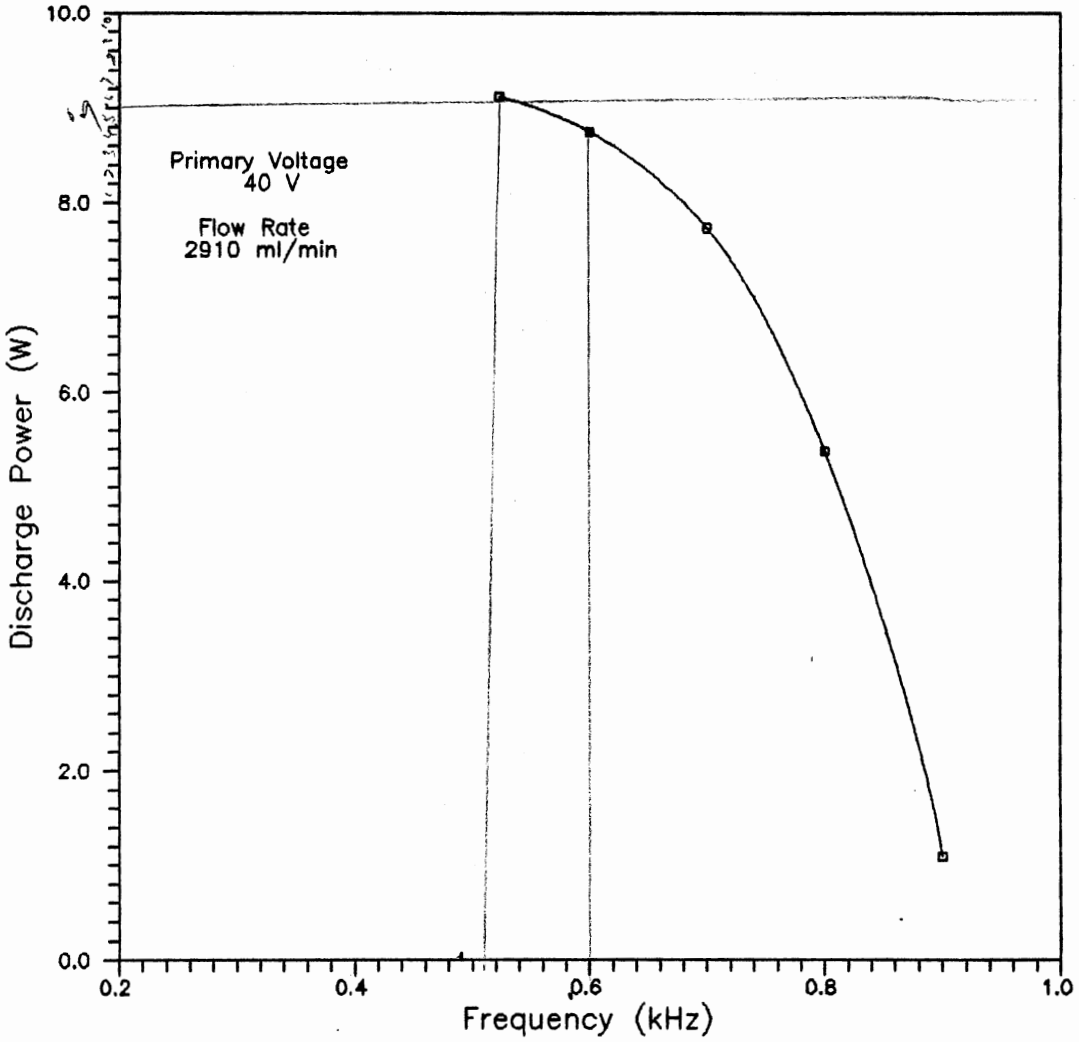

Figure 24. Calculated Discharge Power as a Function of Frequency for Reactor A with Dry Air Discharges.

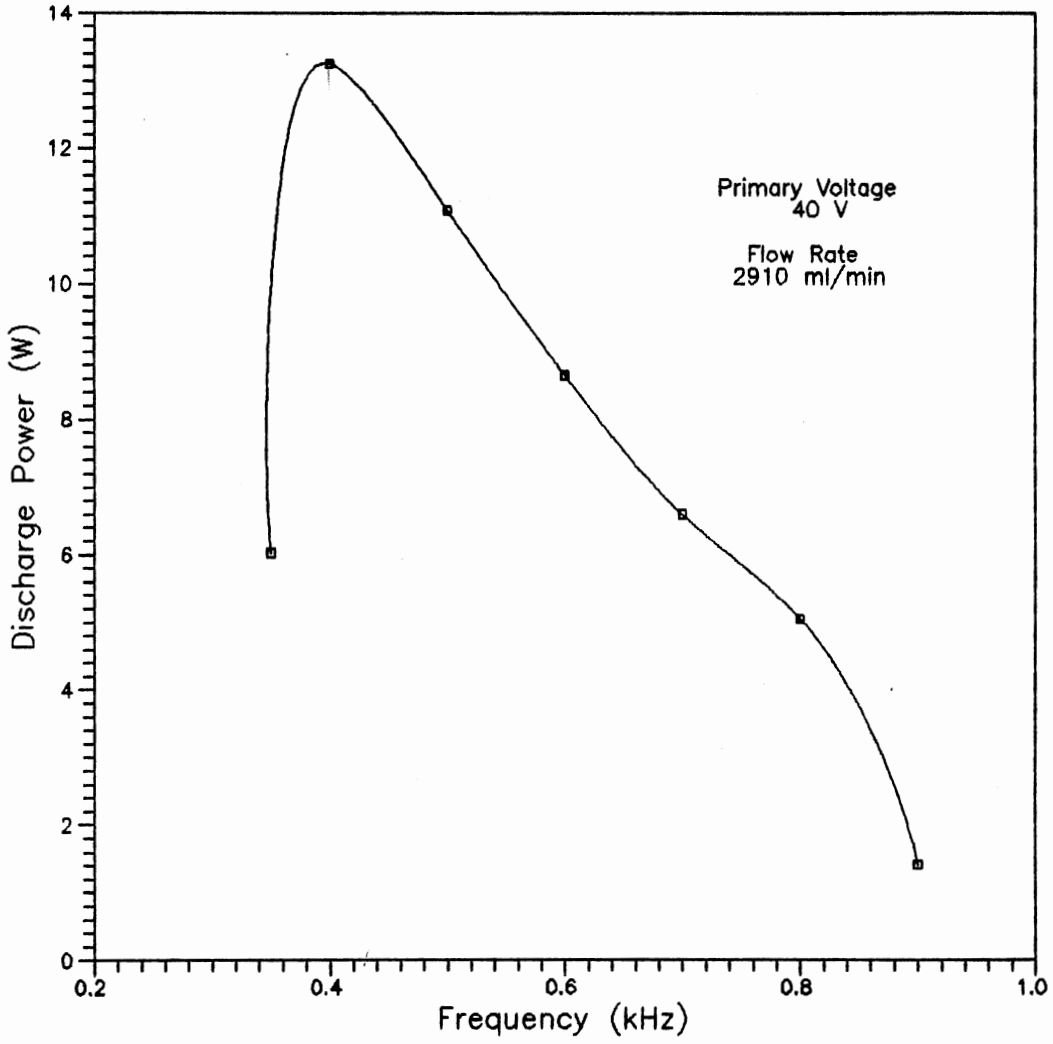

Figure 25. Calculated Discharge Power as a Function of Frequency for Reactor B with Dry Air Discharges.

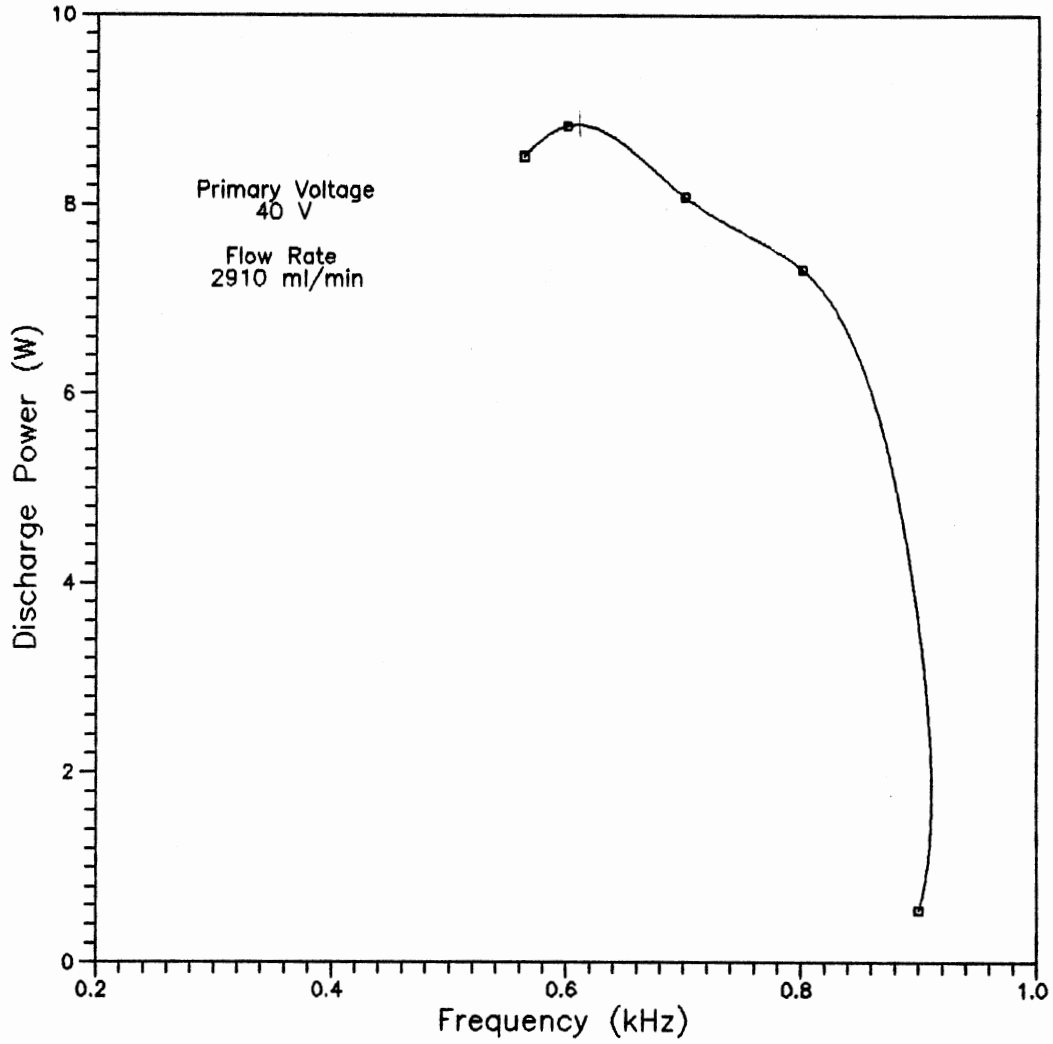

Figure 26. Calculated Discharge Power as a Function of Frequency for Reactor C with Dry Air Discharges.

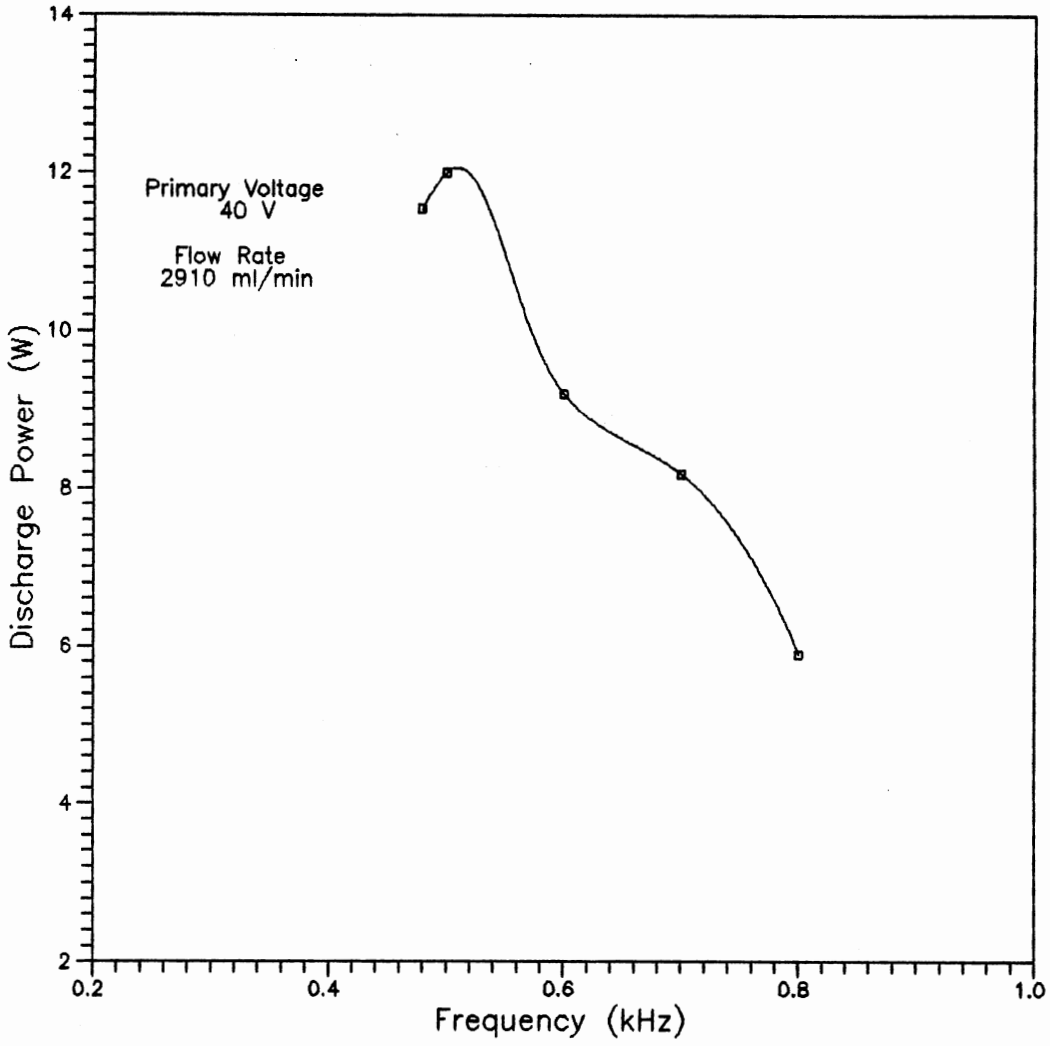

Figure 27. Calculated Discharge Power as a Function of Frequency for Reactor D with Dry Air Discharges.

The presence of TCE in an air discharge has direct influence on the current in the discharge. The discharge draws appreciable current, indicating a high phase shift with respect to the applied voltage. This qualitative finding is in accord with the results reported by Thomas et al. (15). A reasonable explanation for this difference is that organic TCE in a discharge increases the total ion mobility, resulting in a decrease in the impedance of the discharge.

For direct current, the magnitude of current represents the power. With alternating current, however, there is no physical significance to current without considering the power factor. Experimental results confirm that current has no direct effect on conversion. The calculated dynamic capacitances of reactor A are shown in Table XIII. The dynamic capacitance is higher in dry air/TCE discharge than in dry air discharge. The data reveal that higher current causes a higher value of capacitance and that the dynamic capacitance of reactor varies with frequency.

Flamm (45) concluded that the direction of current flow was opposite to the applied field. It is clear that the effect of an increase in capacitance or wall charges is reflected in the voltage. This corresponds to a phase advance of the breakdown in the succeeding half-cycle so that the field resulting from accumulated wall charge is available to reduce the applied field and produce breakdown. This is supported by experimental observation that the

TABLE XII

TOTAL POWER INPUT AND CONVERSION FOR FOUR DIFFERENT REACTORS WITH DRY AIR/TCE DISCHARGES

Reactor	Total Power Input (W)	Conversion (%)
A	95.0	97.77
	93.5	98.07
	90.5	97.35
B	131.5	97.95
	144.0	98.66
	120.5	98.11
C	93.0	97.97
	92.0	94.55
D	108.5	97.97
	106.0	98.57
	109.0	98.86

TABLE XIII

CALCULATED DYNAMIC CAPACITANCES OF REACTOR A

	Dry Air Discharges	Dry Air/TCE Discharges
Frequency (Hz)	Capacitance (pf)	Capacitance (pf)
600	43	179
700	38	153
800	30	107
900	19	91

applied voltage decreases.

Table XIV shows the effect of increasing primary voltage on conversion for reactor C. As the primary voltage increases from 40 to 50 V, an apparent increase in conversion is achieved. For a primary voltage of 40 V, conversion at 900 Hz is below 13 %. By contrast, for a primary voltage of 50 V using the same frequency the conversion is about 87 %.

Volumetric flow rate of feed and gas product determine the residence time of the gas in the discharge zone. Data taken with reactor D are shown in Figure 28. Conversion falls as gas flow rate increases from 2910 to 4410 ml/min. Conversion decrease is not costant and is greater at high

TABLE XIV

EFFECT OF PRIMARY VOLTAGE ON CONVERSION FOR REACTOR C

	Primary Voltage (V)	
	40	50
Frequency (Hz)	Conversion (%)	Conversion (%)
480	NA	97.45
530	NA	98.18
562	97.56	NA
600	97.02	98.80
700	97.97	98.67
800	94.55	97.45
900	12.40	86.56

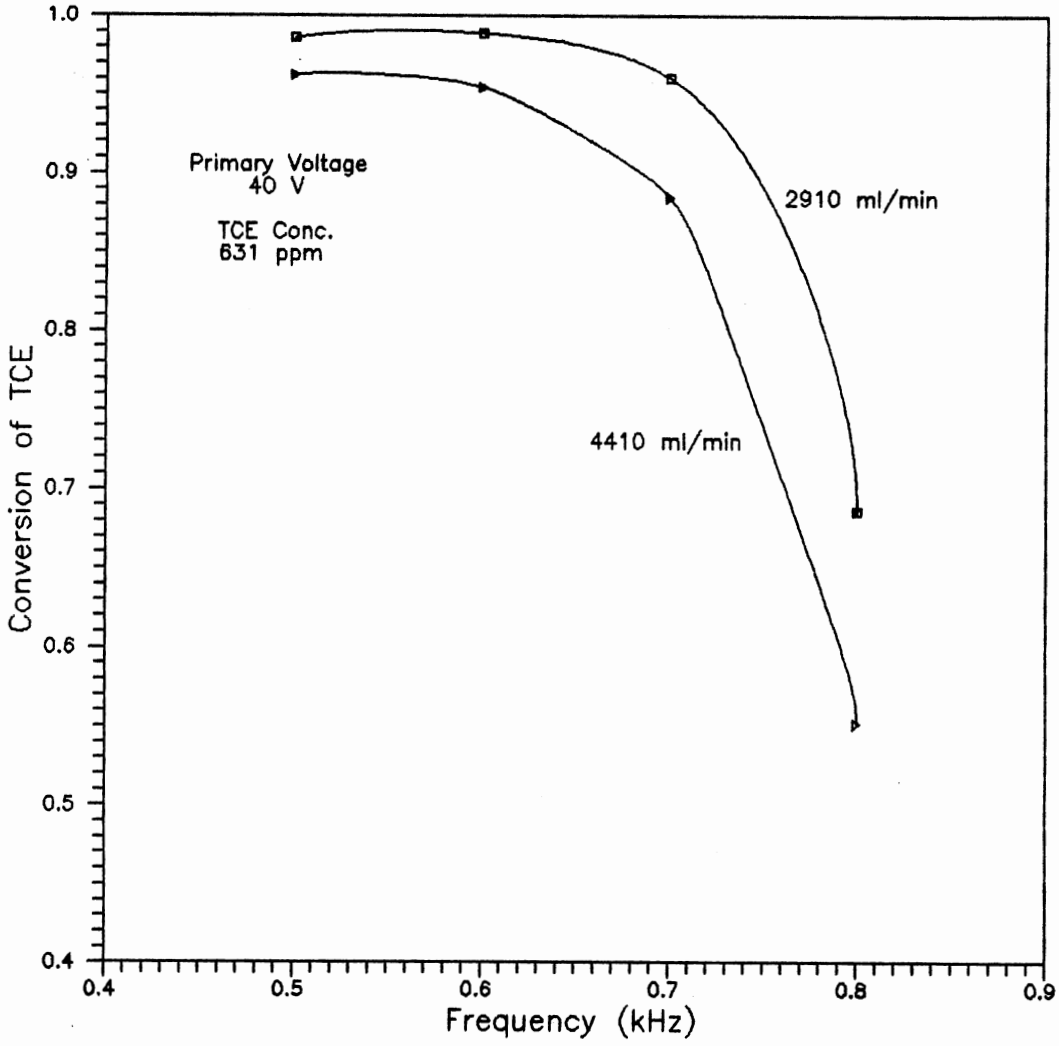

Figure 28. Effect of Flow Rate and Frequency on Conversion of TCE in Dry Air Discharges for Reactor D.

frequency.

For the conditions of low-frequency and relatively high-pressure used in these experiments, the time required for the ions to cross the gap is much less than the period of the applied field. The ions undergo many collisions per transit. Accordingly, the processes of activation occurring in the discharge are fast compared to the mean residence time of the gas. As long as a more uniform discharge is maintained, conversion would be high.

The effects of increasing flow rate are further shown in Tables XV and XVI. An increase in flow rate decreases the total power input and effective current of the reactor. With regard to voltage and gas temperature, the situation is reverse. At high gas flow rate, higher gas temperature is directly related to more discharge power to the reactor. Note that the wall temperature rise of the reactor is partly due to recombination of free radicals on the glass wall.

Figure 29 shows the variation of conversion with TCE concentration for reactors C and D. The observed decrease in conversion with increase in concentration can be explained on the basis of electron density. The data imply that TCE is attacked by electrons easily. Consequently, concentration increases appear to reduce the number of electrons and therefore decreases electron density. Decreases in electron density lead to lower conversions. These conversion curves bear a resemblance to those in Figures 20-23. It is interesting to note that conversion is

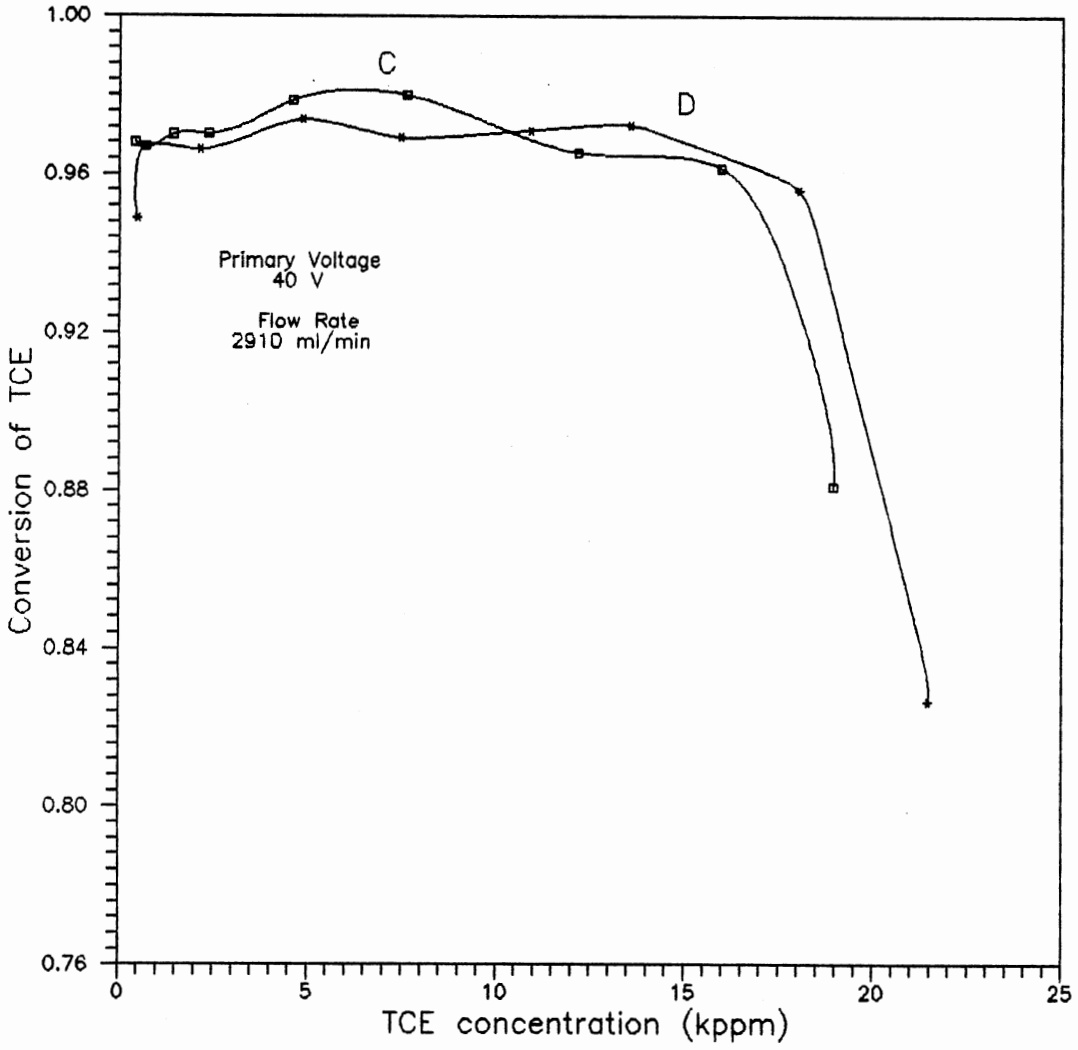

Figure 29. Effect of Concentration on Conversion of TCE in Dry Air Discharges.

TABLE XV

EFFECT OF FLOW RATE ON DISCHARGE CURRENT AND TOTAL POWER INPUT FOR REACTOR D

	Flow Rate (ml/min)			
	2910		4410	
Frequency (Hz)	Discharge Current (mA)	Total Power Input (W)	Discharge Current (mA)	Total Power Input (W)
500	7.508	106.0	5.802	98.5
600	6.485	109.0	5.485	96.0
700	6.143	92.5	5.119	93.5
800	5.460	86.5	4.778	91.0

TABLE XVI

EFFECT OF FLOW RATE ON GAS TEMPERATURE AND VOLTAGE FOR REACTOR D

	Flow Rate (ml/min)			
	2910		4410	
Frequency (Hz)	Voltage (V)	Gas Temp. (°C)	Voltage (V)	Gas Temp. (°C)
500	9220	39.2	10150	44.8
600	9235	37.2	9425	42.8
700	8500	36.2	8995	40.8
800	8230	31.2	8470	32.8

inversely proportional to voltage.

Van Drumpt (16) conducted an experimental investigation of the oxidation of hydrogen chloride in a 50 Hz silent discharge reactor. He concluded that conversion increased almost linearly with the applied voltage. These results seem to qualitatively contradict the present results. In his system increasing the primary voltage raised the applied voltage and hence led to higher power input. Since higher power results in higher conversion, it is obvious that the effect of discharge power was not taken into account in Van Drumpt's analysis. Although the electron is essential condition for gas discharge, discharge reaction is mainly controlled by electron density. The fact that a higher electric field increases the energy of the electrons does not correspond to higher electron density. As discussed previously, the threshold discharge power really controls reaction in the discharge.

Destruction of Trichloroethylene in Wet Air Discharges

In this section, humid air is used in place of dry air. Unless otherwise stated, the oxidation of TCE in the reactors involves wet air discharges.

Figure 30 shows the effect of TCE concentration and flow rate on conversion for wet air discharge in reactor C. A decrease in conversion is observed again due to an increase in flow rate. A visual inspection of the Figure

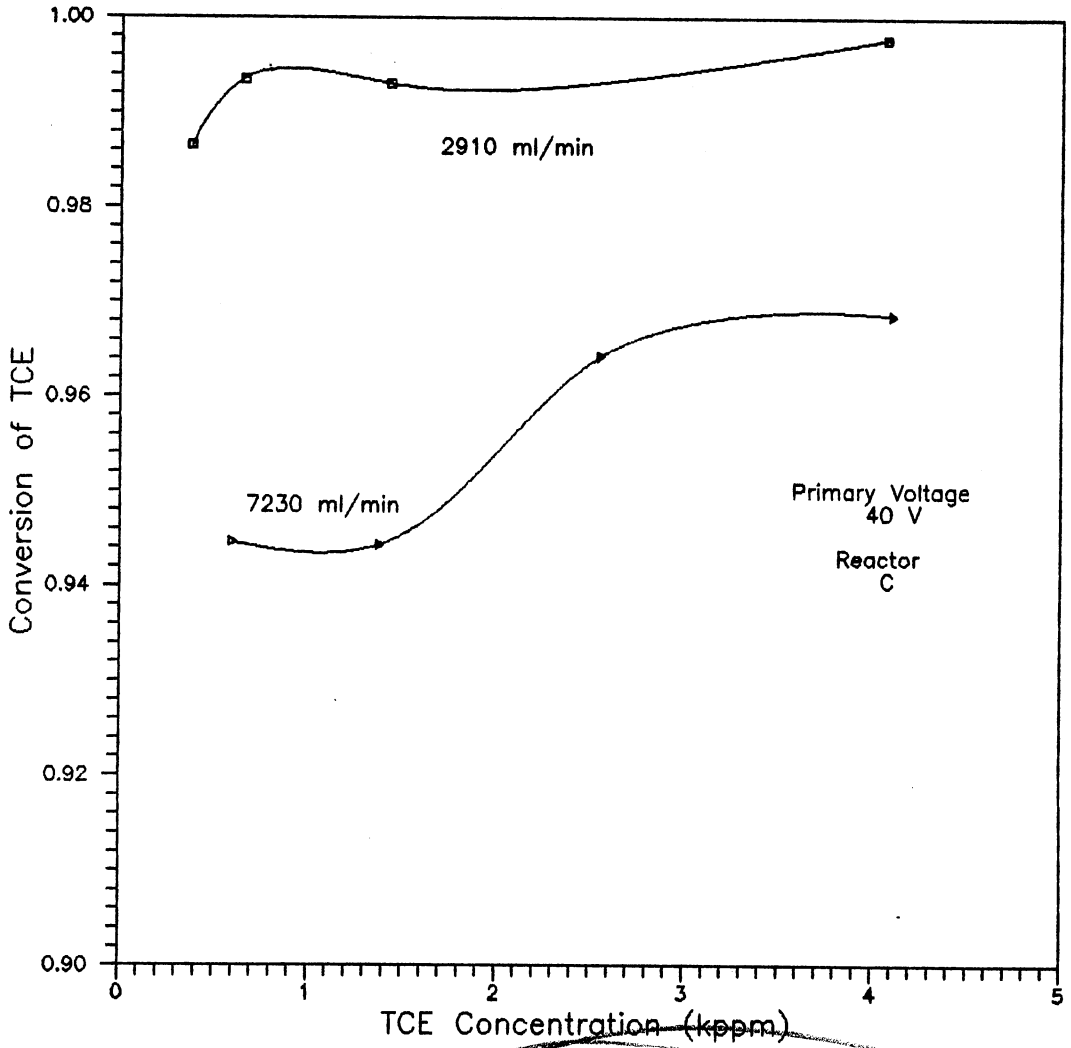

Figure 30. Effect of Concentration and Flow Rate on Conversion of TCE in Wet Air Discharges.

also indicates that the two conversion curves are almost similar except that conversion increases are greater at 7230 ml/min than at 2910 ml/min, as shown from 1300 to 4000 ppm. Further, conversion curves are approximately flat at a certain range of concentration. This shows that reaction mechanism is changed as a critical concentration is reached.

These trends may be explained partly from wall charge and electron density viewpoints. As mentioned previously, at low frequency, the electrons are driven to an electrode surface in each half cycle of the applied field. Under these conditions, the secondary wall process therefore plays a significant role in determining discharge reactions. This wall catalytic process can be affected by air flow rate because of the pressure and air stripping effects. These effects probably clarify the phenomenon that increasing flow rate increases discharge power. It was observed that at a flow rate of 2910 ml/min, the discharge disappears as concentration exceeds 4000 ppm. Obviously, more electrons are consumed by TCE with a lower ionization potential than air. As a result, TCE concentration should have a direct influence over reaction mechanism.

Referring to Figures 22 and 30, the humidification of dry air is shown to have an enhancing effect on conversion. Higher concentration, resulting in an increases conversion, somewhat increases the amount of water vapor in the discharge. With this effect, a high conversion is achieved at a flow rate of 7230 ml/min even though the gas residence

time decreases about 2.5 times. This can occur only when electron density is sufficiently high.

Water vapor is already known to prohibit the formation of ozone (28). In a wet air/TCE discharge, TCE is observed to greatly eliminate the ozone. It is concluded that hydrocarbon derivatives not only prohibit the production of ozone but also are very active in the discharge. The addition of water vapor to dry air discharges was found to quench the discharge and the lowering of the applied voltage and gas temperature resulted. Further tests need to be performed to examine to what extent the humidity affects the oxidation of TCE in the discharge.

For two reactors in parallel, the flow direction of the gas stream affects the performance of the reactors. The data in Table XVII were taken for reactor C-D and reactor D-C at a primary voltage of 40 and 400 Hz. Note that the gases were fed to reactor D and reactor C for reactor D-C and reactor C-D, respectively. As can be seen, comparison of data in Figure 30 and Table XVII shows an apparent improvement in conversion compared to a single reactor. The flow direction of gas stream is also shown to influence the effluent gas temperature. Generally, when the feed gas enters the reactor with a low breakdown voltage, such as reactor D, an intense glow results and the gas temperature is higher. With a high breakdown voltage of the succeeding reactor, the gas temperature of this reactor should be lower due to a low discharge power and the cooling effect caused

TABLE XVII

EFFECT OF FLOW DIRECTION ON CONVERSION AND TOTAL POWER INPUT

Reactor	Concentration (ppm)	Total Power Input (W)	Conversion (%)
C-D[a]	419.23	117.5	99.37
	738.61	116.5	99.58
	1673.52	115.0	>99.99
D-C[a]	355.90	141.5	99.26
	929.30	136.0	99.66
	1126.74	136.5	99.72
D-C[b]	353.15	129.5	98.53
	356.20	131.5	99.85
	1137.93	136.5	99.93
	1696.44	135.5	99.73

a - 2910 ml/min
b - 7230 ml/min

by the environment. As a result, reactor C-D leads to higher effluent temperatures than reactor D-C. Effluent temperatures of these two reactors are referred to the Appendix C (Tables XXXXV and XXXXVI).

Lower gas temperature is generally caused by lower discharge power. However, the data in Table XVII show that reactor D-C has a higher total power input. Apparently, more power is dissipated in the power source as the impedance of the circuit is mismatched. It is interesting to note that increasing the flow rate of the reactor D-C from 2910 to 7230 ml/min gives rise to much higher gas temperature while the total power input is almost the same. Therefore, the total power input is not always a

definite indication of discharge power. This aspect is important in determining optimum condition since electrical discharge is known as an energy-consuming process.

Kinetic Data Correlation

In the case of thermal reactors the extent of reaction is proportional to gas residence time. This is not the case for discharge reactors because the extent of reaction depends on the electron profile in the discharge. It is known that for a silent discharge the plasma is a non-equilibrium mixture in which the electrons have a relatively high temperature, but the neutrals and positives are near ambient. This implies that kinetic modeling in the discharge is very complex. An empirical approach is considered to solve this kinetic problem.

From experimental observations, TCE destruction in dry air discharges appears to be most sensitive to the threshold power and determines the reaction mechanism and the types of reaction products. Above threshold power, conversion is relatively high once reaction equilibrium is reached. However, discharge power much higher than the threshold power has little advantage of increasing conversion. TCE conversions is found to be approximately constant over a wide range of TCE concentrations in humid air. The reaction kinetic of TCE is either first-order or second-order. Increasing flow rate decreases the destruction efficiency.

Since the discharge power is an implicit function of TCE

concentration, the empirical correlation is therefore based on the premise that below the threshold power, conversion increases with increasing discharge power and can be expressed in the following way

$$X_a = 1 - \exp(-0.3939 W_s/(1+0.076 Q^{1.2})) \qquad (5.3)$$

where X_a = TCE conversion

Q = flow rate of gas feed, l/min

Equation (5.3) provides a means of estimating a possible threshold power. The calculated power can be used to determine possible operating conditions of discharge reactors. The data used for the correlation and the predicated values of conversion are listed in Table XVIII. Note that the discharge powers which are used are the predicted values obtained from non-destructive (dry air discharge) data.

TABLE XVIII

DATA FOR CORRELATION AND ESTIMATED CONVERSION

Q (l/min)	W_s (W)	X_a (%)	X_{apre} (%)
2.91	8.58	97.77	93.77
2.91	8.14	98.07	92.81
2.91	7.01	97.35	89.64
2.91	4.53	93.05	76.94
2.91	10.98	98.11	97.13
2.91	8.47	96.24	93.55
2.91	6.35	90.71	87.18
2.91	7.53	97.56	91.25
2.91	7.80	97.02	91.99
2.91	6.91	97.97	89.30
2.91	6.11	94.55	86.15
2.91	1.33	12.50	34.99
2.91	11.45	98.57	97.54
2.91	8.51	98.86	93.63
2.91	7.37	95.98	90.79
4.41	7.69	90.63	89.73
4.41	10.40	96.18	95.40
7.23	12.52	94.46	95.92

CHAPTER VI

CONCLUSIONS AND RECOMMENDATIONS

The double frequency-tuned capacitive discharge reactor system used in this work is an impedance-changing circuit. The output of the power source is connected to a transformer coupled to a capacitive discharge reactor. The system characteristics are that for a given primary voltage the impedances of these three devices are tuned simultaneously by an oscillator in the power source . This greatly increases the versatility in transferring power to the reactor. Since the impedance of the discharge reactor is high, more energy is dissipated in the power source if a good match is not achieved. Accordingly, examination of the factors affecting the power consumption in the operation and design of a discharge reactor is extremely important.

This research attempts to search for a more general criterion for operating discharge reactors at high conversion and low total power input and explores a conceptual approach to the design of a capacitive discharge reactor for a specific power system. A series of experiments were undertaken to examine the nature of the system and the effects of operating conditions on conversion of trichloroethylene (TCE) in air discharges.

The following conclusions are drawn from the results of this investigation:

1. The use of a double frequency-tuned capacitive discharge reactor system has been shown to be a highly effective technique for the decomposition of TCE. High destruction efficiency of TCE is achieved for a gas residence time of 0.1 -0.8 s, which is in the laminar flow regime.
2. A breakdown model was developed to predict the breakdown voltage and frequency. The predicted results are in good agreement with the experimental data. The breakdown voltage increases with the primary voltage. This is because, at a lower frequency, the electric field must be raised to increase electron energy to effectively initialize the discharge. Increasing the primary voltage decreases the breakdown frequency. The capacitance of a reactor shows a considerable influence over the breakdown frequency. Breakdown data of a single reactor can be used for the scale-up of a reactor with the same diameter as a single reactor.
3. The maximum voltage of a reactor usually corresponds with high discharge power but sometimes more energy is consumed in the power source due to a mismatch in the circuit. This phenomenon can be avoided by choosing a higher frequency. In other words, from the power-frequency curve of dry air discharges, the frequency which is chosen is with a discharge power slightly greater than the threshold power.

4. For all reactors, the breakdown frequency is below the resonance frequency of the transformer under no load conditions. At the start of gas discharge, the reactor leads to either partial breakdown or direct breakdown, depending on the internal diameter and type of gas. A value of internal diameter ratio greater than 1.46 causes a direct breakdown with the discharge being more uniform.
5. Humid air enhances the oxidation of TCE in the discharge. TCE similar to water vapor inhibits the formation of ozone but introduces higher discharge currents than both dry air and humid air. This effect excludes the possibility of direct prediction of discharge power using a power model because of the drastic increase in capacitance. The power can be evaluated indirectly using dry air discharge data since these two discharges have almost the same primary current which is an indication of the power transferred from the power source to the transformer.
6. A threshold power level exists for each reactor, below which there is a drastic decrease in conversion. High flow rate through the discharge gives rise to a high discharge power, which a high conversion results.
7. A kinetic equation was correlated in terms of discharge power and gas flow rate. A dynamic model was developed to evaluate the dynamic capacitance and resistance in the discharge. Combination of the breakdown and power models coupled to the kinetic and energy equations allows

determination of the appropriate geometry and operating conditions for a reactor with a given power transfer system.

The following recommendations are made based on the results of this study.

1. The discharge power is a crucial factor in the destruction efficiency of TCE and in evaluating the performance of discharge reactors. The power model appears to make reasonable predictions of discharge power. Since the experimental data are not allowed to support its validity, a better apparatus such as an oscilloscope is required to measure the actual power.
2. The humidification of air has been shown to increase conversion. The extent that the humidity enhances the oxidation of TCE is unknown. Further investigation on this effect should be performed in future work.
3. The static capacitance of a reactor has great effect on the breakdown frequency. Although the breakdown model is available to predict breakdown frequency for the present power system, more breakdown data for large-scale reactors should be collected to check the model.
4. For commercial application of this technology, one of the most desirable operating conditions is a high flow rate and high pressure. Higher pressure increases breakdown voltage but reduces gas volume and increases residence time of the gas. The effect of higher pressure must therefore be studied.

5. Detailed analysis of the gas product is needed to examine possible toxic hazards. Elimination of toxic materials may require additional engineering evaluation. This is an important step before the technique is utilized for large-scale decomposition of TCE.

BIBLIOGRAPHY

1. Alston, L. L., High-Voltage Technology, Oxford Univ. Press, (1968).

2. Peek, F. W. Dielectric Phenomena in High Voltage Engineering, McGraw-Hill, New York (1915).

3. Chapman, B., Glow Discharge Processes, John Wiley & Sons, New York (1980).

4. Maxfield, F. A. and R. R. Benedict, Theory of Gaseous Conduction and Electronics, McGraw-Hill, New York (1941)

5. Birk, J. B. and J. H. Schulman, Progress in Dielectrics, John Wiley & Sons, New York, 1 (1959).

6. Birk, J. B. and J. H. Schulman, Progress in Dielectrics, John Wiley and Sons, New York, 2 (1960).

7. Thorpe, M., "Plasma Energy: the Ultimate in Heat Transfer." Chem. Eng. Prog., 85(7), 43-53 (1989).

8. Loeb, L. B., Fundamental Processes of Electrical Discharge in Gases, John Wiley & Sons, New York (1939).

9. Works, C. N. and T. W. Dakin, "Dielectric Breakdown of Sulfur Hexafluoride in Non-uniform Fluids." Trans. AIII, 72, 682-689 (1951).

10. Plaumbo, F. J. and F. Fraas, "The Removal of Sulfur from Stack Gases by an Electrical Discharge." J. Air Pollut. Contr. Assoc., 21(3), 143-144 (1971).

11. Penning, F. M., Electrical Discharges in Gases, Macmillan, New York, 37 (1957).

12. Klyarfel'd. B. N., Investigation into Electrical Discharges in Gases, Macmillan, New York, (1964).

13. Leedy, H. A., "Ozone Chemistry and Technology", Adv. Chem. Soc. Ser., 21 (1959).

14. Fraser, M. E., H. G. Eaton and R. S. Sheinson, "Initial Decomposition Mechanisms and Products of Dimethyl Methylphosophonate in an Alternating Current Discharge." Environ. Sci. Tech., 19(10), 946-949 (1985).

15. Thomas, C. L., Egloff, G. and J. C. Morrel, "Reactions of Hydrocarbons in Electrical Discharges." Chem. Revs., 28 (1941).

16. Van Drumpt, J. D., "Oxidation of Hydrogen Chloride with Molecular Oxygen in a Silent Electrical Discharge." Ind. Eng. Chem., Fundam., 11, 594-595 (1972).

17. Bailin, L. J., M. E. Sibert, M. E. Jonas and A. T. Bell, "Microwave Decomposition of Toxic Vapor Simulants." Envir. Sci. & Tech., 9, 254-258 (1975).

18. Tevault, D. E., M. Chester, P. Simmons and J. G. Birmingham, "NOx Production in a Silent Electric Discharge as a Function of Humidity, Frequency and Power." Unpublished results.

19. Clothiaux, E. J., J. A. Koropchak and R. R. Moore, "Decomposition of an Organophosphorus Material in a Silent Electric Discharge." Plasma Chem. Plasma Process., 4(1), 15-20 (1984).

20. Moore, R. R. and J. G. Birmingham, "The Decomposition of Toxic Chemicals in a Low Temperature Plasma Device." HAZPRO '87 Conference Proceedings, Chatanooga, Tennessee (June 8-12, 1987).

21. Fraser, M. E. and R. S. Sheinson, "Electric Discharge-Induced Oxidation of Hydrogen Cyanide." Plasma Chem. Plasma Process., 6(1), 27-37 (1986).

22. Moore, R. R., J. G. Birmingham and J. A. Koropchak, " The Decomposition of Cyanide Compounds in an AC Silent Discharge Plasma Reactor." Unpublished results.

23. McInally, M. "Light Emission and Ozone Formation in Ozonizers, " Electrochimica Acta, 14, 1167-1171 (1969).

24. Davis, S. R. and D. E. Tevault, "FTIR Studies of Plasma-Induced Decomposition of Dimethylsulfide in an Air-like Environment." HAZPRO '87 Conference Proceedings, Chatanooga, Tennessee (April 8-12, 1987).

25. Sheinson, R. S., "Contaminant Destruction Chemistry in Electric Discharge." HAZPRO '87 Conference Proceedings, Chatanooga, Tennessee (April 8-12, 1987).

26. Neely, W. C., S. R. Best and E. J. Clothiaux, "The Decomposition of Gas Phase Formaldehyde by Plasma Discharge." Proceedings of the 1984 Scientific Conference on Chemical Defense Research, Aberdeen, Maryland (1984).

27. Coffman, J. A. and W. R. Browne, "Corona Chemistry." Sci. Am., 89, 91-97 (1965).

28. My, N. L. and P. N. Sahgal, "Generation of Ozone in Two-Dielectric Ozonizer." J. Chem. Eng., 40, 175-179 (1989).

29. Piatt, M. A., "Methane Destruction in an Alternating Current Plasma Reactor." MS thesis, Oklahoma State Univ., Stillwater (1988).

30. Hosselft, L. M. L. F., "Increased Efficiency of Ozone-Production by Electric Discharges." Electrochimica Acta, 18, 1033-1041 (1973).

31. Dibelius, N. R., J. C. Fraser, M. Kawahata and C. D. Doyle, "Corona Processing of Coal." Chem. Eng. Prog., 60(6), 41-44 (1964).

32. Lunt, R. W. and K. G. Emeleus, "Chemical Reaction in Ionized Gases." Nature, 137, 404 (1936).

33. Giao, T. N. and J. B. Jordan, "Modes of Corona Discharge in Air." IEEE Trans., 87(5), 1207-1212 (1968).

34. Manley, T. C., "The Electric Characteristics of the Ozonator Discharge." Trans. Electrochem. Soc., 84, 83-96 (1943)

35. Gould, R. F., Chemical Reactions in Electrical Discharges, Adv. Chem. Ser., 80, 29-47) (1969).

36. Birmingham, J. G., R. R. Moore and Jerome P. Gilman, "The Application of Electrical Discharge Plasmas for the Destruction of Environmental Contaminants. " HAZPRO 87' Conference Proceeding, Chatanooga, Tennessee (April 8-12, 1987).

37. Masuda, S. and E. Kiss, "On Streamer Discharges in Ceramic-Based Ozonizer Using High Frequency Surface Discharge." Inst. Phys. Conf., 85, 243-254

(1987).

38. Lind, S. C. and G. Glockler, " III. The Chemical Effects of Semi-Corona Discharge in Gaseous Hydrocarbon." J. Am. Chem. Soc., 51, 2811-2822 (1929).

39. Lind, S. C. and G. Glockler, "The Chemical Effects of Electrical Discharges in Butane. Fractionation of the Liquid Production." J. Am. Chem. Soc., 51, 3655-3660 (1929).

40. Faes, Y., "Ozoneurs: Leur Théorie et Application des Techniques Nouvelles à Semi-Conducteurs à Leur Alimentation." R.G.E., 84(1), 13-23 (1975).

41. Kunhardt, E. E. and L. H. Luessen, Electrical Breakdown and Discharge in Gases, NATO ASI Ser. B, 89b, Plenumn Press, New York (1983).

42. Honda, K. and Y. Naito, "On the Nature of Silent Electric Discharge." J. Phys. Soc. Jap., 10, 1007-1011 (1955).

43. McEachron, K. B., "The Production of Nitric Oxides and Ozone by High Voltage Electric Discharge." Bull. Purdue Univ., 9, 160 (1922).

44. Thornton, W. M., "The Electric Strength of Gases, Measured by Corona Discharge." Phil. Mag. 28, 666-678 (1939).

45. Flamm, D. L., "On the Oxidation of Hydrogen Chloride in a Silent Discharge." Ind. Eng. Chem., Fundam., 13 (1), 91-92 (1974).

APPENDICES

APPENDIX A

REPRODUCIBILITY

The experimental data were taken under identical conditions in order to estimate the reproducibility of the testing procedures. For reactor C, dry air discharge and breakdown data were considered, as shown in Tables XXXXVIII AND XXXXIV. The standard deviations and probable errors for electrical parameters and gas temperature are shown in Table XIX. For the same reactor, data from Table XXXXVI were used to estimated the standard deviation and probable error for TCE concentration and conversion and are shown in Table XXI.

TABLE XIX

ERROR ANALYSIS OF NON-DESTRUCTIVE DATA

	I_p (mA)	V_s (V)	W_t (W)	T (°C)
	483	11580	93.0	48.5
	482	11590	87.5	49.5
	478	11570	87.5	46.5
	496	11510	88.5	49.5
	502	11510	90.0	49.5
SD	10	39	2.3	1.3
PE	7	26	1.6	0.9

SD - Standard Deviation
PE - Probable Error

TABLE XX

ERROR ANALYSIS OF BREAKDOWN DATA

	Primary Voltage (V)	Breakdown Frequency (Hz)	Breakdown Voltage (V)
	40	550	10500
		552	10620
		548	10400
SD		2	110
PE		1	74
	45	525	10840
		512	10460
		518	10560
		518	10520
		522	10700
SD		5	153
PE		3	103

TABLE XXI

ANALYSIS OF DESTRUCTIVE DATA OF TCE

TCE Concentration	Conversion (%)
325.26	97.98
334.88	99.80
353.15	98.53
356.20	99.85
302.43	98.46
306.29	99.83
SD 22.76	0.84
PE 15.39	0.57

APPENDIX B

BREAKDOWN VOLTAGE CALCULATION

The breakdowm voltage can be predicted using equation (4.3). The data used in the calculation are shown as follows:

tube diameters of reactor A:

$D_1 = 1.27$ cm $D_2 = 1.5$ cm $D_3 = 2.19$ cm $D_4 = 2.5$ cm

dielectric constant:

$K_g = 4.6$ (glass) $K_a = 1$ (air)

dry air:

pressure: 76.2 cm Hg temperature: 23 °C

The air is assumed to be an ideal gas and the relative density of the air can be obtained from equation (4.4).

$$\delta = \frac{(3.921)(76.2)}{296} \approx 1.009$$

Inserting the numercial values into equation (4.3) gives

$$V_b = (10.96)(1.5)(1.009)\left(1 + \frac{0.308}{\{(1.5)(1.009)\}^{\frac{1}{2}}}\right)$$

$$\left\{\left(\frac{1}{4.6}\right)\left(\ln \frac{(1.5)(2.5)}{(1.27)(2.19)}\right) + \ln \frac{2.19}{1.5}\right\}$$

$$\approx 9{,}200 \text{ V}$$

APPENDIX C

PROGRAM LISTING FOR POWER AND DYNAMIC MODELS

```
C*************************************************************
C                                                            C
C      THIS PROGRAM IS MAINLY AVAILABLE FOR PREDICTING       C
C                        DISCHARGE POWER                     C
C                                                            C
C*************************************************************
C                            NOTATIONS                       C
C                                                            C
C      D(I) : TUBE DIAMETERS, START FROM INNER TUBE (cm)     C
C        RL : LENGTH OF THE REACTOR (m)                      C
C      CK(I) : DIELECTRICS, START FROM INNER TUBE            C
C       V(I) : APPLIED VOLTAGE (V)                           C
C      FR(I) : APPLIED FREQUENCY (Hz)                        C
C       T(I) : EXIT GAS TEMPERATURE (oC)                     C
C       IFO  : REFERENCE FREQUENCY WHICH GAS TEMPERATURE     C
C              STARTS TO INCREASE                            C
C         TO : INLET GAS TEMPERATURE (oC)                    C
C         FC : CORRECTION FACTOR OF FREQUENCY                C
C         N  : SET OF DATA                                   C
C*************************************************************C
      DIMENSION D(5),CK(10),V(10),FR(10),T(10)
      OPEN(UNIT=7, FILE='POWER.DAT')
      READ(6,*) N,RL                          20.2
      READ (6,*) (D(I),I=1,4)  1.27 1.50 2.19 2.56
      READ (6,*) N,TO,IFO,FC   1, 25, 5, 580, 0.2
      READ (6,*) (CK(I),I=1,N)   3
      READ (6,*) (V(I),I=1,N)
      READ (6,*) (FR(I),I=1,N)
      READ (6,*) (T(I),I=1,N)
      WRITE(7,30) NO
      ESC=55.63*15500
      FO=IFO
      DO 50 J=1,3                  * RL
50    C(J)=55.63*CK(J)/ALOG(D(J+1)/D(J))
      CA=C(2)
      CD=C(1)*C(3)/(C(1)+C(3))
      DO 200 J=1,N
      FRR=FR(J)
      IFR=FRR
      TT=0.5*(TO+T(J))
      DEN=298/(298+TT)
      VA=(FO/FRR)**FC*ESC*D(2)*DEN*(1+0.308/(DEN*D(2))**0.5)/CA
      VO=VB*2**0.5                 VB=V(I)
      VR=VA/VO
      CR=CA/CD
      APHA=2*VR*(1+CR)-1
      IF (ABS(APHA).GT.1) THEN
      WRITE (7,35)
      WRITE (7,55)
      GO TO 99
      ENDIF
      A=ASIN(APHA)
      PI=3.1415927
      PR=0.25*PI
```

```
      BETA=0.5*A+0.25*SIN(2*A)
      SIGM=(CR/(CR+1))**2
      BD=(PR-BETA+SIGM*(PR+BETA))**0.5
      W=2*PI*FRR
      EIF=1000*CD*RL*W*VO*BD*1.E-12/PI**0.2
      P=4*FRR*VA*VO*CD*RL*(1-VR*(1+VR))*1.E-12
      EID=EIF/1000
      DYC=EID**2/(W*((EID*VO)**2-P**2)**0.5)
      IDY=DYC
      IOHM=P/EID**2
      PFA=P/(EID*VB)
      VAM=VA/2**0.5
99    WRITE(7,30)
      WRITE(7,90) IFO
      WRITE(7,80) IFR
      WRITE(7,60) VB
      WRITE(7,40) TT
      WRITE(7,15) VAM
      IF (ABS(APHA).GT.1) THEN
      GO TO 100
      ENDIF
      WRITE(7,20) EIF
      WRITE(7,25) P
      WRITE(7,70) IDY
      WRITE(7,65) IOHM
200   WRITE(7,10) PFA
 10   FORMAT(12X,'Power factor :',16x,F5.3,//)
 15   FORMAT(12X,'Gas breakdown voltage (V) :',F7.1)
 20   FORMAT(12X,'Secondary current (mA) :'4X,F7.3)
 25   FORMAT(12X,'Discharge power (W) :'8x,F7.3)
 30   FORMAT(12X,'Reactor No.:'19X,I1)
 35   FORMAT(12X,'The gas breakdown of the reactor does not
 40   FORMAT(12X,'Gas temperature (oC) :',8XF4.1)
 55   FORMAT(12X,'-- check tube diameters')
 60   FORMAT(12X,'Applied voltage (V) :',10x,F7.1)
 65   FORMAT(12X,'Discharge resistance (ohm) :'I10)
 70   FORMAT(12X,'Dynamic cpacitance (pf) :'3x,I10)
 80   FORMAT(12X,'Applied frequency (Hz) :',6x,I4)
 90   FORMAT(12X,'Reference frequency (Hz) :',4x,I4)
100   END
```

APPENDIX D

EXPERIMENTAL DATA

TABLE XXII

OPEN-CIRCUIT TEST OF TRANSFORMER
RUN 1

V_p (V)	f (Hz)	I_p (mA)	V_s (V)
40	60	159	5375
	100	118	5400
	150	93	5405
	200	84	5350
	250	71	5390
	300	60	5470
	350	51	5640
	400	50	5830
	450	52	6000
	500	57	6230
	550	66	6530
	600	79	6920
	650	95	7380
	700	116	7980
	750	143	8770
	800	178	9820
	850	224	11180
	900	289	13120
	925	NA	14950
50	60	189	6700
	100	136	6740
	150	108	6770
	200	93	6730
	250	78	6790
	300	68	6900
	350	61	7120
	400	65	7360
	450	69	7590
	500	78	7900
	550	91	8300
	600	109	8820
	650	130	9430
	700	159	10250
	750	195	11310
	800	243	12760
	850	308	14750
	856	316	15050

TABLE XXII (Continued)

V_p (V)	f (Hz)	I_p (mA)	V_s (V)
60	60	225	8040
	100	155	8130
	150	122	8170
	200	104	8130
	250	89	8220
	300	79	8350
	350	73	8630
	400	81	8940
	450	88	9220
	500	99	9610
	550	116	10100
	600	138	10735
	650	165	11530
	700	201	12590
	750	245	13910
	780	280	14990
70	60	266	9330
	100	174	9470
	150	135	9540
	200	116	9500
	250	100	9610
	300	90	9780
	350	86	10100
	400	97	10490
	450	106	10830
	500	120	11330
	550	141	11890
	600	168	12670
	650	200	13610
	700	243	14920
	705	246	15010
80	60	312	10550
	100	192	10740
	150	147	10840
	200	126	10910
	250	110	11040
	300	100	11240
	350	101	11620
	400	113	12080
	450	124	12480
	500	143	13030
	550	167	13750
	600	199	14650
	623	210	15000

TABLE XXIII

OPEN-CIRCUIT TEST OF TRANSFORMER
RUN 2

V_p (V)	f (Hz)	I_p (mA)	W_p (W)	W_t (W)
40	60	165	4.35	81.0
	70	281	4.30	76.0
	80	250	4.20	72.5
	90	229	4.00	70.0
	100	214	3.95	67.5
	110	201	3.70	66.0
	120	191	3.55	63.5
	130	184	3.45	61.5
50	60	200	6.70	95.0
	70	181	6.40	84.0
	80	167	6.15	80.5
	90	156	5.94	76.5
	100	149	5.75	73.5
	110	141	5.55	71.5
	120	135	5.40	70.0
	130	130	5.30	68.5
60	60	237	9.30	101.5
	70	181	6.40	93.5
	80	193	8.50	88.5
	90	179	8.17	84.0
	100	170	7.85	81.0
	110	161	7.72	78.5
	120	153	7.48	76.0
	130	148	7.30	74.0
70	60	280	12.25	114.0
	70	243	11.64	103.5
	80	220	11.18	96.0
	90	203	10.83	91.5
	100	191	10.50	87.5
	110	181	10.15	84.5
	120	173	9.92	84.0
	130	165	9.70	80.0
80	60	332	15.70	136.0
	70	281	14.75	116.5
	80	250	14.15	106.5
	90	229	13.17	100.0
	100	214	13.30	95.0
	110	201	12.90	91.5
	120	191	12.55	88.5
	130	184	12.30	86.0

TABLE XXIV

NON-DESTRUCTIVE TEST
RUN 3

Reactor: A Status: Instantaneous
Gas: Dry Air Flow Rate: 2910 ml/min
Room Temp.: 19.3 °C Pressure: 762 mm Hg

V_p (V)	f (Hz)	I_p (mA)	W_p (W)	V_s (V)	W_t (W)
40	60	166	4.70	5020	80.0
	70	152	4.65	5040	75.5
	80	141	4.45	5060	72.5
	90	132	4.30	5070	69.5
	100	124	4.10	5080	66.0
	110	117	4.03	5090	64.5
	120	112	3.90	5100	62.5
	130	107	3.75	5120	61.0
70	60	278	12.84	8640	115.0
	70	242	12.40	8710	103.5
	80	218	11.95	8770	96.5
	90	203	11.62	8810	91.5
	100	190	11.30	8850	87.5
	110	179	11.08	8800	85.0
	120	173	11.05	8920	92.5
	130	225	15.25	8900	96.5
80	60	357	19.30	9890	141.0
	70	314	19.05	9960	126.0
	80	294	19.44	10100	120.0
	90	282	19.70	10090	116.0
	100	281	20.45	10105	115.5
	110	279	21.48	10275	115.5
	120	285	22.28	10485	115.5
	130	295	23.10	10520	119.0

TABLE XXV

NON-DESTRUCTIVE TEST
RUN 4

Reactor: B Status: Instantaneous
Gas: Dry Air Flow Rate: 2910 ml/min
Room Temp.: 18 °C Pressure: 762 mmHg

V_p (V)	f (Hz)	I_p (mA)	W_p (W)	V_s (V)	W_t (W)
40	60	163	4.65	5020	69.0
	70	148	4.60	5060	74.5
	80	137	4.50	5175	70.5
	90	128	4.31	5095	68.5
	100	120	4.15	5110	65.5
	110	113	4.10	5130	63.5
	120	107	3.90	5150	61.0
	130	102	3.85	5180	59.5
60	60	251	11.30	6245	95.5
	70	229	11.30	7550	98.5
	80	218	11.30	7540	95.0
	90	212	11.55	7430	93.5
	100	207	11.93	7740	91.5
	110	210	11.95	7830	91.5
	120	218	12.45	7830	94.0
	130	228	13.25	7830	95.5
70	60	297	15.10	8680	119.5
	70	269	15.10	8790	111.0
	80	254	15.30	8870	105.5
	90	247	15.50	8870	103.5
	100	243	16.10	8990	101.5
	110	250	16.50	9010	103.5
	120	263	17.10	9270	106.5
	130	267	17.50	9330	108.5
80	60	348	19.43	9880	136.0
	70	308	19.15	9950	123.5
	80	285	19.45	10130	116.5
	90	280	19.65	10190	114.0
	100	275	20.32	10265	113.5
	110	278	20.91	10510	113.5
	120	292	21.41	10650	116.5
	130	307	22.35	10770	121.5

TABLE XXVI

NON-DESTRUCTIVE TEST
RUN 5

Reactor: C Status: instantaneous
Gas: Dry Air Flow Rate: 2910 ml/min
Room Temp.: 19 °C Pressure: 762 mm Hg

V_p (V)	f (Hz)	I_p (mA)	W_p (W)	V_s (V)	W_t (W)
40	60	167	4.85	5050	81.0
	70	153	4.65	5170	76.5
	80	142	4.45	5090	73.5
	90	133	4.30	5100	72.0
	100	125	4.13	5120	66.5
	110	118	4.05	5125	64.5
	120	113	3.90	5140	62.5
	130	108	3.85	5160	62.5
50	60	201	7.15	6280	91.0
	70	181	6.85	6315	85.0
	80	166	6.55	6340	81.0
	90	156	6.33	6360	76.5
	100	147	6.15	6390	74.5
	110	139	5.98	6400	71.5
	120	132	5.81	6420	70.5
	130	126	5.75	6440	68.0
80	60	332	16.70	9860	132.5
	70	282	15.93	9960	116.0
	80	251	15.40	10060	106.5
	90	230	14.90	10120	99.5
	100	214	14.55	10190	95.0
	110	201	14.15	10220	91.0
	120	191	13.92	10260	88.5
	130	261	20.10	10240	105.0

TABLE XXVII

NON-DESTRUCTIVE TEST
RUN 6

Reactor: D Status: Instantaneous
Gas: Dry Air Flow Rate: 2910 ml/min
Room Temp.: 20 °C Pressure: 762 mm Hg

V_p (V)	f (Hz)	I_p (mA)	W_p (W)	V_s (V)	W_t (W)
40	60	165	4.85	5060	79.0
	70	150	4.70	5080	75.0
	80	139	4.50	5100	71.5
	90	130	4.33	5120	68.5
	100	123	4.22	5125	65.5
	110	115	4.10	5140	63.5
	120	110	3.95	5160	61.5
	130	105	3.90	5180	59.5
70	60	299	14.90	8730	121.5
	70	272	15.13	8790	113.5
	80	256	15.30	8800	108.5
	90	251	15.70	8900	105.5
	100	248	16.43	9020	104.5
	110	244	16.90	9175	103.5
	120	149	17.10	9120	104.0
	130	263	18.05	9055	108.5
80	60	360	19.75	9920	141.0
	70	319	19.70	10020	126.5
	80	299	20.35	10140	121.5
	90	293	20.90	10100	121.5
	100	292	21.85	10200	119.5
	110	294	22.90	10510	120.0
	120	306	23.65	10570	120.0
	130	316	24.50	10610	125.0

TABLE XXVIII

NON-DESTRUCTIVE TEST
RUN 7

Reactor: A Status: instantaneous
Gas: Dry Air Flow Rate: 2910 ml/min
Room Temp.: 17 °C Pressure: 762 mm Hg

V_p (V)	f (Hz)	I_p (mA)	V_s (V)	I_s (mA)	W_t (W)
20	60	100	2720	1.4	31.5
	100	73	2730	2.0	27.5
	200	39	2780	1.4	22.5
	300	29	3030	2.0	21.0
	400	45	2430	2.0	23.5
	500	84	4230	2.0	28.5
	600	172	6360	2.0	41.0
	670	323	9160	2.0	61.5
	700	377	9420	2.0	71.0
	800	410	8840	2.0	75.0
	900	284	5260	1.4	55.5
	1000	191	2730	1.4	22.5
30	60	126	4070	2.0	36.0
	100	92	4090	2.0	31.0
	200	52	4160	1.4	25.0
	300	46	4550	2.0	23.5
	400	75	5180	1.4	26.5
	500	138	6450	2.0	36.0
	597	309	5570	2.0	59.5
	600	334	9790	2.0	58.5
	700	459	9830	2.0	82.5
	800	456	9094	2.7	81.5
	900	415	7500	1.4	75.5
	1000	281	2930	2.0	57.5

TABLE XXVIII (Continued)

V_p (V)	f (Hz)	I_p (mA)	V_s (V)	I_s (mA)	W_t (W)
40	60	153	5390	2.0	40.0
	100	109	5440	1.4	33.5
	200	64	5570	2.0	26.5
	300	69	6120	1.4	26.5
	400	112	7000	1.4	32.5
	500	199	8770	2.0	45.0
	520	240	9510	2.0	50.0
	565	501	10615	3.4	88.5
	600	523	10390	3.4	91.5
	700	519	9615	3.1	91.0
	800	488	8755	2.4	86.0
	900	457	7685	1.7	81.5
	1000	367	5010	2.0	67.5
50	60	183	6710	2.0	44.0
	100	127	6790	2.0	36.5
	200	76	6970	2.0	28.5
	300	92	7680	1.4	30.0
	400	149	8810	2.0	37.5
	440	199	9730	1.4	44.5
	500	724	10700	5.5	123.5
	600	625	9290	4.8	108.5
	700	557	8440	2.7	97.5
	800	482	7160	3.4	86.0
	900	444	6335	2.0	80.0
	1000	403	5090	2.0	72.5

TABLE XXIV

NON-DESTRUCTIVE TEST
RUN 8

Reactor: B Status: instantaneous
Gas: Dry Air Flow Rate: 2910 ml/min
Room Temp.: 19 °C Pressure: 762 mmHg

V_p (V)	f (Hz)	I_p (mA)	V_s (V)	I_s (mA)	Wt (W)
20	60	99	2740	1.4	31.5
	100	70	2760	1.4	26.5
	200	35	2850	2.0	21.5
	300	36	3190	2.0	21.5
	400	74	3860	1.4	26.5
	500	157	5430	2.0	38.5
	529	207	6355	2.4	35.5
	600	366	7280	2.7	68.5
	700	363	6670	2.0	68.5
	800	306	5280	1.4	59.0
	900	201	2910	2.0	44.0
	1000	151	1690	2.0	36.5
30	60	124	4070	2.0	36.0
	100	88	4010	2.0	30.5
	200	46	4260	1.4	23.5
	300	64	4800	1.4	27.5
	400	124	5860	1.4	34.0
	420	166	6435	1.7	40.0
	500	496	8690	3.4	87.5
	600	461	7520	2.7	81.5
	700	420	6720	2.7	76.0
	800	372	5900	1.4	68.5
	900	295	4440	1.4	56.0
	1000	222	2410	2.0	46.0
40	60	150	5410	2.0	40.0
	100	105	5480	1.4	32.5
	200	60	5690	2.0	25.5
	316	105	6630	2.0	21.5
	400	890	11070	3.4	151.5
	500	678	8150	3.4	116.5
	600	521	6530	3.4	92.5
	700	444	5730	2.0	80.0
	800	392	5130	2.0	71.5
	900	349	4420	1.3	67.5
	1000	293	3100	1.3	56.5

TABLE XXX

NON-DESTRUCTIVE TEST
RUN 9

Reactor: C Status: instantaneous
Gas: Air Flow Rate: 2910 ml/min
Room Temp.: 19 °C Pressure: 762 mmHg

V_p (V)	f (Hz)	I_p (mA)	V_s (V)	I_s (mA)	W_t (W)
20	60	100	2720	1.4	31.5
	100	73	2720	1.4	26.5
	200	39	2770	2.0	22.5
	300	28	3030	2.0	21.0
	400	44	3430	2.0	23.5
	500	85	4240	2.0	28.5
	600	172	6110	2.0	40.0
	689	400	10000	1.4	73.5
	700	416	10000	2.7	76.0
	800	430	9140	1.4	77.5
	900	288	5380	1.4	56.0
	1000	191	2730	2.0	41.5
30	60	126	4080	1.4	36.5
	100	93	4100	1.4	31.0
	200	54	4150	2.0	26.0
	300	45	4530	2.0	23.5
	400	72	5150	2.0	26.5
	500	134	6400	1.4	35.5
	600	272	9360	1.4	55.0
	626	458	10920	2.0	73.5
	660	460	11700	2.7	82.5
	700	486	10780	2.7	86.5
	800	490	9930	2.0	86.5
	900	419	7600	1.4	76.0
	1000	283	3955	1.7	55.5

TABLE XXX (Continued)

V_p (V)	f (Hz)	I_p (mA)	V_s (Vs)	I_s (mA)	Wt (W)
40	60	154	5390	2.0	40.0
	100	110	5450	2.0	32.5
	200	65	5580	1.4	26.5
	300	69	6130	2.0	26.5
	400	112	7000	1.4	32.5
	500	200	8780	1.4	45.5
	560	413	11625	2.4	76.5
	600	539	11740	3.4	93.5
	700	565	11050	2.7	98.5
	800	540	10140	2.0	93.5
	900	500	8720	2.0	88.5
	1000	367	5030	2.0	69.5
50	60	185	6690	2.0	43.5
	100	127	6780	2.7	43.5
	200	77	6970	2.0	28.5
	300	91	7670	2.0	29.5
	400	148	8790	2.0	37.5
	500	601	12790	3.4	105.0
	600	682	11120	4.8	114.5
	700	625	10660	3.4	106.0
	800	578	9900	2.0	99.5
	900	534	8740	2.0	91.5
	1000	457	6210	2.0	91.5

TABLE XXXI

NON-DESTRUCTIVE TEST
RUN 10

Reactor: D Status: instantaneous
Gas: Air Flow Rate: 2910 ml/min
Room Temp.: 16 °C Pressure: 2910 mm Hg

V_p (V)	f (Hz)	I_p (mA)	V_s (V)	I_s (mA)	W_t (W)
20	60	100	2750	2.0	31.5
	100	72	2750	2.0	26.5
	200	38	2840	1.4	22.5
	300	31	3130	2.0	20.5
	400	55	3650	2.0	24.5
	500	112	4740	1.4	21.5
	600	256	7730	2.0	51.5
	618	310	8830	2.0	59.0
	700	429	9160	2.0	76.5
	800	399	7930	2.0	81.5
	900	241	4060	1.4	48.5
	1000	172	2250	2.0	39.0
30	60	126	4060	1.4	36.0
	100	91	4090	2.0	31.0
	200	52	4190	2.0	25.0
	300	52	4630	2.0	24.5
	400	94	5430	2.0	30.0
	500	182	7150	2.0	41.5
	553	346	9590	2.7	66.0
	600	460	9850	3.4	82.0
	700	484	9235	2.4	86.0
	800	452	8280	2.4	81.5
	900	345	5560	1.7	64.5
	1000	248	3090	2.0	50.0

TABLE XXXI (Continued)

V_p (V)	f (Hz)	I_p (mA)	V_s (V)	I_s (mA)	Wt (W)
40	60	154	5400	1.4	40.0
	100	110	5450	2.0	33.5
	200	63	5610	2.0	28.5
	300	77	6230	2.0	27.5
	400	137	7350	2.0	36.0
	475	225	9040	2.0	48.5
	500	482	10650	3.4	84.5
	600	572	10130	5.5	98.5
	700	540	9325	2.4	94.0
	800	503	8540	2.0	88.5
	900	433	6975	1.7	67.5
	1000	326	4060	1.4	61.0
50	60	181	6690	2.0	43.5
	100	124	6790	2.0	35.5
	200	75	7010	2.0	28.5
	300	104	7830	2.0	31.5
	392	173	9130	2.0	41.5
	400	196	9430	2.0	46.0
	430	998	13670	4.1	169.0
	450	952	12170	5.5	158.5
	500	808	10430	5.5	146.5
	600	642	8680	4.1	111.0
	700	558	7785	3.1	97.5
	800	504	7210	1.4	91.5
	900	458	6260	2.0	81.5
	1000	406	4830	2.0	73.5

TABLE XXXII

NON-DESTRUCTIVE TEST
RUN 11

Reactor: A	Primary Voltage: 40 V	Status: steadystate
Gas: Dry Air	Flow Rate: 2910 ml/min	
	Room Temp.: 21.2 °C	Pressure: 762 mm Hg

f (Hz)	I_p (mA)	V_s (V)	I_s (mA)	W_t (W)	T_e (°C)
60	153	5390	2.0	40.0	21.2
100	109	5440	1.4	33.5	21.2
200	68	5550	2.0	26.5	21.2
250	56	5830	2.0	25.0	21.2
300	66	6090	2.0	26.0	21.2
350	81	6440	1.4	28.5	21.2
400	107	6960	1.4	31.5	21.2
450	142	7660	1.4	36.5	21.2
500	193	8700	1.4	43.5	21.2
523	477	10130	2.7	86.0	38.2
550	507	10080	2.7	89.5	39.2
600	511	9715	2.4	90.0	39.2
650	508	9420	2.7	89.5	38.2
700	504	9225	2.4	89.5	38.2
750	494	8935	2.7	86.0	38.2
800	484	8650	2.0	85.0	38.2
850	471	8255	1.4	83.5	38.2
900	473	8040	1.4	83.5	29.7
950	450	7060	1.4	80.0	22.2
1000	370	5060	1.4	67.5	21.2

TABLE XXXIII

NON-DESTRUCTIVE TEST
RUN 12

Reactor: B	Primary Voltage: 40 V	Status: steady state
Gas: Dry Air	Flow Rate: 2910 ml/min	
	Room Temp.: 20 °C	Pressure: 762 mm Hg

f (Hz)	I_p (mA)	V_s (V)	I_s (mA)	W_t (W)	T_e (°C)
60	150	5410	2.0	40.0	20.0
100	105	5480	1.4	32.5	20.0
200	62	5670	2.0	25.0	20.0
250	71	6060	1.4	26.5	20.0
300	97	6480	1.4	31.0	20.0
311	106	6620	1.4	31.5	20.0
350	341	8460	2.7	64.5	29.0
400	861	10890	3.4	146.0	40.5
450	819	10090	3.4	139.5	38.5
500	688	9100	3.8	118.5	37.5
550	614	8370	2.7	106.0	36.0
600	555	7780	2.7	96.5	34.5
650	505	7220	2.7	90.0	33.5
700	477	6900	2.7	85.0	30.5
750	456	6640	2.7	81.5	29.5
800	436	6330	2.0	78.5	26.5
850	413	5925	1.7	76.0	24.5
900	390	5360	1.4	71.5	22.0
950	337	4100	1.4	63.5	20.5
1000	296	3120	1.4	56.5	20.0

TABLE XXVI

NON-DESTRUCTIVE TEST
RUN 13

Reactor: C Primary Voltage: 40 V Status: steady state
Gas: Dry Air Flow Rate: 2910 ml/min
Room Temp.: 21.2 °C Pressure: 762 mm Hg

f (Hz)	I_p (mA)	V_s (V)	I_s (mA)	W_t (W)	T_e (°C)
60	155	5390	2.0	40.0	20.2
100	111	5440	1.4	32.5	20.2
200	65	5540	1.4	26.0	20.2
250	56	5830	2.0	25.0	20.2
300	67	6090	2.0	25.5	20.2
350	82	6450	2.0	28.5	20.2
400	109	6960	1.4	31.5	20.2
450	145	7690	2.0	36.5	20.2
500	195	8730	2.0	43.5	20.2
550	272	10380	1.4	55.0	20.2
563	496	11075	2.4	87.5	35.7
600	532	10975	2.4	92.5	35.7
650	548	10755	2.4	95.0	36.2
700	549	10530	2.0	95.0	37.7
750	546	10380	2.0	94.5	38.2
800	542	10195	1.7	93.5	38.2
850	535	9840	1.4	91.5	35.2
900	525	9190	1.4	91.0	25.2
950	446	6940	1.4	78.5	21.2
1000	369	5000	1.4	66.5	20.2

TABLE XXXV

NON-DESTRUCTIVE TEST
RUN 14

Reactor: D	Primary Voltage: 40 V	Status: steady state
Gas: Dry Air	Flow Rate: 2910 ml/min	
	Room Temp.: 20.3 °C	Pressure: 762 mm Hg

f (Hz)	I_p (mA)	V_s (V)	I_s (mA)	W_t (W)	T_e (°C)
60	154	5400	1.4	40.0	20.3
100	110	5450	2.0	33.5	20.3
200	62	5620	1.4	26.0	20.3
250	66	5990	2.0	26.0	20.3
300	77	6250	2.0	27.5	20.3
350	101	6710	2.0	30.5	20.3
400	137	7380	1.4	36.0	20.3
450	188	8340	1.4	42.5	20.3
479	534	10325	3.0	93.5	31.8
500	568	10275	3.0	98.5	32.8
550	568	9725	3.0	98.5	32.8
600	550	9360	2.7	96.0	32.3
650	535	9140	2.7	93.5	31.8
700	523	8910	2.0	93.5	31.0
750	511	8690	2.0	89.5	30.8
800	499	8410	2.0	87.5	29.3
850	486	8055	1.7	86.0	26.8
900	454	7140	1.4	81.0	20.3
950	385	5340	1.4	70.5	20.3
1000	326	3910	1.4	60.5	20.3

TABLE XXXVI

DESTRUCTION TEST
RUN 15

Reactor: A Primary Voltage: 40 V Status: steady state
Gas: Dry Air/TCE Flow Rate: 2910 ml/min
Room Temp.: 22.8 °C Pressure: 762 mm Hg

f (Hz)	C_i (ppm)	C_o (ppm)	I_p (mA)	V_s (V)	I_s (mA)	Wt (W)	Te (°C)	Ef (%)
518	624.82	13.95	561	9265	6.5	95.0	41.8	97.77
600	622.24	12.01	543	9190	6.1	93.5	42.8	98.07
700	629.66	18.07	526	9220	6.1	90.5	37.8	97.35
800	625.24	43.44	503	8920	4.8	86.5	37.8	93.05
900	618.35	353.76	479	7990	4.1	86.5	29.8	42.79

TABLE XXXVII

DESTRUCTIVE TEST
RUN 16

Reactor: B Primary Voltage: 40 V Status: steady state
Gas: Dry air/TCE Flow Rate: 2910 ml/min
Room Temp.: 23 °C Pressure: 762 mm Hg

f (Hz)	C_i (ppm)	C_o (ppm)	I_p (mA)	V_s (V)	I_s (W)	Wt (oC)	T (oC)	Ef (%)
285	627.82	533.93	100	6210	16.8	31.5	25.0	15.96
320	622.65	356.76	176	6980	14.3	40.0	28.0	42.70
360	623.23	12.80	798	11340	13.0	131.5	44.0	97.95
400	624.69	8.34	855	10690	14.3	144.0	45.0	98.66
500	627.62	11.84	716	8850	13.7	120.5	40.0	98.11
600	633.46	23.79	559	7590	13.7	96.5	37.0	96.24
700	631.42	58.68	482	6800	9.6	84.0	33.0	90.71

TABLE XXXVIII

DESTRUCTIVE TEST
RUN 17

Reactor: C Primary Voltage: 40 V Status: steady state
Gas: Dry Air/TCE Flow Rate: 2910 ml/min
Room Temp.: 20.5 °C Pressure: 762 mm Hg

f (Hz)	C_i (ppm)	C_o (ppm)	I_p (mA)	V_s (V)	I_s (mA)	W_t (W)	T_e (°C)	E_f (%)
562	622.36	15.16	NA	9940	3.4	NA	39.5	97.56
600	613.56	18.28	NA	9790	3.4	NA	39.5	97.02
700	638.00	11.88	544	10241	3.4	93	NA	97.97
800	541.28	29.51	528	9240	2.0	92	NA	94.55
900	515.04	450.61	531	9035	1.7	NA	NA	12.50

TABLE XXXIX

DESTRUCTIVE TEST
RUN 18

Reactor: D Primary Voltage: 40 V Status: steady state
Gas: Dry Air/TCE Flow Rate: 2910 ml/min
Room Temp.: 23.2 °C Pressure: 762 mm Hg

f (Hz)	C_i (ppm)	C_o (ppm)	I_p (mA)	V_s (V)	I_s (mA)	W_t (W)	T_e (°C)	E_f (%)
453	631.28	12.80	650	9745	7.2	108.5	39.2	97.97
500	640.97	9.15	623	9220	7.5	106.0	39.2	98.57
600	629.64	7.21	568	9235	6.5	109.0	37.2	98.86
700	624.16	25.09	533	8500	6.1	92.5	36.2	95.98
800	630.12	198.13	505	8230	5.5	86.5	31.2	68.56

TABLE XXXX

DESTRUCTIVE TEST
RUN 19

Reactor: C Primary Voltage: 50 V Status: steady state
Gas: Dry Air/TCE Flow Rate: 2910 ml/min
Room Temp.: 20 °C Pressure: 762 mm Hg

f (Hz)	C_i (ppm)	C_o (ppm)	I_p (mA)	V_s (V)	I_s (mA)	W_t (W)	T_e (°C)	E_f (%)
480	629.18	15.09	713	10810	6.8	120.0	46	97.45
530	628.90	11.46	682	10325	6.5	116.0	44	98.18
600	627.79	7.53	636	9740	6.1	111.0	41	98.80
700	628.25	9.03	600	9390	5.5	104.5	42	98.67
800	652.00	16.64	578	9140	4.1	101.5	43	97.45
900	636.34	85.54	542	8080	4.1	96.0	34	86.56

TABLE XXXXI

DESTRUCTIVE TEST
RUN 20

Reactor: D Primary Voltage: 40 V Status: steady state
Gas: Dry Air/TCE Flow Rate: 4410 ml/min
Room Temp.: 20.8 °C Pressure: 764 mm Hg

f (Hz)	C_i (ppm)	C_o (ppm)	I_p (mA)	V_s (V)	I_s (mA)	W_t (W)	T_e (°C)	E_f (%)
462	630.93	59.09	401	9755	5.8	66.0	36.8	90.63
500	623.86	23.82	557	10150	5.8	98.5	44.8	96.18
600	623.19	28.49	562	9425	6.5	96.0	42.8	95.43
700	626.15	72.39	536	8995	5.1	93.5	40.8	88.44
800	630.00	282.84	507	8470	4.8	91.0	32.8	55.10

TABLE XXXXII

DESTRUCTIVE TEST
RUN 21

Reactor: C Primary Voltage: 40 V Status: steady state
Frequency: 558 Hz
Gas: Wet Air/TCE Flow Rate: 2910 ml/min
Room Temp.: 22 °C Pressure: 762 mm Hg

C_i (ppm)	C_o (ppm)	I_p (mA)	V_s (V)	I_s (mA)	Wt (W)	Te (°C)	Ef (%)
6.82	*	545	9620	6.1	93.5	38.5	>99.99
6.96	*	544	9600	6.1	93.5	38.5	>99.99
374.40	5.04	531	10300	5.5	93.5	38.5	98.65
655.38	4.23	541	9930	5.5	93.5	38.5	99.35
1431.60	10.00	NA	NA	NA	NA	38.5	99.30
4074.60	9.06	518	10530	5.1	93.5	39.5	99.78
7388.30	27.13	498	10700	5.5	91.5	37.5	99.63
10207.00	41.82	487	10830	5.5	90.0	37.5	99.59
14361.00	43.92	476	10930	4.8	88.5	35.5	99.69
15945.00	86.53	470	10990	4.8	86.5	34.5	99.46

* Undetected

TABLE XXXXIII

DESTRUCTIVE TEST
RUN 22

Reactor: C Primary Voltage: 40 V Status: steady state
Frequency: 558 Hz
Gas: Wet Air/TCE Flow Rate: 7723 ml/min
Room Temp.: 23 °C Pressure: 773 mm Hg

C_i (ppm)	C_o (ppm)	I_p (mA)	V_s (V)	I_s (mA)	Wt (W)	T (°C)	Ef (%)
8.55	1.76	544	10560	4.8	91.5	54.0	79.46
599.72	33.23	517	11400	4.8	89.0	54.0	94.46
1382.57	76.99	478	11630	4.1	83.5	51.0	94.43
2151.48	77.04	484	11590	4.1	84.0	53.0	96.42
2557.33	86.69	486	11590	4.1	84.3	54.0	96.86
4112.94	80.98	486	11590	4.1	85.0	54.0	98.03

TABLE XXXXIV

DESTRUCTIVE TEST
RUN 23

Reactor: C-D* in parallel Status: steady state
Primary Voltage: 40 V
Gas: Wet Air/TCE Flow Rate: 2910 ml/min
Room Temp.: 21 °C Pressure: 762 mm Hg

f (Hz)	C_i (ppm)	C_o (ppm)	V_s (V)	I_s (mA)	W_t (W)	T_c (°C)	T_d (oC)	E_f (%)
389	462.47	258.23	9375	3.8	60.0	21	23	44.16
	980.99	409.97	9335	3.8	60.0	24	25	58.21
	3430.62	2780.85	9310	3.4	60.0	21	23	18.94
400	355.90	2.61	10970	6.1	141.5	25	42	99.26
	929.30	3.19	10930	6.1	136.0	25	41	99.66
	1126.74	6.42	10865	5.8	136.5	25	43	99.72
	4846.25	-	10780	6.1	125.5	25	41	>99.99
500	630.29	1.76	9140	5.5	119.5	23	38	99.72
	1513.00	2.91	9470	7.2	120.0	24	39	99.80
	4776.60	11.32	9425	7.2	120.0	25	38	99.76
600	470.53	15.71	8490	7.2	97.5	24	37	97.01
	1300.73	12.89	8785	5.1	108.5	24	37	99.00
	2362.50	8.18	8920	4.8	111.0	26	35	99.65

* Entrance of Feed
\- Undetected

TABLE XXXXV

DESTRUCTIVE TEST
RUN 24

Reactor: D-C* in parallel — Status: steady state
Primary Voltage: 40 V — Frequency: 400 Hz
Gas: Wet Air/TCE — Flow Rate: 2910 ml/min
Room Temp.: 22 °C — Pressure: 762 mm Hg

C_i (ppm)	C_o (ppm)	I_p (mA)	V_s (V)	I_s (mA)	Wt (W)	T_c (°C)	T_d (°C)	E_f (%)
419.23	2.63	706	10720	6.1	117.5	32.5	57.5	99.37
444.37	**	702	10605	5.8	117.5	32.5	52.5	100.00
738.61	3.10	696	10660	6.1	116.5	32.5	52.5	99.58
1673.52	**	684	10770	5.5	115.0	32.5	52.5	100.00
2469.71	4.39	690	10810	5.5	115.5	32.5	57.5	99.82
4405.74	NA	NA	NA	NA	NA	NA	NA	NA

* Entrance of Gas Feed
** Undetected

TABLE XXXXVI

DESTRUCTIVE TEST
RUN 25

Reactor: C-D* in parallel — Status: steady state
Primary Voltage: 40 V — Frequency: 400 Hz
Gas: Humid Air/TCE — Flow Rate: 7230 ml/min
Room Temp.: 22 °C — Pressure: 774 mm Hg

C_i (ppm)	C_o (ppm)	I_p (mA)	V_s (V)	I_s (mA)	Wt (W)	T_c (°C)	T_d (°C)	E_f (%)
325.26	6.56	783	11080	6.1	136.5	58.0	30.0	97.98
353.15	5.18	794	11090	6.8	129.5	59.0	30.0	98.53
334.88	0.67	797	11090	6.8	130.0	59.0	30.0	99.80
356.20	0.53	800	11060	6.1	131.0	59.0	31.0	99.85
302.43	4.67	801	11070	5.5	131.5	59.0	30.5	98.46
306.29	0.53	802	11040	6.1	133.5	59.0	30.0	99.83
1137.93	0.74	817	11285	5.8	136.5	63.0	28.5	99.93
1696.44	4.64	806	11245	5.8	135.5	63.0	28.0	99.73
2510.08	9.01	794	11205	5.8	131.5	65.0	28.0	99.64
3974.07	10.33	772	11140	6.1	127.5	65.0	29.0	99.74

* Entrance of Gas Feed

TABLE XXXXVII

DESTRUCTIVE TEST
RUN 26

Reactor: C Primary Voltage: 40 V Status: steady state
Frequency: 548 Hz
Gas: Dry Air/TCE Flow Rate: 2910 ml/min
Room Temp.: 20.6 °C Pressure: 762 mm Hg

C_i (ppm)	C_o (ppm)	I_p (mA)	V_s (V)	I_s (mA)	W_t (W)	T_e (°C)	E_f (%)
862.87	28.67	546	10010	5.5	91.5	35.6	96.68
2140.98	72.48	527	10250	5.5	91.3	36.6	96.61
4869.04	9.03	512	10450	5.5	90.0	35.6	97.63
7445.43	16.64	491	10820	5.5	88.5	32.6	96.71
10899.83	85.54	474	10860	5.5	90.0	28.6	97.09
13561.64	376.81	465	11000	5.5	84.5	26.6	97.22
18043.54	796.51	451	11090	4.8	81.5	27.6	95.58
21468.40	2344.00	441	11130	4.1	80.5	28.6	89.08
24297.02	4211.86	436	11130	2.7	80.0	28.6	82.66

TABLE XXXXVIII

DESTRUCTIVE TEST
RUN 27

Reactor: C Primary Voltage: 40 V Status: steady state
Frequency: 548 Hz
Gas: Dry Air Flow Rate: 2910 ml/min
Room Temp.: 23.0 °C Pressure: 762 mm Hg

I_p (mA)	V_s (V)	W_t (W)	T (°C)
483	11580	93.0	48.5
482	11590	87.5	49.5
478	11570	87.5	46.5
496	11510	88.5	49.5
502	11510	90.0	49.5

TABLE XXXXIV

DUPLICATED BREAKDOWN TEST
RUN 28

Reactor: C	Room Temp.: 23 °C Gas: Dry Air	Pressure: 762 mm Hg Flow Rate: 2910 ml/min
Primary Voltage	Breakdown Frequency	Breakdown Voltage
40	550	10500
	552	10620
	548	10400
45	525	10840
	512	10460
	518	10560
	518	10520
	522	10700

2

VITA

Ven-Yen Tsai

Candidate for the Degree of

Doctor of Philosophy

Thesis: CONCEPTUAL DESIGN AND PERFORMANCE ANALYSIS OF FREQUENCY-TUNED CAPACITIVE DISCHARGE REACTORS

Major Field: Chemical Engineering

Biographical:

Personal Data: Born in Ching Shui, Taiwan, Republic of China, April 28, 1956, the son of Shing Cheng and Wen Chuan Tsai.

Education: Received Bachelor of Engineering Degree in Chemical Engineering from Chung Yuan Christian University, Chungli, Taiwan, in June 1978; received Master of Science Degree in Chemical Engineering from Mississippi State University, Starkville, Mississippi, in December 1986; completed requirements for the Doctor of Philosophy Degree at Oklahoma State University in May 1991.

Professional Experience: Technician, Assistant Researcher, Associate Engineer and Project Leader, Energy Research Laboratory, Industrial Technology Research Institute, Taiwan, 1981-1984; Graduate Teaching and Research Assistant, School of Chemical Engineering, Oklahoma State University, Stillwater, Oklahoma, 1987-1991.

Membership in Professional Society: Omega Chi Epsilon; Chinese Institute of Chemical Engineers, Taiwan; Society of Optical Engineering, Taiwan; Chinese Institute of Engineers, Taiwan; German Carl Duisberg Association/Taiwan.